

**UNIVERSITÉ DU QUÉBEC À TROIS-RIVIÈRES**

**RÔLE DU COLLAGÈNE DE TYPE IV SUR L'ACTIVITÉ DE GLP-1/NOTCH DANS  
LA LIGNÉE GERMINALE DE *C. ELEGANS***

**ROLE OF TYPE IV COLLAGEN ON GLP-1/NOTCH ACTIVITY IN THE *C.*  
*ELEGANS* GERMLINE**

**THÈSE PRÉSENTÉE  
COMME EXIGENCE PARTIELLE DU  
DOCTORAT EN BIOLOGIE CELLULAIRE ET MOLÉCULAIRE**

**PAR  
PIER-OLIVIER MARTEL**

**JUILLET 2024**

Université du Québec à Trois-Rivières

Service de la bibliothèque

Avertissement

L'auteur de ce mémoire, de cette thèse ou de cet essai a autorisé l'Université du Québec à Trois-Rivières à diffuser, à des fins non lucratives, une copie de son mémoire, de sa thèse ou de son essai.

Cette diffusion n'entraîne pas une renonciation de la part de l'auteur à ses droits de propriété intellectuelle, incluant le droit d'auteur, sur ce mémoire, cette thèse ou cet essai. Notamment, la reproduction ou la publication de la totalité ou d'une partie importante de ce mémoire, de cette thèse et de son essai requiert son autorisation.

UNIVERSITÉ DU QUÉBEC À TROIS-RIVIÈRES  
BIOLOGIE CELLULAIRE ET MOLÉCULAIRE (DOCTORAT)

**Direction de recherche :**

---

Patrick Narbonne Directeur de recherche

**Jury d'évaluation**

---

Patrick Narbonne Directeur de recherche

---

Hugo germain Président de jury

---

Jean-Philippe Leduc Gaudet Évaluateur interne

---

Richard Roy Évaluateur externe

Je dédie cette thèse à la mémoire de ma tante  
Marielle, emportée par le cancer et dont le souvenir  
m'a gardé motivé dans mes recherches.

## Remerciements

Tout d'abord, je tiens sincèrement à remercier le professeur Patrick Narbonne, sans qui les études supérieures auraient été hors de portée. Je n'ai pas eu de facilité lors de mon premier cycle, durant lequel j'ai entrepris deux autres baccalauréats et fait face à de nombreux échecs avant de trouver ma place en biologie. C'est pendant ce baccalauréat que j'ai retrouvé de la confiance en mes capacités. Malgré mon historique de performances académiques désastreuses, Patrick a accepté de me donner une chance de prouver que je valais plus que mon relevé de notes. Grâce à lui, j'ai pu développer une passion pour la recherche ces dernières années. Dans son laboratoire j'ai acquis un large éventail de compétences scientifiques qui me serviront tout au long de ma carrière. Il m'a offert une grande liberté autour de mon projet de recherche tout en étant toujours très disponible, ce qui m'a permis de développer mon autonomie, ma débrouillardise et ma pensée critique, des traits qui me seront utiles toute ma vie. En bref, merci infiniment de m'avoir donné cette chance, merci pour ta patience et surtout merci d'avoir contribué à faire de moi le scientifique que je suis aujourd'hui.

Je voudrais également remercier tous les collègues de laboratoire que j'ai côtoyés ces dernières années. Nous ne partageons peut-être pas toujours les mêmes points de vue, mais je ne serais pas là où j'en suis aujourd'hui sans vous tous.

Je tiens à remercier Malika Nadour, Claire Bénard, David Sherwood et Joe Culotti pour les réactifs, conseils et souches qui ont été d'une grande aide tout au long du projet. Je remercie également Judith Kimble et Sarah Crittenden avec qui chaque rencontre a été extrêmement instructive! Je les remercie également pour leurs conseils, les souches, les matériaux ainsi que leur disponibilité pour répondre à mes questions. De plus, je les remercie d'avoir proposé l'utilisation du senseur SALSA qui a été essentiel à l'avancement du projet. Enfin, je remercie Hugo Germain de m'avoir donné accès à sa licence du logiciel Imaris, qui a été largement utilisée pendant ce projet.

Je remercie mes parents pour leur soutien tout au long de mes études. Je remercie particulièrement ma mère qui a consacré beaucoup de son temps à la correction grammaticale et à améliorer la clarté de cette thèse. Je remercie aussi mon père qui l'a lue avant le dépôt initial et qui m'a tenu compagnie en ligne lors des longues soirées d'analyse.

Enfin, je voudrais remercier ma conjointe Marie-Ève qui m'a soutenu durant toutes ces années. Merci pour ta patience et pour toutes ces soirées et fins de semaine que tu as passées en solitaire alors que j'étais au laboratoire ou bien collé devant mon ordinateur.

Grammarly a été utilisé dans les chapitres I et III de ce document pour aider à corriger les erreurs grammaticales et en améliorer la clarté.

## Résumé

La régulation de la prolifération des cellules souches est essentielle au sein d'un organisme, car sa dérégulation peut conduire à la déplétion des cellules souches ou à la formation de tumeurs. La niche des cellules souches assume une partie de ce rôle en empêchant leur différenciation et en permettant leur prolifération, empêchant ainsi leur perte. Chez *C. elegans*, les cellules d'extrémité distale de la gonade forment la niche des cellules souches germinales, qui existent en tant que deux populations situées aux extrémités distales de deux bras de gonade. Ces cellules d'extrémité distale expriment un ligand à leur membrane, LAG-2, qui se lie au récepteur Notch, GLP-1, exprimé à la surface des cellules souches germinales adjacentes. L'activation de la signalisation Notch dans les cellules souches germinales empêche leur différenciation et permet leur prolifération. Pour mieux comprendre la régulation de la prolifération des cellules souches germinales par la signalisation Notch, nous avons effectué un criblage génétique afin d'isoler des mutations amplifiant un allèle gain de fonction (*gf*) de *glp-1/Notch*. Cela a conduit à l'isolement d'un nouvel allèle hypomorphe (*qz2*) de *mig-6L*, qui augmente de manière synergique la formation de tumeurs germinales dans un fond *glp-1(gf)*. Cette synergie se produit sans aucun changement détectable dans l'expression de *lag-2* ou de *glp-1*. MIG-6L est un homologue de la Papiline des mammifères, connue pour réguler négativement les dépôts de collagène de type IV (COL IV), le principal composant structurel de la membrane basale. Comme MIG-6L est spécifiquement exprimé par les cellules d'extrémité distale, nous avons pensé qu'il pourrait modifier la membrane basale associée aux cellules d'extrémité distale et aux cellules souches germinales et ainsi influencer la signalisation Notch. En effet, nous avons mesuré une augmentation significative des niveaux de COL IV associé aux cellules d'extrémité distale et aux cellules souches germinales, en particulier dans les gonades postérieures des mutants *mig-6L(qz2)*, qui entraîne une augmentation de l'activation de GLP-1 dans la gonade postérieure et de la taille de la population postérieure de cellules souches germinales. En plus d'affecter la signalisation *glp-1/Notch*, *mig-6L(qz2)* entraîne le développement de gonades distales plus courtes. Cependant, nous avons constaté que l'élongation des gonades était régulée indépendamment des niveaux de COL IV. Par ailleurs, les effets positifs de l'augmentation des niveaux de COL IV sur l'activation de GLP-1

n'étaient pas spécifiques aux mutants *mig-6(qz2)*. L'augmentation des niveaux de COL IV adjacents aux cellules d'extrémité distale par le biais de mutations dans les composants de signalisation TGF- $\beta$  augmente aussi l'activation de GLP-1 dans les cellules souche germinale(CSG). Enfin, en manipulant directement le COL IV associé aux cellules d'extrémité distale, nous avons confirmé qu'il favorise l'activation de GLP-1 dans les cellules souches germinales. De plus, nous avons montré que les niveaux de COL IV associé aux cellules d'extrémité distale étaient considérablement augmentés dans les mutants perte de fonction (pf) *glp-1(pf)*, qui perdent leurs populations de CSG par différenciation. À l'inverse, les niveaux de COL IV associé aux cellules d'extrémité distale étaient plus faibles dans les *glp-1(gf)* qui forment des tumeurs, indiquant une relation négative directe entre l'activité de *glp-1/Notch* et les niveaux de COL IV associé aux cellules d'extrémité distale. Enfin, nous fournissons la preuve que l'augmentation du COL IV associé aux cellules d'extrémité distale observée dans les *glp-1(pf)* peut résulter de la perte des cellules souches germinales plutôt que de la perte de l'activité de Notch en tant que telle. Ces résultats ont été quelque peu surprenants puisque la suraccumulation de collagène, également connue sous le nom de fibrose, est souvent considérée comme une conséquence d'une activité Notch élevée en raison de leur cooccurrence fréquente. Nos résultats montrent plutôt que les niveaux de COL IV favorisent l'activation du récepteur Notch, ce qui suggère que le contenu en collagène de la membrane basale peut influencer considérablement la signalisation médiée par les récepteurs intercellulaires.

## Abstract

The regulation of stem cell proliferation within an organism is critical as deregulation can lead to either stem cell depletion or tumour formation. The stem cell niche fulfills part of this role by preventing stem cell differentiation and allowing for their proliferation, altogether preventing their loss. In *C. elegans*, the distal tip cells (DTCs) act as niches for the germline stem cells (GSCs), which exists as two pools located at the distal extremities of two gonad arms. These DTCs express LAG-2, a membrane-bound ligand for the Notch receptor, GLP-1, expressed at the surface of the nearby GSCs. Activation of Notch signaling in GSCs prevents their differentiation and allows for their mitotic proliferation. To gain insights into the regulation of GSC proliferation by Notch signaling, we carried out a *glp-1*/Notch gain-of-function (gf) enhancer forward genetic screen. This led to the isolation of a new hypomorphic allele (*qz2*) of *mig-6L* that synergistically enhances germline tumour formation in a *glp-1(gf)* background. This synergy occurs without any detectable changes in *lag-2* or *glp-1* expression in *mig-6(qz2)* mutants. MIG-6L is homologous to mammalian Papilin, which is known to negatively regulate type IV collagen (COL IV) deposition, the main basement membrane structural component. As MIG-6L is specifically expressed by the DTCs, we reasoned that it could modify the basement membrane separating the DTCs and GSCs and thereby influence Notch signal transmission. Indeed, we measured a significant increase in COL IV levels at the DTC/GSC interface, specifically in the posterior gonad arms of *mig-6L(qz2)* mutants, while this was associated with increased posterior *glp-1* signaling and posterior GSC pool size. In addition to affecting *glp-1*/Notch signaling, *mig-6L(qz2)* causes animals to develop shorter distal gonads. However, we found that gonad elongation was regulated independently from COL IV levels. We found that the positive effects of increased COL IV levels on GLP-1 activation was not specific to *mig-6(qz2)* mutants as increasing DTC-associated COL IV (DTC-AC) levels through mutations in TGF- $\beta$  signaling components similarly increased GLP-1 activation in GSCs. Finally, by directly manipulating DTC-AC levels, we confirmed that they promote GLP-1 activation in GSCs. Moreover, we showed that DTC-AC levels were dramatically increased in *glp-1* loss of function (lf) mutants, which lose their GSC pools to differentiation. Conversely, DTC-AC levels were lower in tumorous *glp-1(gf)*, indicating a direct negative relationship between *glp-1*/Notch



activity and DTC-AC levels. Finally, we provide evidence that the increase in DTC-AC observed in *gfp-1(lf)* may result from the loss of the GSC pool rather than the loss of Notch activity per se. These results came somewhat as a surprise since in the literature, collagen overaccumulation, also known as fibrosis, is often deemed a consequence of high Notch activity due to their frequent co-occurrence. Instead, our results show that COL IV levels promote Notch receptor activation, suggesting basement membrane collagen contents can sizably influence intercellular receptor-mediated signalling.

## TABLE OF CONTENTS

Remerciements.....	i
Résumé .....	ii
Abstract .....	iv
TABLE OF CONTENTS.....	vi
LIST OF FIGURES AND TABLES .....	viii
LIST OF ABBREVIATIONS AND ACRONYMS .....	ix
CHAPTER I .....	1
Introduction .....	1
1.1 Cancer .....	1
1.2 Stem Cells.....	3
1.3 <i>Caenorhabditis elegans</i> as a model.....	5
1.4 <i>C. elegans</i> gonads .....	6
1.5 Notch signalling.....	7
1.6 Homeostatic regulation of stem cells in <i>C. elegans</i> .....	10
1.7 Screening for new genes involved in homeostatic regulation of GSCs	11
1.8 Mig-6/Papilin .....	12
1.9 The Basement membrane.....	13
1.10 TGF beta.....	14
1.11 Interaction between the basement membrane and SC .....	20
1.12 Inhibitors of gamma-secretase .....	21
Chapter II.....	23
Objectives and preliminary results .....	23
2.1 Research objectives.....	23
2.1.1 Objective 1: Defining the impact of the <i>mig-6(qz2)</i> mutation. ....	23
2.1.2 Objective 1.1: Defining the nature of the interaction between <i>mig-6</i> and <i>glp-1</i> . ....	23
2.1.3 Objective 1.2: Defining the impact of <i>mig-6(qz2)</i> on collagen IV levels. ....	24
2.1.4 Objective 1.3: Define whether reduced <i>mig-6l</i> function improves Notch signalling. ....	25
2.1.5 Objective 1.4: using the SALSA sensor to define Notch activity more precisely. ....	26

2.1.6 Objective 2: does collagen deposition correlate with Notch activity in <i>C. elegans</i> ?	28
2.1.7 Objective 2.1: Does a decrease of collagen levels cause a reduction in Notch activity?	29
2.1.8 Objective 2.2: How will other collagen-affecting mutations affect Notch activity?	29
2.1.9 Objective 3: Determine whether collagen IV regulates notch activity or Notch activity regulates collagen IV	30
2.1.10 Objective 3.1: How will a decrease in the expression of LAG-2, the Notch ligand, impact collagen IV?	30
2.1.11 Objective 3.2: How will changes in Notch receptor-dependent activity impact COL IV?	30
Submitted manuscript	31
Niche-associated Type IV collagen promotes GLP-1/Notch receptor activation in the <i>C. elegans</i> germline	31
Abstract	31
Main	32
A basement membrane glycoprotein synergistically interacts with <i>glp-1</i> /Notch	32
MIG-6L limits collagen accumulation at the DTC-GSC interface	35
MIG-6L reduces GLP-1(NICD) presence at the GSC plasma membrane	38
GLP-1/Notch activation varies together with DTC-AC Col IV levels	39
GLP-1/Notch activity inversely affects COL IV levels	40
GLP-1/Notch activation is tied to DTC-associated COL IV levels	42
DTC-associated COL IV promotes GLP-1/Notch receptor activation	45
Discussion	45
Methods	46
<i>C. elegans</i> maintenance	46
Cloning of the <i>mig-6(qz2)</i> allele	46
Transgenics	46
Imaging	46
Tumour formation assay	47
Distal gonad length measurement	47
Brood size, embryonic and larval lethality	48
<i>Plag-2::GFP</i> and <i>EMB-9::mCherry</i> fluorescence intensity quantification	48
Notch signaling quantification using <i>GLP-1(NICD)::GFP</i>	48
Notch signaling quantification using SALSA	48
PZ size evaluation	49

Statistics .....	49
Acknowledgements .....	49
Extended Data .....	50
Chapter III .....	59
Discussion .....	59
3.1 MIG-6 PLAC domain .....	59
3.2 How does <i>mig-6(qz2)</i> interact with <i>glp-1(qr202)</i> ? .....	60
3.3 Anterior/posterior gonad asymmetry .....	61
3.4 Type IV collagen promotes Notch ligand/receptor activity .....	61
3.5 Notch activity does not promote collagen production. ....	63
3.6 Mutation in the <i>daf-7</i> gene could cause changes in COL IV levels through its impact on Notch activity .....	64
3.7 Conclusion .....	64
3.8 Research Perspectives .....	65
3.8.1 How exactly does COL IV promote Notch activity? .....	65
3.8.2 Investigating the role of TGF- $\beta$ signalling in COL IV production. ...	66
3.8.3 Investigating the impact of gamma-secretase inhibitors on COL IV levels. ....	67
References .....	68

## LIST OF FIGURES AND TABLES

Figure 1: Tumours subtypes origin models .....	2
<b>Figure 2: Stem cell development in mammals</b> .....	3
<b>Figure 3: The relationship between the number of stem cell divisions in the lifetime of a given tissue and the lifetime risk of cancer in that tissue.</b> Adapted from Tomasetti and Vogelstein <sup>1</sup> .....	4
<b>Figure 4: C. elegans life cycle</b> .....	6
<b>Figure 5: Graphical representation of C. elegans anatomy.</b> .....	6
<b>Figure 6: Graphical representation of gonadogenesis.</b> .....	7
<b>Figure 7: The core of Notch signalling pathway</b> .....	9
<b>Figure 8: simplified genetic pathway showing how Notch activity prevents differentiation.</b> .....	10
<b>Figure 9: The C. elegans GSC niche</b> .....	10
<b>Figure 10: Identification of <i>mig-6(qz2)</i> following a mutagenic screen</b> .....	12
<b>Figure 11: The novel <i>mig-6(qz2)</i> interacts with <i>glp-1(ar202)</i></b> .....	13
<b>Figure 12: Basement Membrane matrix Components and Receptors in C. elegans.</b> .....	14
<b>Figure 13: Effect of collagen IV and MIG-6L mutant alleles</b> .....	15
<b>Figure 14: Cell signalling pathway of TGF-<math>\beta</math> superfamily of ligands.</b> .....	16

Figure 15 : TGF- $\beta$ superfamily signalling is highly conserved in metazoans. ....	17
Figure 16: The Dauer TGF- $\beta$ -related pathway. ....	18
Figure 17: The Sma/Mab TGF $\beta$ -related pathway. ....	19
Figure 18: Basement membrane surrounding tumours are stiffer.....	20
Figure 19: The gamma-Secretase Complex Members.....	21
Figure 20: COL IV quantification workflow.....	25
Figure 21 : Cleaving assay workflow.....	26
Figure 22: Graphical representation of the two techniques used to assess Notch activity.....	27
Figure 23: SALSA sensor explanation.....	28
Figure 24: Silencing of <i>emb-9</i> expression by RNAi causes gonad rupture.....	29
Figure 25: Keeley et al. COL IV quantification.....	60

## LIST OF ABBREVIATIONS AND ACRONYMS

ADAMTS	A Disintegrin and Metalloproteinase with Thrombospondin Motifs
ANOVA	ANalysis Of VAriance
APH	Anterior PHarynx defective
BMP	Bone Morphogenic Proteins
BRA	BMP Receptor Associated protein family
CBF	C-promoter binding factor (in mammals)
<i>C. elegans</i>	<i>Caenorhabditis Elegans</i>
COL IV	Type IV collagen
CO-TFS	CO-Transcription Factors
CSL	CBF1/Su(H)/Lag-1
DAF	abnormal DAuer Formation
DAPI	4',6-diamidino-2-phenylindole
DIC	Differential Interference Contrast microscopy
DTC	Distal Tip Cell
DTC-AC	DTC Associated Collagen
EMB	abnormal EMBryogenesis
EMS	Ethyl Methane Sulfonate
EpCAM	Epithelial Cell Adhesion Molecule
ERK	Extracellular signal-Regulated Kinase
FBF	Fem-3 mRNA Binding Factor
FEM	FEMinization of animals
FOG	Feminization Of Germline
FRET	Förster Resonance Energy Transfer
gf	gain of function
GFP	Green Fluorescent Protein
GLD	defective in Germ Line Development
GLP	abnormal Germ Line Proliferation
GSC	Germline Stem Cell
HIS	HIStone
IGF	Insulin-like Growth Factor
IIS	insulin-like/IGF-1 signalling
LAG	Lin-12 And Glp-1 phenotype

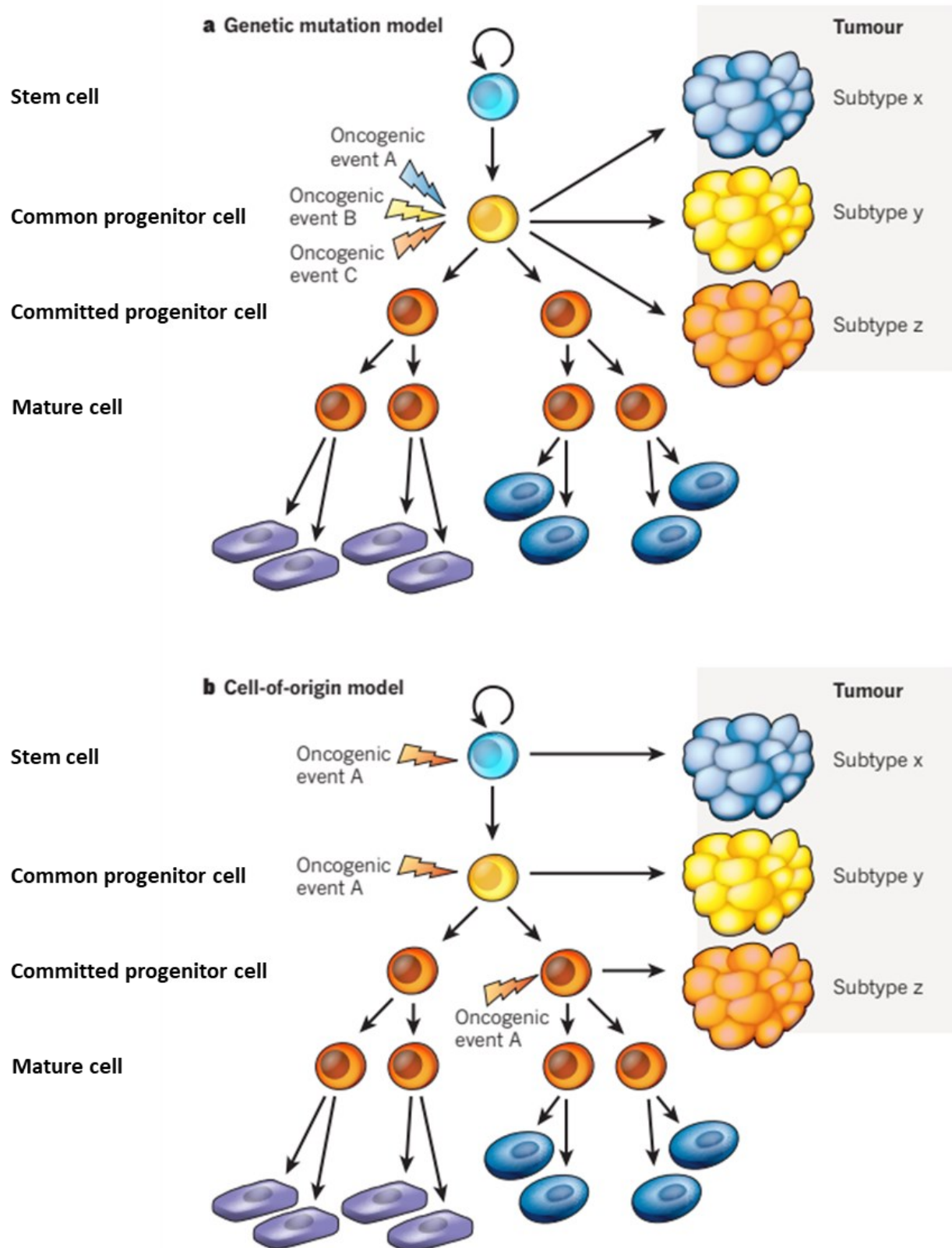
LAR	Leukocyte-common Antigen Related
If	loss of function
LIN	abnormal cell LINEage
LON	LONG
LST	Lateral Signaling Target
MAB	Male ABnormal
MAPK	Mitogen-Activated Protein Kinase
mCherry	monomer Cherry
MIG	abnormal cell MIGration
MIG-6L	MIG-6 long isoform
MIG-6S	MIG-6 short isoform
mRNA	messenger RiboNucleic Acid
MSP	Major Sperm Protein
NECD	Notch ExtraCellular Domain
NICD	Notch IntraCellular Domain
NOS	NanOS related
PEN	Presenilin Enhancer
PIE	Pharynx and Intestine in Excess
PLAC	Protease and LACunin
PUF	PUmilio and FBF
PZ	Progenitor Zone
RFP	Red Fluorescent Protein
RPTP	Receptor-like Protein Tyrosine Phoshatases
R-SMAD	Receptor-associated SMAD
SALSA	Sensor Able to detect Lateral Signaling Activity
SC	Stem Cell
SMA	SMALL
SMAD	Suppressor of Mothers against Decapentaplegic
Su(H)	Suppressor of Hairless (in <i>drosophila</i> )
SYGL	SYnthetic GerMLine proliferation defective
TAG	Temporarily Assigned Gene name
tevP	tobacco etch virus Protease
TGF- $\beta$	Transforming Growth Factor- $\beta$

## CHAPTER I

### Introduction

#### 1.1 Cancer

Cancer is known as one of the leading causes of mortality worldwide. Only in Canada, an estimated 233,900 new cancer cases and 85,000 cancer deaths occurred 2022<sup>11</sup>. Its social and economic impacts have made it a prime research interest. However, one could ask, how can the cure for a disease that has been investigated since the 19<sup>th</sup> century still be elusive? Part of the problem we are facing is that cancer is not just one disease, but a collection of diseases that can affect any tissue. These diseases however share common characteristics. By definition, cancer is a malignant tumour of potentially unlimited growth that expands locally by invasion and systemically by metastasis<sup>12,13</sup>. A tumour is an abnormal benign or malignant growth of tissue that possesses no physiological function and arises from uncontrolled, usually rapid cellular proliferation<sup>10,13</sup>. In other words, the difference between a benign and a malignant tumour is that a malignant tumour can undergo metastasis, which means it can spread from the initial site of the disease to another part of the organism. But how does a tumour arise in the first place? While other origins likely exist, it is believed that most tumours originate from the accumulation of mutations and epigenetic changes that progressively increase the growth potential and the normal function of stem cells (SCs), to promote tumour development, and eventually cancer (Fig. 1). Therefore, it would seem more unlikely that a mature cell that has no or very low division potential regains such potential<sup>9,14,15</sup>.



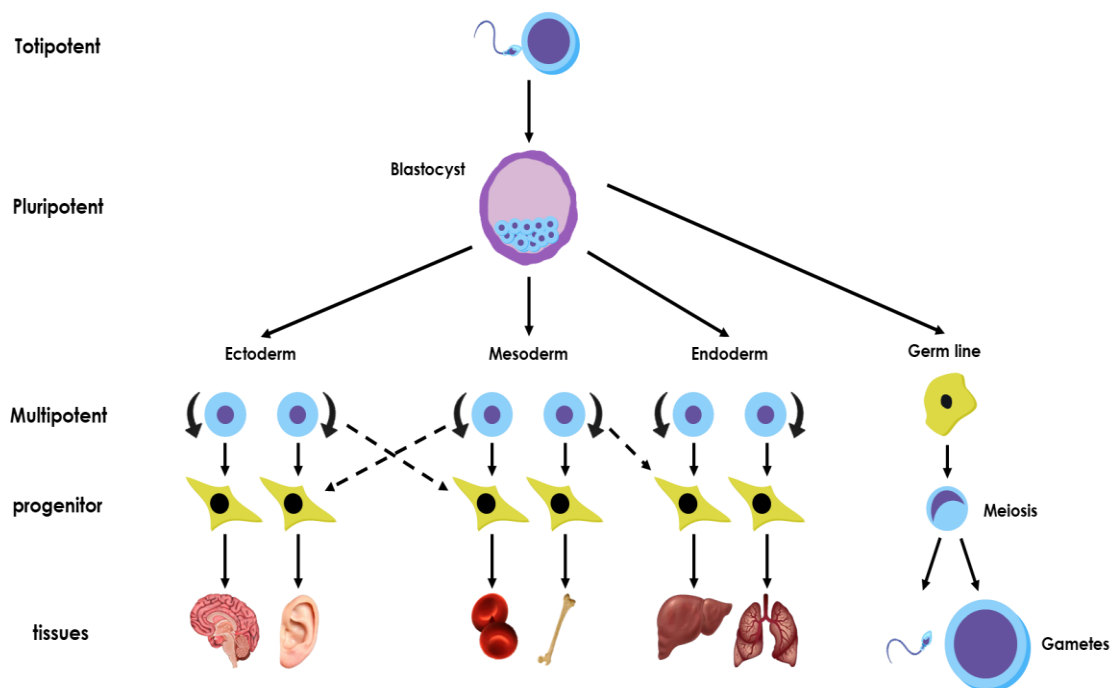
**Figure 1: Tumours subtypes origin models**

**a.** In the genetic (and epigenetic) mutation model, mutations primarily determine the tumour phenotype, such that different mutations on the same cell-of-origin result in different tumour morphologies. **b.** In the cell-of-origin model, different cell populations in the lineage hierarchy serve as cells of origin for the different cancer subtypes arising within that organ or tissue. Figure adapted from Visvader<sup>9</sup>.



## 1.2 Stem Cells

SC are undifferentiated cells with two defining characteristics: they are capable of long-term self-renewal and, depending on their differentiation potential, can give rise to a range of differentiated cells in an organism (Fig. 2)<sup>16</sup>.

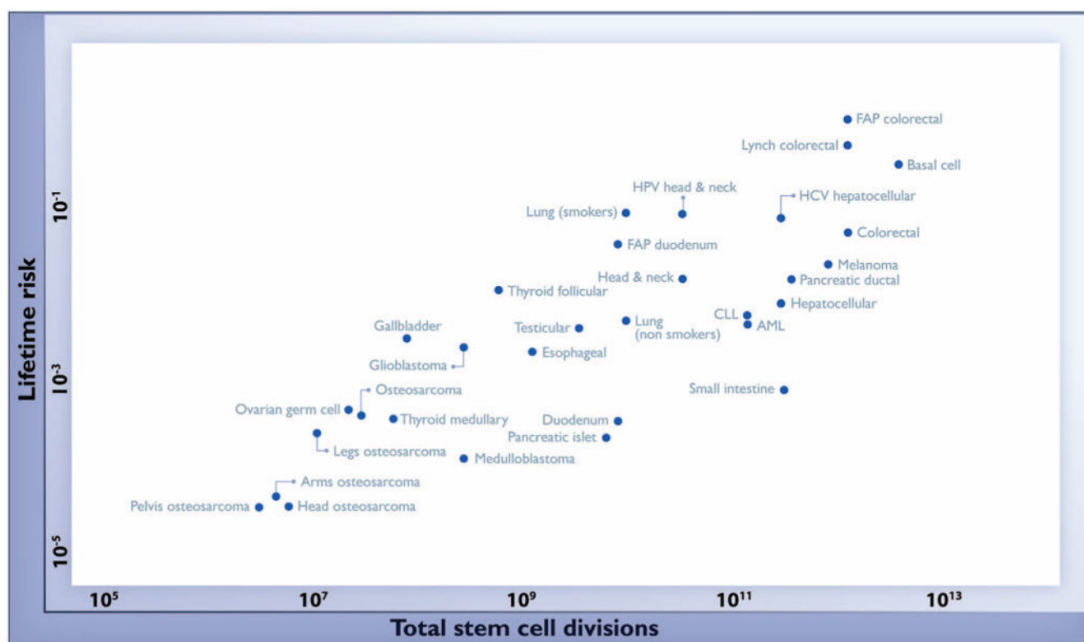


**Figure 2: Stem cell development in mammals**

From the highest to the lowest differentiation potential, totipotent cells come first. They originate from a male and female gamete fusion when they form the zygote and can differentiate into every cell type, including the extra-embryonic tissue, such as the placenta. Next, derived from the totipotent cells are the pluripotent SCs, also known as embryonic SCs, which can differentiate into any cell type of the embryo proper, but not into extraembryonic tissue. Further differentiation yields the multipotent SCs, also called adult SCs, that can differentiate into a narrower subset of specialised cells in the organ they serve. Progenitor cells are no longer considered SCs as they have more limited self-renewal and differentiation capacities.

SCs play a pivotal role during embryonic development, as embryonic SCs allow tissue generation, while adult SCs will be crucial for tissue regeneration, renewal and repair to maintain tissue homeostasis. Therefore, the SCs should divide only when there is a need for more undifferentiated or differentiated cells so that the tissue contains just the right amount of each needed to fulfil their purpose. The fulfilment of SC functions

shares a common requirement for cell division and, consequently, replication of genetic material. Despite the intricate cellular processes in place to minimise errors during replication ( $\approx 10^{-10}$  mutations per base pair per cell division)<sup>17</sup>, the more division a cell undergoes, the more at risk it is to commit replication errors. Consistent with this, cancer will be more frequent in tissues in which SCs undergo an overall greater number of SC divisions than those in which SCs divide rarely<sup>1</sup> (Fig. 3) as mutations in multiple genes are usually required for SC's over proliferation to occur. Therefore, the genes' identity, functions and interaction partners that lead to tumour formation



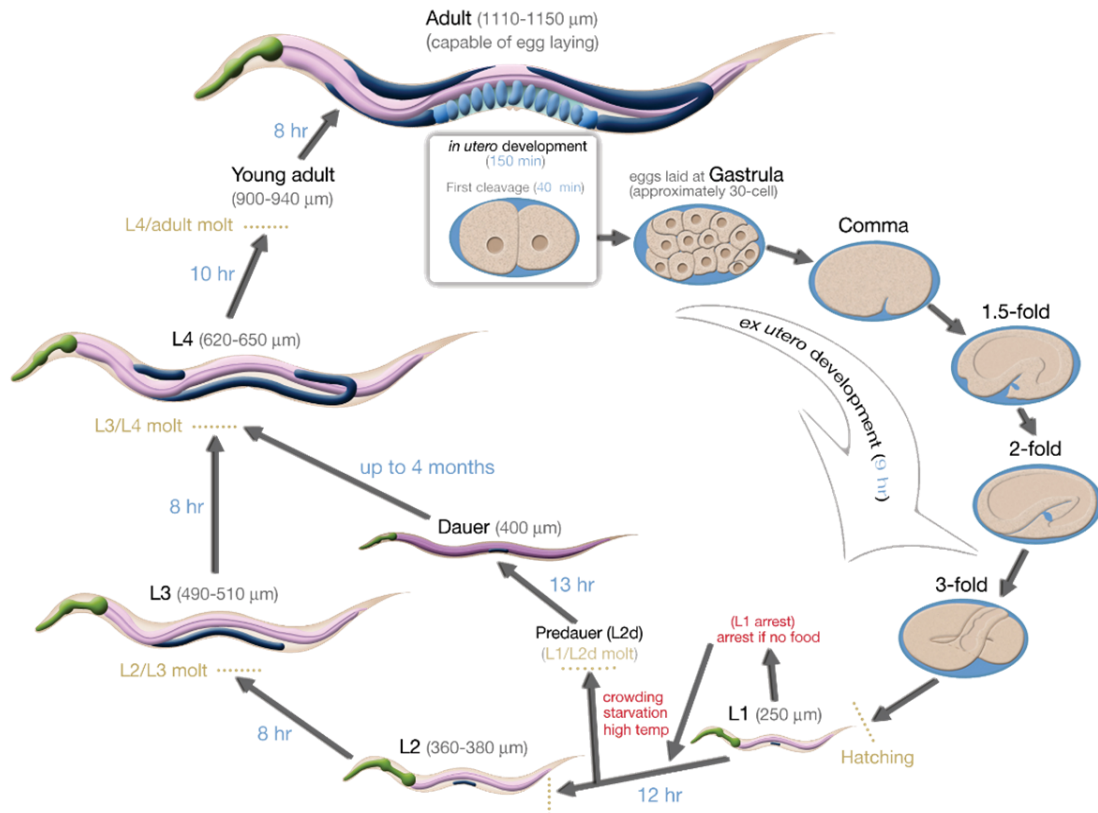
**Figure 3: The relationship between the number of stem cell divisions in the lifetime of a given tissue and the lifetime risk of cancer in that tissue.** Adapted from Tomasetti and Vogelstein<sup>1</sup>.

have long been investigated. However, the study of SCs within a living organism has faced many challenges due to their restricted accessibility, necessitating a continual advancement and refinement of techniques up to the present day<sup>9,10</sup>.

As an alternative, *in vitro* SC culture has been widely used since its introduction<sup>18</sup>. While it has multiple advantages that have significantly enhanced our understanding of SC biology, *in vitro* cell culture also has limitations. One such drawback is its inability to encompass the impact of both the macro and microenvironment on stem cell proliferation<sup>19</sup>. Acknowledging these limitations, our research program, centered on the homeostatic regulation of SCs, takes advantage of a model organism that allows for straightforward *in vivo* observation of SCs, specifically, the nematode *C. elegans*.

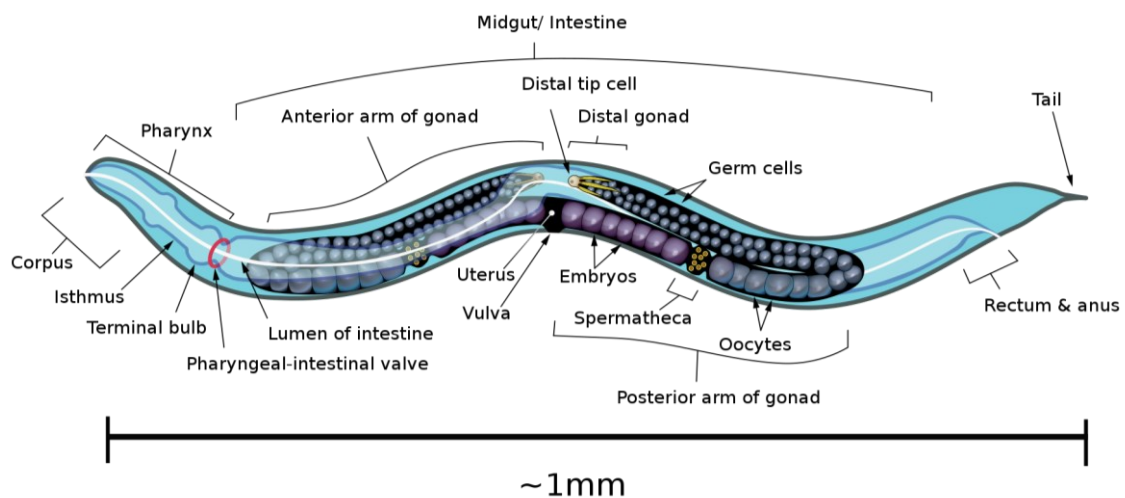
### **1.3 *Caenorhabditis elegans* as a model**

Since its introduction as a genetically tractable model organism more than 50 years ago<sup>20</sup>, *C. elegans* has proven to be a powerful and versatile model organism that has allowed critical advancement in biological research. It was the first animal whose entire genome, encompassing 20,000 protein-coding genes, was completely sequenced<sup>21</sup>. Many key features and aspects of *C. elegans* make it a model organism of choice. First, they are small, about 1 millimetre long, nonparasitic, non-pathogenic and easy-to-grow nematodes with a simple anatomy comprising a total of 959 somatic cells and approximately ~2000 germ cells<sup>22,23</sup>. Furthermore, its transparent cuticle allows for easier *vivo* observation of biological processes and the use of fluorescent-tagged proteins. They are hermaphrodites, meaning they can produce both sperm and then oocytes that they use to self-fertilize and lay roughly 300 eggs, which is a significant asset for maintaining complex mutation combinations as every offspring will conserve the same genetic makeup as their parent without the need for a specific mate. Fortunately, male *C. elegans* exist in a small proportion of the population and allow researchers to carry out genetic crosses. They also have a short life cycle as it takes 2-3 days to go from an egg to an egg-laying adult (Fig. 4). They are a model of choice to help us investigate the homeostatic regulation of SCs as opposed to mammals, for example, that have a multitude of hardly accessible SC populations dispersed throughout their body, *C. elegans* only have two well characterised and easily observable pools of multipotent germline stem cells (GSC), each located at the distal end of their two gonad arms<sup>24</sup> (Fig. 5).



**Figure 4: *C. elegans* life cycle**

Source: Girard, et al. <sup>8</sup>.



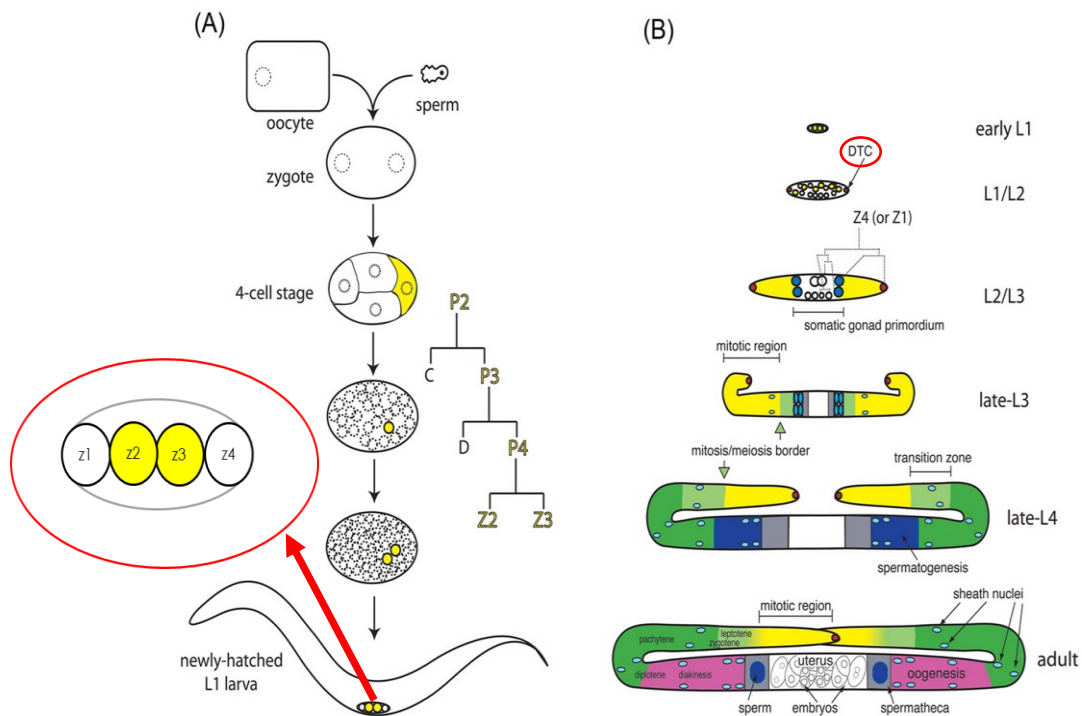
**Figure 5: Graphical representation of *C. elegans* anatomy.**

The anterior is left, and the posterior is right. The ventral side is down like the vulva, and the dorsal side is up. Source: Wikipedia.

### 1.4 *C. elegans* gonads

*C. elegans* develops two U-shaped somatic gonad arms that, in the adult, contain more than a thousand cells that originated from two germ precursor cells. Each gonad arm contains a pool of undifferentiated GSCs in their most distal part (Fig. 6). These GSCs will have two roles: maintain themselves by mitosis or differentiate by meiosis

into a finite quantity of sperm during the L4 stage or into oocytes in the adult stage (Fig. 6). This decision between mitosis and meiosis is spatially regulated by a niche, the distal tip cell (DTC), which is both necessary and sufficient for germline proliferation during the larval stage and later on in adults, and will maintain the most distal cells into an undifferentiated state through a Notch signal<sup>23,25</sup>.



**Figure 6: Graphical representation of gonadogenesis.**

At the L1 stage, we find the two yellow cells, Z2 and Z3, that will give rise to the germline, while Z1 and Z4 will yield the somatic gonad, including the stem cells' two niche cells displayed as red dots on the right developmental image series. These are called distal tip cells (DTCs), and they play a role in gonad migration and the maintenance of the SC stemness. During development, the gonad will undergo 3 phases of migration. First, it will elongate ventrally both anteriorly and posteriorly. Second, toward the end of the L3 stage, the gonad arms will make two-step U-turns, dorsally and then toward the centre of the animal. During the third phase of migration that takes place from the L4 stage to early adulthood, the gonads will elongate dorsally toward the center—adapted from Girard, et al. <sup>8</sup>.

### 1.5 Notch signalling

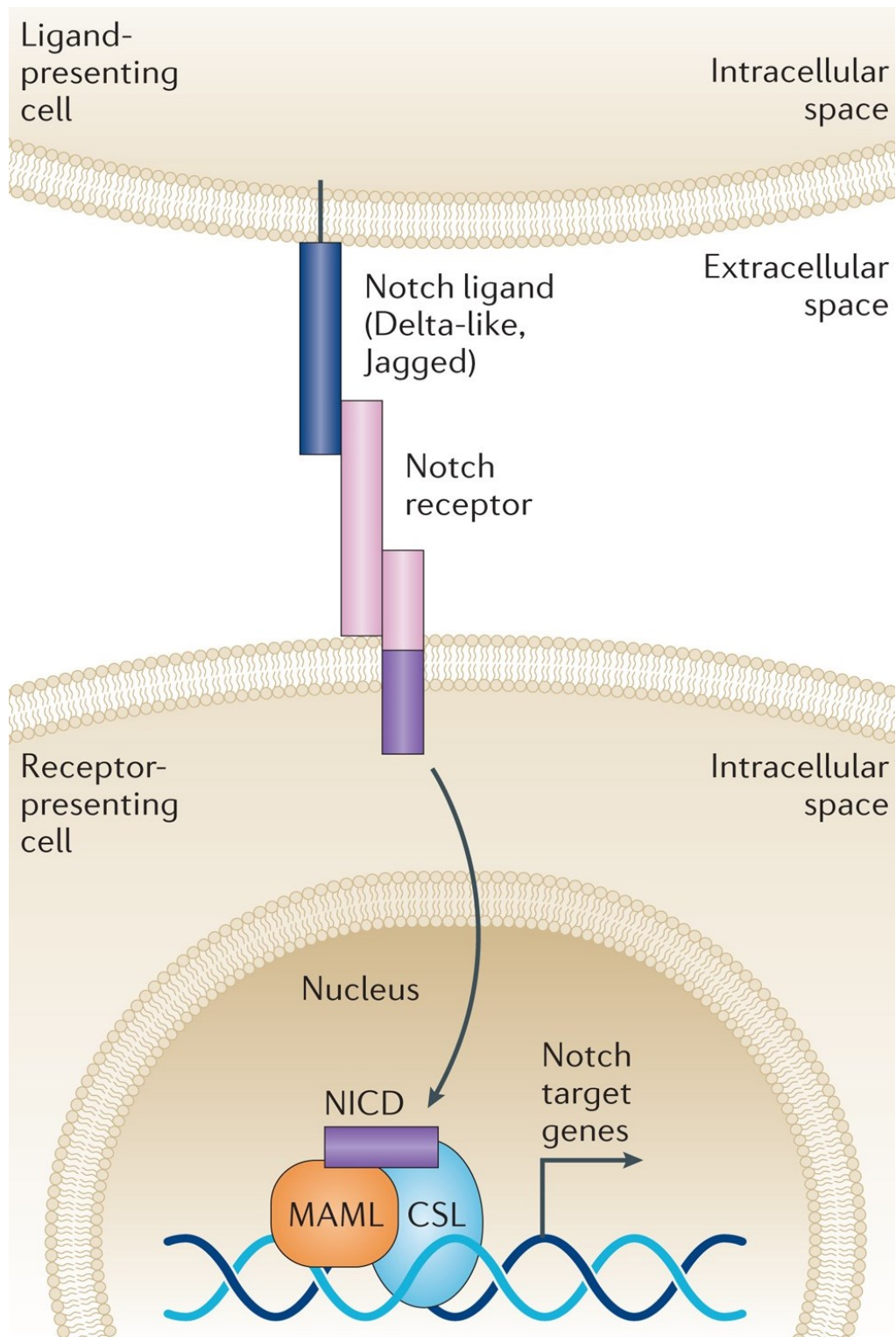
Notch signalling is an evolutionary conserved cell-cell communication pathway essential for diverse cell fate decisions and is, therefore, crucial to the development and maintenance of many multicellular organisms. It has been extensively studied as

its

deregulation leads to multiple human diseases, including cancers<sup>26-28</sup>. In humans, the Notch signalling pathway is composed of four receptors Notch(1-4) and four ligands Delta-like(1,4) and Jagged(1,2) plus their downstream target genes<sup>28</sup>. Both the ligand and receptors are transmembrane proteins expressed at the surface of neighbouring cells that can bind to one another to initiate Notch signalling (Fig. 7).

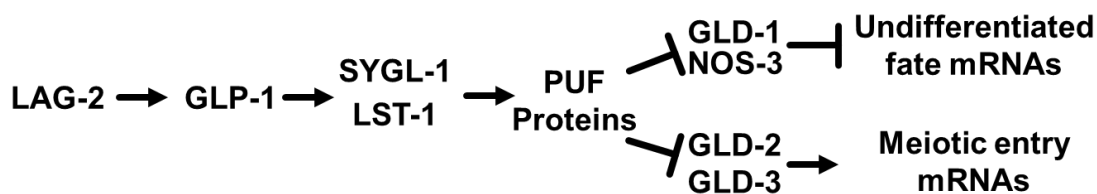
In *C. elegans*, the DTC is a jellyfish-looking cell that enwraps the most distal part of the gonad. It produces a Notch ligand, LAG-2, that will bind to its receptor, GLP-1, expressed by the GSCs and allows for Notch target genes transcription. Upon binding of the ligand to the Notch extracellular domain (NECD) a proteolytic cleavage will free the Notch intracellular domain (NICD) that can translocate to the nucleus and form a heterotrimeric complex with LAG-1/CSL DNA binding protein and LAG-3/SEL-8/Mastermind transcription co-activator to promote the transcription of Notch two primary target genes in *C. elegans*, *sygl-1* and *lst-1*<sup>8,10,29,30</sup>. These two genes encode for two redundant proteins that act upstream of Pumilio and FBF (PUF) proteins, which are eukaryotic, conserved mRNA translational repressors<sup>31,32</sup>. SYGL-1 and LST-1, together with PUFs will repress the translation of *gld-(1-3)* and *nos-3* mRNAs that would otherwise promote differentiation<sup>33,34</sup>. Notch activity, therefore, maintains a pool of undifferentiated cells by repressing differentiation (Fig. 8).

As division occurs, some GSCs are pushed further away from the DTC, where Notch signalling is reduced due to its distance from the ligand producing DTCs, thus allowing the cells to differentiate<sup>6</sup> (Fig. 9). In any organism, maintaining this delicate balance between SC division and differentiation is crucial<sup>35</sup>. Without sufficient division in the presence of active differentiated cell production, the SC pool can be depleted, resulting in the incapacity to produce additional differentiated cells. This means the tissue loses its renewal capacity and, here, the ability to make more sperm or oocytes, depending on the sex and developmental stage<sup>8,36</sup>. The opposite scenario, where there is too much division, will lead to an aberrant volume of undifferentiated SC, in other words, a tumour<sup>37</sup>.

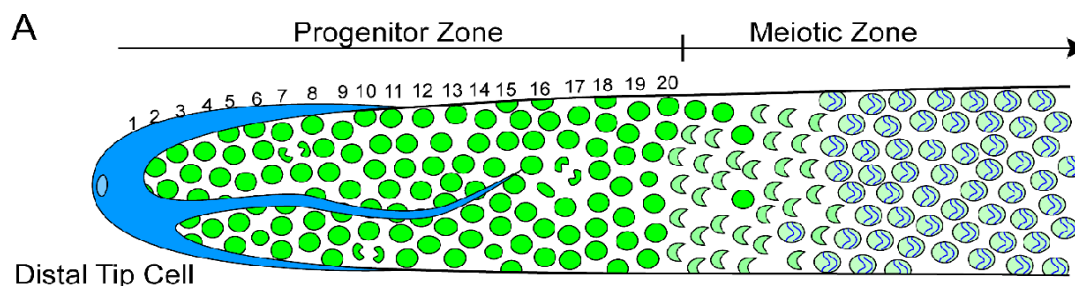


**Figure 7: The core of Notch signalling pathway**

The ligand on the presenting cell upon its binding with the Notch receptor extracellular domain (NECD) induces a series of proteolytic cleavage events in the receiving cell. These cleavage events release the Notch intracellular domain (NICD), which translocates to the nucleus to activate the transcription. Adapted from Andersson and Lendahl <sup>10</sup>.



**Figure 8: simplified genetic pathway showing how Notch activity prevents differentiation.**



**Figure 9: The *C. elegans* GSC niche**

(A) Schematic representation of the GSC niche (progenitor zone) in *C. elegans* oriented with the distal tip cell to the left. DTC is in blue with a cytoneme extending into the progenitor region, germ cells are in green with GSCs (solid green), meiotic cells (crescent shaped and green circles with blue lines). Numbers mark each cell row with a typical 20 cell diameters from the distal tip cell to the end of the progenitor region. Source: Trimmer<sup>6</sup>.

### 1.6 Homeostatic regulation of stem cells in *C. elegans*

Homeostasis is not only about the balance between division and differentiation. It's also about the tissue need for differentiated cells. Therefore, when no more differentiated cells are needed, the SC must periodically enter a quiescent state, which is a reversible phase of inactivity<sup>38</sup>. Failing to do so can result in an overabundance of differentiated tissue, once again leading to the formation of a tumour.

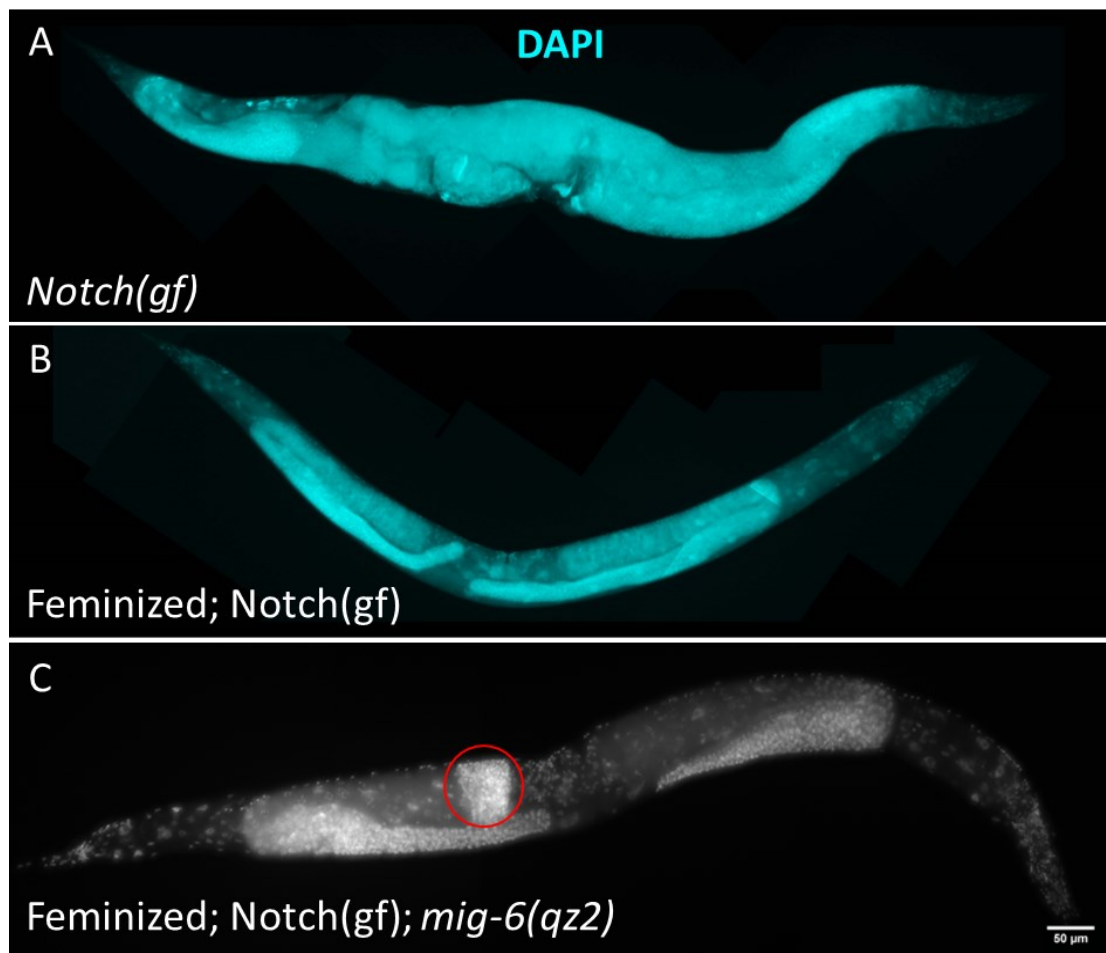
There are two known mechanisms that regulate GSC proliferation in adult *C. elegans*. First, the animal's nutritional status systemically regulates SC proliferation through insulin-like/IGF-1 signalling (IIS), In absence of food, reduced IIS activity will decrease cell proliferation to conserve energy and limited resources<sup>39,40</sup>.

The second mechanism would be the tissue need for differentiated cells, oocytes in adult hermaphrodites, that is believed to maintain activation of MAPK-1/ERK in the animals gut and/or somatic gonad, from where it non-autonomously promotes GSC proliferation<sup>41</sup>.



### **1.7 Screening for new genes involved in homeostatic regulation of GSCs**

Additional GSC proliferation regulatory mechanisms may also exist and require to be investigated. In pursuit of this, a mutagenic screen was conducted using ethyl methane sulfonate (EMS) on a mutant strain of *C. elegans* carrying two pertinent alleles. The first, *fog-1(q785)* allele, where FOG stands for feminisation of the germline, which prevents sperm formation and causes oocytes to accumulate early into adulthood, consequently diminishing GSC proliferation. The second is a temperature-sensitive gain-of-function (gf) allele of the Notch receptor, *glp-1(ar202)*, allowing for constitutive activation of Notch signalling under restrictive conditions, here 25°C. This impedes differentiation and leads to GSC tumour formation. Wild-type *C. elegans* are adapted to temperatures between 15°C and 25°C<sup>8</sup>, which allows for the use of temperature-sensitive alleles in experimental conditions. By raising those double mutant animals in permissive conditions, at 15°C until the late L4 stage, no tumours or sperm formation occurs. Upon shifting to a restrictive condition, oocytes rapidly accumulate due to the lack of sperm and tumour formation is prevented by inhibiting GSC proliferation. Subsequently, F2 progeny of the EMS-mutagenized animals were screened to identify mutants exhibiting tumour formation even in the presence of the homeostatic signalling induced by oocyte overaccumulation. Only one mutant fulfilling those criteria was isolated and identified as carrying a novel allele of *mig-6*, a homolog of human papilin<sup>3</sup> (Fig. 10).



**Figure 10: Identification of *mig-6(qz2)* following a mutagenic screen**

DAPI staining of animals of the indicated genotype. (A) *Notch(gf)/glp-1(ar202)* animals raised in restrictive conditions (25°C) develop massive GSC tumours. (B) In feminized worms the lack of sperm leads to oocyte accumulation and triggers the homeostatic signalling, thus preventing tumour formation. (C) triple mutants still form tumours in those same conditions. Source: Patrick Narbonne's preliminary analyses of *mig-6(qz2)* mutants.

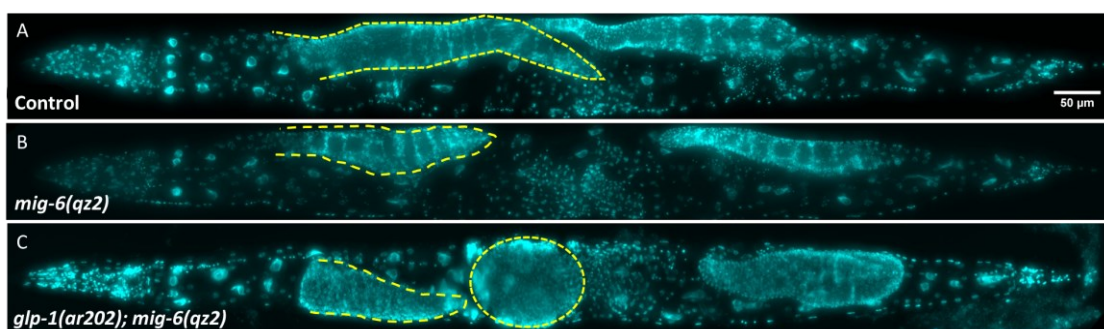
### 1.8 Mig-6/Papilin

MIG-6 is a large protein of the basement membrane that is conserved in both vertebrates and invertebrates<sup>42,43</sup>. *C. elegans* encodes two distinct isoforms, MIG-6S and MIG-6L, playing distinct roles in the gonad formation by respectively promoting cell non-autonomously or autonomously the DTC migration<sup>3</sup>. The *mig-6(qz2)* allele specifically affects the long MIG-6 isoform in its conserved C-terminal protease and lacunin (PLAC) domain, the exact function of which remains unknown but is commonly found in the « A Disintegrin and Metalloproteinase with Thrombospondin Motifs » (ADAMTS) family. These proteins, known for their roles as peptidases, play a significant role in tissue development and maintenance<sup>44-46</sup>. Interestingly, *mig-6* has

not previously been implicated in SC regulation. This aligned with our initial goal to identify unknown genes involved in the homeostatic regulation of SCs. However, upon isolation, we found that on their own, *mig-6(qz2)* single mutants did not cause any homeostatic regulation defect and did not lead to germline tumour formation (fig. 11). Instead, it appears this allele was a false positive that interacted with Notch signalling instead of being involved in homeostatic signalling.

### 1.9 The Basement membrane

This prompted us to investigate the interaction between a protein in the basement membrane and the Notch receptor. The basement membrane consists of thin, dense proteinaceous sheets of specialised extracellular matrix that envelop most animal

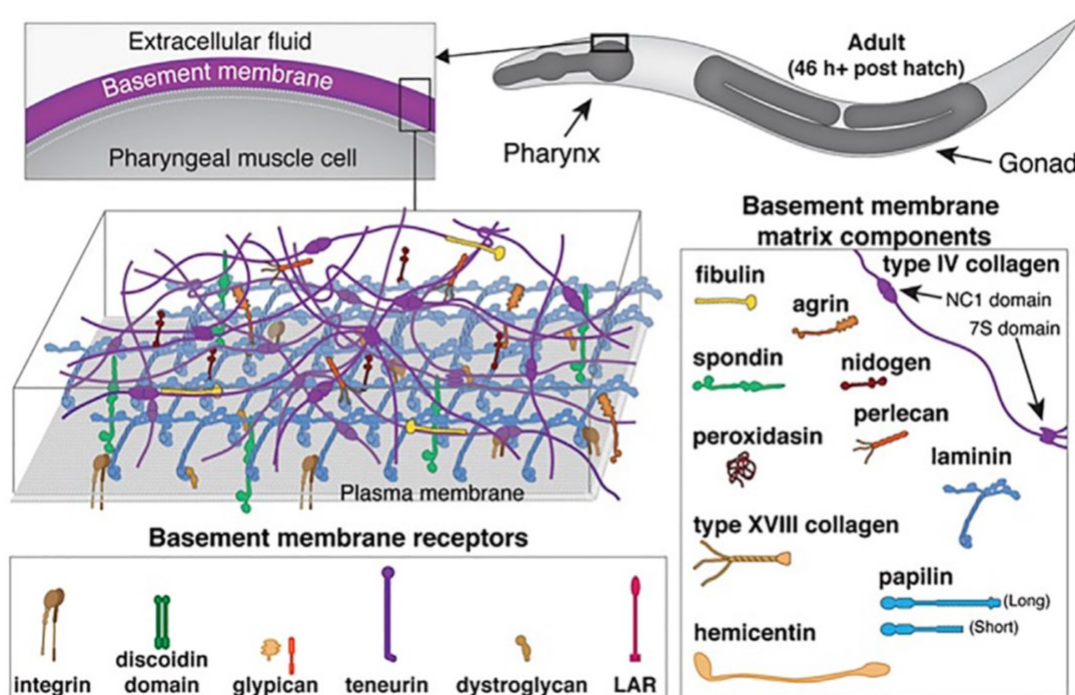


**Figure 11: The novel *mig-6(qz2)* interacts with *glp-1(ar202)***

DAPI staining of animals of the indicated genotype. (A) Control (B) *mig-6(qz2)* single mutants have shorter gonads but do not develop tumours (C) Double *glp-1(ar202); mig-6(qz2)* mutants also have shorter gonads and develop GSC tumours even when raised in permissive conditions.

tissues<sup>47</sup>. Although the mechanism regulating their structure and composition are poorly understood, they are known to be important in development and homeostasis as null mutations of proteins irreplaceable for basement membrane assembly lead to embryonic lethality<sup>48</sup>. One such essential component is type IV collagen (COL IV), a heterotrimer composed of COL IV  $\alpha 1$  and  $\alpha 2$  chains. It is the basement membrane's most abundant protein that assembles into a cross grid that serves as its primary structural foundation<sup>2,49,50</sup>. This COL IV grid is interconnected to a Laminin network that, in turn, binds to the cell<sup>2,50,51</sup>. Various other proteins, such as MIG-6, assume distinct roles and are present in varying abundance within this complex assembly (Fig. 12)<sup>2</sup>. MIG-6L is specifically expressed by the DTC and has recently been shown to negatively regulate procollagen peptidase access to the basement membrane, thereby locally reducing COL IV assembly<sup>2</sup>. Interestingly, null *mig-6L* mutants exhibit

severely slowed gonad elongation defect and sterility, similar to some COL IV mutants<sup>3</sup>(Fig. 13). Therefore, collagen assembly in the basement membrane is regulated by MIG-6 in part, which makes it a protein of interest for this study. However, we can next ask what controls collagen synthesis in the first place?

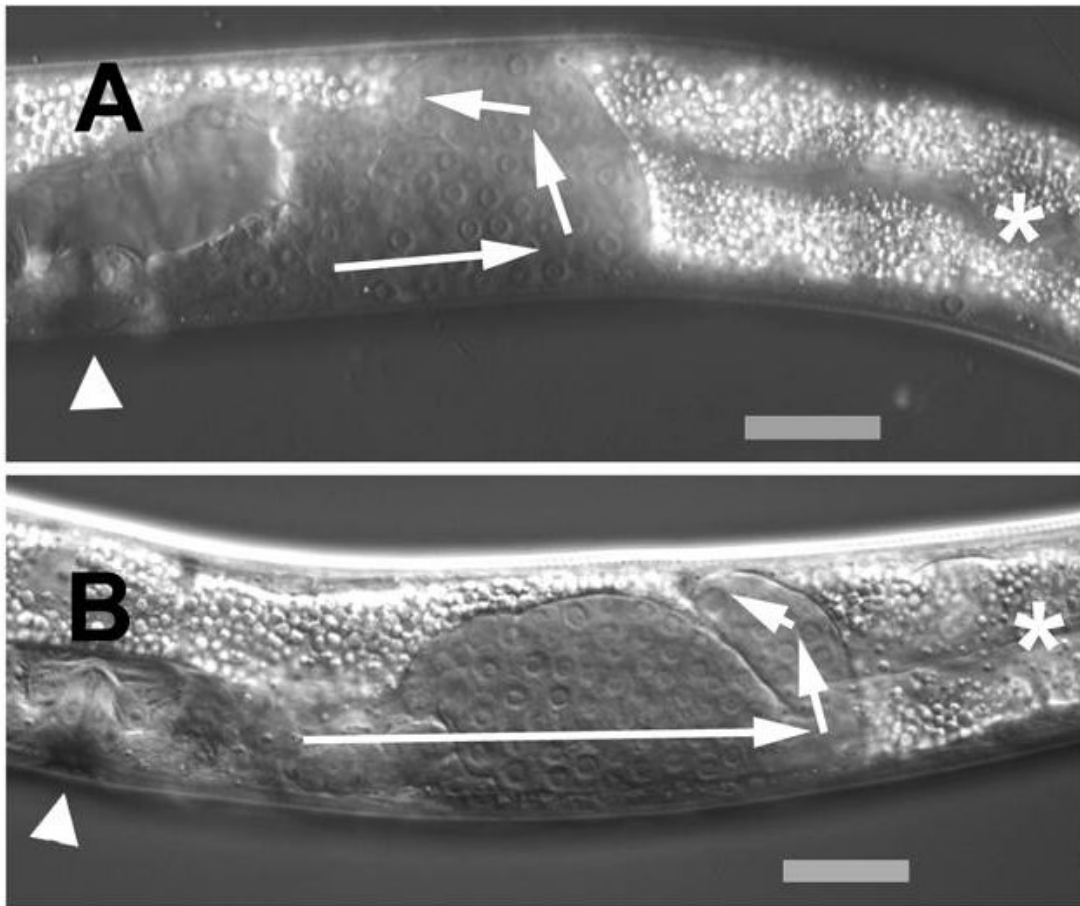


**Figure 12: Basement Membrane matrix Components and Receptors in *C. elegans*.**

A schematic of basement membrane composition showing the major families of conserved basement membrane matrix components and receptors in *C. elegans*. Adapted from Keeley, et al. <sup>2</sup>.

### 1.10 TGF beta

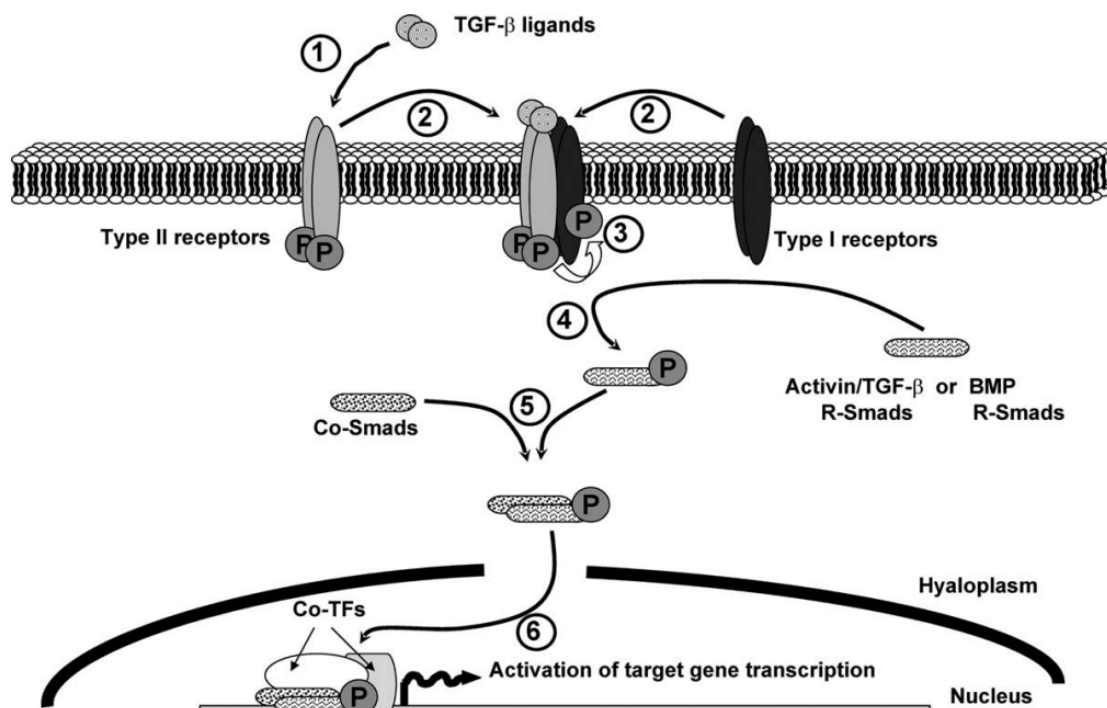
Transforming growth factor beta (TGF- $\beta$ ) superfamily signalling is a network translating signals from more than 30 ligands in humans, orchestrating several essential processes, such as cell proliferation, tissue development, and homeostasis<sup>5,8,52</sup>. Unsurprisingly, dysregulation of TGF- $\beta$  family members is



**Figure 13: Effect of collagen IV and MIG-6L mutant alleles**

Temperature-sensitive collagen IV mutant *emb-9(g23)* cultured at a non-permissive temperature from L2 to L4 larval stages showed slow gonad elongation (B), which is similar to class-I defect of *mig-6(e1931)* (A). Scale bars: 20  $\mu\text{m}$ . Adapted from Kawano, et al.<sup>3</sup>.

commonly implicated in cancer in ways that are still poorly understood<sup>53</sup>. The complexity and widely diversified array of cellular responses generated by this system are partly responsible for the current limited understanding. However, this system has a simple conserved signalling cascade as its core across vertebrates and invertebrates alike (Fig. 14).



**Figure 14: Cell signalling pathway of TGF-β superfamily of ligands.**

(1) TGF-β ligands interact with constitutively phosphorylated type II receptors. (2) Formation of heterotetramers by recruitment of two type I receptors that form a complex with two type II receptors. (3) The type I receptor is transphosphorylated by the type II receptor. (4) This leads to the recruitment and phosphorylation of active receptor-associated Smads (R-Smads). (5) This is followed by dimerization of the now phosphorylated R-Smad with a Co-Smad (6) This dimer can then enter the nucleus and with co-transcription factor (CO-TFs) activate the Transcription of target genes. Adapted from Herpin, et al. <sup>5</sup>.

Many components of the system have been identified in *C. elegans* (Fig. 15), including only two type I and one type II receptor, therefore allowing for only two different combinations: the Dauer TGF-β-related pathway, and the Sma/Mab TGFβ-related pathway (Fig. 16,17) that have both been linked by transcriptome analyses to the regulation of collagen gene expression<sup>54</sup>.

First, the dauer-related TGF-β pathway (Fig. 16) implicates, as its name implies, genes involved in dauer formation. When an L1-L2 *C. elegans* larva encounters unfavourable conditions such as high population density, food shortage or inadequate ambient temperature, it can, instead of becoming an L3, switch to a facultative diapause stage called the dauer larva (Fig. 4), which can survive and wait for a long period for better

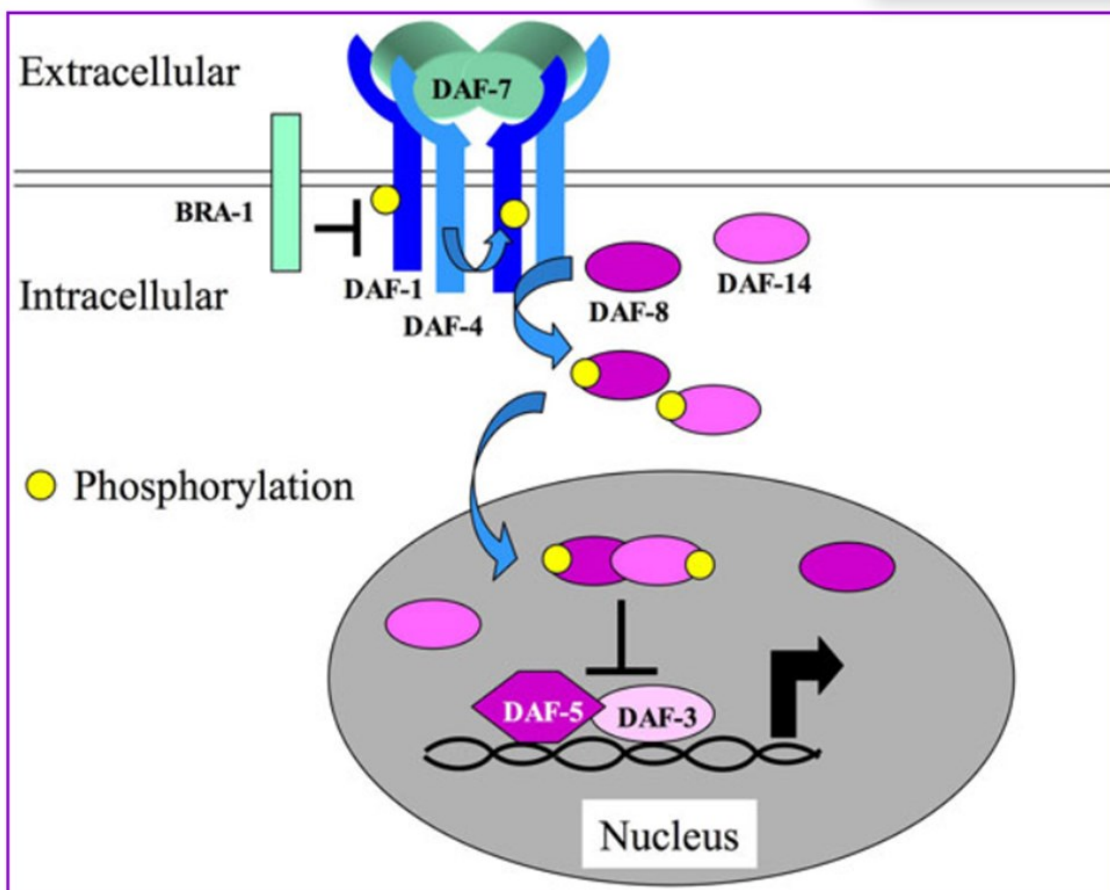
Component	<i>C. elegans</i> gene name	<i>Drosophila</i> gene name	Human gene name	Molecule or family
Ligand	<a href="#">dbl-1</a>	<i>app</i>	BMP5	Transforming Growth Factor- $\beta$
	<a href="#">daf-7</a>	<i>dawdle</i>	GDF11	
	<a href="#">unc-129</a>	-	-	
	<a href="#">tig-2</a>	<i>gbb</i>	BMP8	
	<a href="#">tig-3</a>	dActivin	BMP2	
Type I receptor	<a href="#">sma-6</a>	<i>tkv</i>	BMPRIB	ser/thr kinase receptor
	<a href="#">daf-1</a>	<i>babo</i>	TGF- $\beta$ RI	
Type II receptor	<a href="#">daf-4</a>	<i>put</i>	ACTRIIB	
R-Smad	<a href="#">sma-2</a>	<i>Mad</i>	Smad1	Smad
	<a href="#">sma-3</a>	<i>Mad</i>	Smad5	
	<a href="#">daf-8</a>	<i>Smox</i>	Smad8	
	<a href="#">daf-14</a>	<i>Smox</i>	Smad2	
Co-Smad	<a href="#">sma-4</a>	<i>Medea</i>	Smad4	
	<a href="#">daf-3</a>	<i>Medea</i>	Smad4	
I-Smad	<a href="#">tag-68</a>	<i>Dad</i>	Smad6	
Transcription Factors	<a href="#">sma-9</a>	<i>schurri</i>	Shn1/Shn2/Shn3	
	<a href="#">lin-31</a>	<i>fd96C</i>	FoxB1	HNF3/forkhead family
	<a href="#">mab-31</a>	-	-	
	<a href="#">daf-5</a>	-	Sno/Ski	Proline-rich protein
	<a href="#">daf-12</a>	Hr96	Vitamin D receptor	nuclear hormone receptor
	<a href="#">lon-1</a>	-	-	CRISP PR-protein
Extracellular Regulators	<a href="#">lon-2</a>	Dally, Dally-like	GPC1-GPC6	glypican
	<a href="#">sma-10</a>	kekkon	LRIG	leucine rich and immunoglobulin-like domains protein
	<a href="#">crm-1</a>	CRIM	CRIM/CHRD/chordin	cysteine-rich
	<a href="#">drag-1</a>	-	RGMA, RGMB	repulsive guidance molecule (RGM)
	<a href="#">dat-2</a>	-	-	ADAMTS

**Figure 15 : TGF- $\beta$  superfamily signalling is highly conserved in metazoans.**

Source: Girard, et al. <sup>8</sup>.

conditions<sup>8</sup>. While those genes are involved in dauer formation during larval development, they also have functions in the adult. They can be studied using temperature-sensitive alleles as long as the animals are upshifted in restrictive conditions after the L2 stage from where it is too late to switch to the facultative dauer stage (Fig. 4). In this work, we used mutants of the *daf-7* gene that encode one of the 5 TGF- $\beta$  pathway ligands in *C. elegans* and works in favourable conditions by inhibiting dauer entry<sup>55</sup>. Few have investigated its role in adult worm; interestingly, however, *daf-7* mutants were found to impact LAG-2 levels, making it a gene of interest in our aim to link the basement membrane and Notch signalling together<sup>56</sup>.

Secondly, there is the the Sma/Mab TGF $\beta$ -related pathway (Fig. 17). It is named so as it was first associated with two mutant phenotypes, small body size (Sma) and male



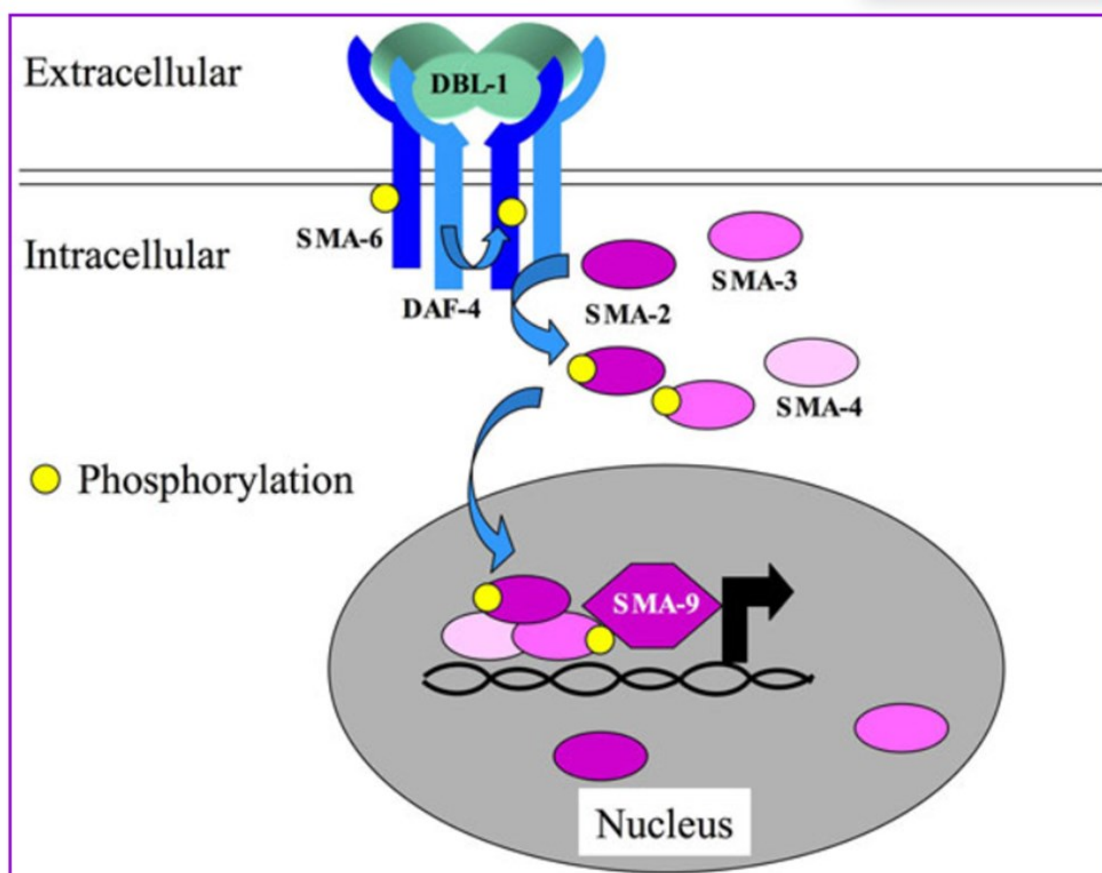
**Figure 16: The Dauer TGF- $\beta$ -related pathway.**

DAF-7 promotes continuous, non-dauer development. The DAF-7 signal is transduced by the DAF-1 type I receptor, DAF-4 type II receptor, and DAF-8 and DAF-14 Smads. These components, when activated, inhibit the functions of DAF-3 Smad and DAF-5 Sno/Ski, which promote Dauer development. BRA-1 is a negative regulator of DAF-1. Girard, et al. <sup>8</sup>.

tail abnormal morphology (Mab)<sup>20,57,58</sup>. Subsequent genetic screening led to the identification of the DBL-1 ligand, a homologue to the vertebrate bone morphogenic proteins (BMPs)<sup>59,60</sup>. In vertebrates, BMP refers to a family of ligands involved in various processes during embryonic development and adult homeostasis<sup>61</sup>. For example, BMP-2,3 are involved in bone and cartilage formation<sup>61-63</sup> while administration of exogenous BMP-7 to mice was shown to have a positive effect on chronic renal fibrosis models<sup>64</sup>. In *C. elegans*, the DBL-1 ligand works in a dose-dependent manner, with its downstream effectors regulating body size<sup>59</sup>. Overexpression of DBL-1 leads to long (lon) phenotype while loss of function mutants leads to the opposite small (sma) phenotype<sup>59,65</sup>. It does so through transcriptional regulation of cuticle collagen genes<sup>66</sup>.



LON-2 is an extracellular regulator of the Sma/Mab TGF $\beta$ -related pathway that sequesters the DBL-1 ligand, which prevents its binding to its type two receptor<sup>67</sup>. Therefore, the loss of LON-2 function results in a phenotype like DBL-1 overexpression. In this study, we used a mutant allele of *lon-2* to overactivate DBL-1 signalling, as it could hypothetically lead to an increase of COL IV levels in the gonad basement membrane, just as it does for cuticle collagens.

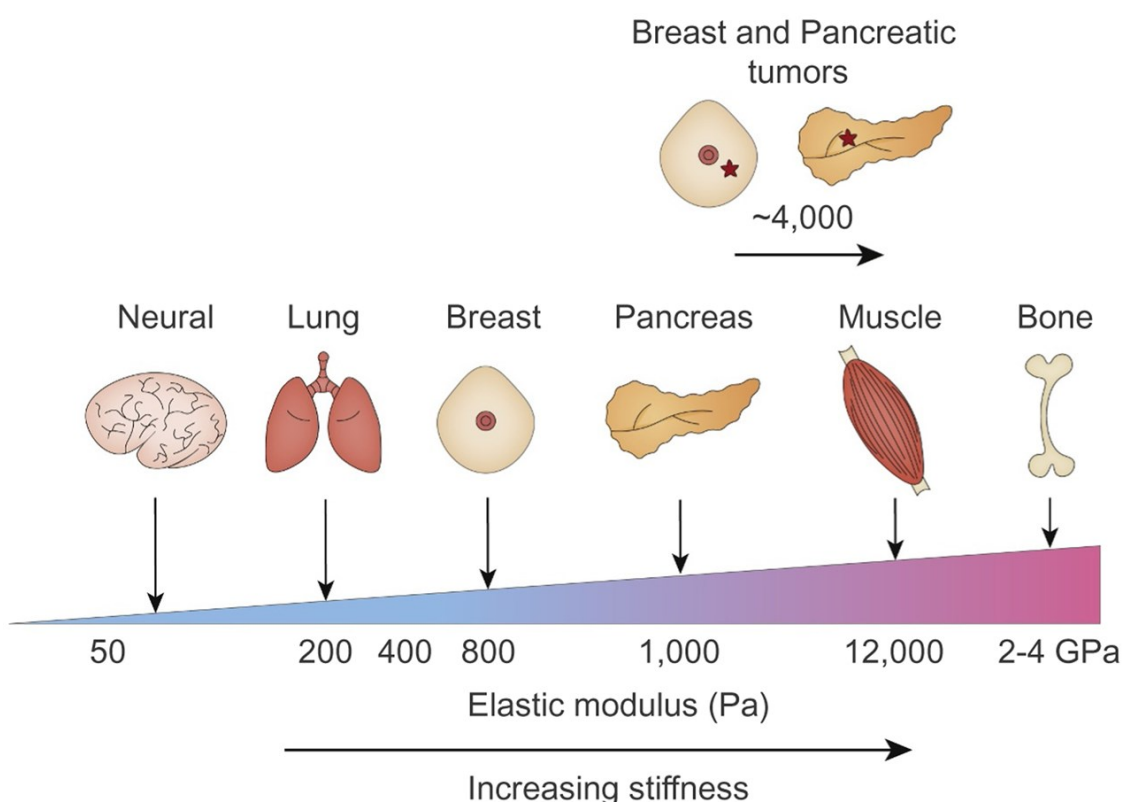


**Figure 17: The Sma/Mab TGF $\beta$ -related pathway.**

DBL-1 regulates body size and male tail morphogenesis. The DBL-1 signal is transduced by SMA-6 type I receptor, DAF-4 type II receptor, SMA-2, SMA-3, and SMA-4 Smads, and SMA-9 Schnurri. Source: Girard, et al. <sup>8</sup>.

### 1.11 Interaction between the basement membrane and SC

How can we establish a connection between *mig-6* and *glp-1*? Could the basement membrane composition affect the regulation of SCs? Since MIG-6 has been suggested as regulating the localization of ADAMTS and is thought to be important for the assembly and removal of COL IV during the BM expansion<sup>2,3</sup>. Alterations in the basement membrane likely occur in the *mig-6(qz2)* mutant, as COL IV assembly is no longer properly downregulated, this mutant may have an increase in COL IV abundance. COL IV is the primary structural component of the basement membrane, and an increase in its concentration has been shown to provoke a stiffening of the basement membrane<sup>68</sup>. An abnormal increase in basement membrane stiffness is a phenomenon commonly called fibrosis, a hallmark observed in various diseases, notably cancer<sup>4,69</sup>. Tumours are indeed often surrounded by a stiffer basement membrane compared to their healthy host tissue (Fig. 18). To our knowledge, there are no instances of a solid tumour with an overall reduced surrounding basement



**Figure 18: Basement membrane surrounding tumours are stiffer**

Different tissues serve different functions and have different basement membrane stiffnesses. Here we graphically depict breast and pancreatic tumours that both have increased stiffness when compared to their healthy counterpart, 4000 Pa vs 800 Pa and 1000 Pa, respectively. Adapted from <sup>4</sup>

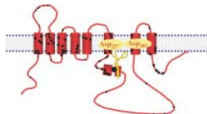

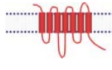

membrane stiffness compared to the healthy tissue. Upregulation of Notch signalling is also a hallmark of cancer and is seen in the literature as one of the causes of fibrosis<sup>28,70</sup>.

For examples, inhibition of Notch activity was shown to attenuate fibrosis in rat peritoneal and hepatic tissues<sup>71,72</sup>. Notch is also described as a pro-fibrotic regulator in the epidermis and kidneys<sup>73,74</sup>. However, all cited examples have one thing in common: the use of gamma-secretase inhibitors as a means to shut down Notch activity.

### 1.12 Inhibitors of gamma-secretase

The gamma-secretase is a protein complex consisting of four essential subunits, presenilin (PS), nicastrin, anterior pharynx defective 1 (APH1), and presenilin enhancer 2 (PEN2), responsible for the cleavage of multiple proteins transmembrane domain<sup>7</sup> (Fig. 19).

Out of the four subunits, only the presenilin was shown to have a catalytic domain responsible for the complex activity<sup>7,75</sup>. Gamma-secretase inhibitors have long been

Name (Generic)	<i>C. elegans</i>	Mammalian	Functions	
Presenilin		HOP-1, SEL-12 (PSEN in <i>Drosophila</i> )	PS1, PS2	Catalytic subunit and assembly of $\gamma$ -secretase (glycosylation of Nct, Pen-2 expression); $\beta$ -catenin phosphorylation
Nicastrin		APH-2	Nct	Assembly of $\gamma$ -secretase (stabilization of PS, Pen-2)
Aph-1		APH-1 (PEN-1)	Aph1aL and Aph1aS; Aph1b (Aph1c in rodents)	Assembly of $\gamma$ -secretase (stabilization of PS/Nct)
Pen-2		PEN-2	Pen-2	Assembly of $\gamma$ -secretase (proteolytic processing PS)

**Figure 19: The gamma-Secretase Complex Members**

Source: De Strooper <sup>7</sup>.

exploited as inhibitors of Notch activity as its activity is required for the release of the NICD<sup>72,76,77</sup>. The issue is that gamma-secretase is not specific to Notch signalling and has, at the very least, 90 additional substrates<sup>78,79</sup>, including components of the TGF- $\beta$  signalling pathway<sup>80</sup>. For example, betaglycan, also known as TGF- $\beta$  type III receptor, is an accessory receptor that facilitates TGF- $\beta$ 1 ligand binding to the type II

receptor, which generally promotes fibrosis<sup>81,82</sup>. Additionally, betaglycan possesses an intracellular domain that is released in the cytoplasm as a result of gamma-secretase activity and plays a yet-to-be fully described function in further regulation of TGF- $\beta$ 1 activity<sup>83,84</sup>.

Another example would be the role involvement of gamma-secretase with RPTP, LAR, EpCAM, and E-cadherin, all playing roles in cell adhesion but additionally being involved in  $\beta$ -catenin activity whose upregulation is linked to fibrosis, probably downstream of TGF- $\beta$ 1<sup>80,85,86</sup>. This quick examination of only 5 out of the 90 potential gamma secretase substrates highlights the possible bias when trying to link fibrosis to Notch activation when using gamma-secretase inhibitors.

## Chapter II

### Objectives and preliminary results

#### 2.1 Research objectives

Despite not being implicated in a homeostatic regulation process, *mig-6(qz2)* genetically interacted with *glp-1(ar202)*, leading to increased tumour formation. Consequently, the focus of this study shifted toward identifying how exactly this novel allele of *mig-6L* promoted Notch signalling. Completing the related objectives stated below led to the article presented in the second chapter of this thesis.

##### 2.1.1 Objective 1: Defining the impact of the *mig-6(qz2)* mutation.

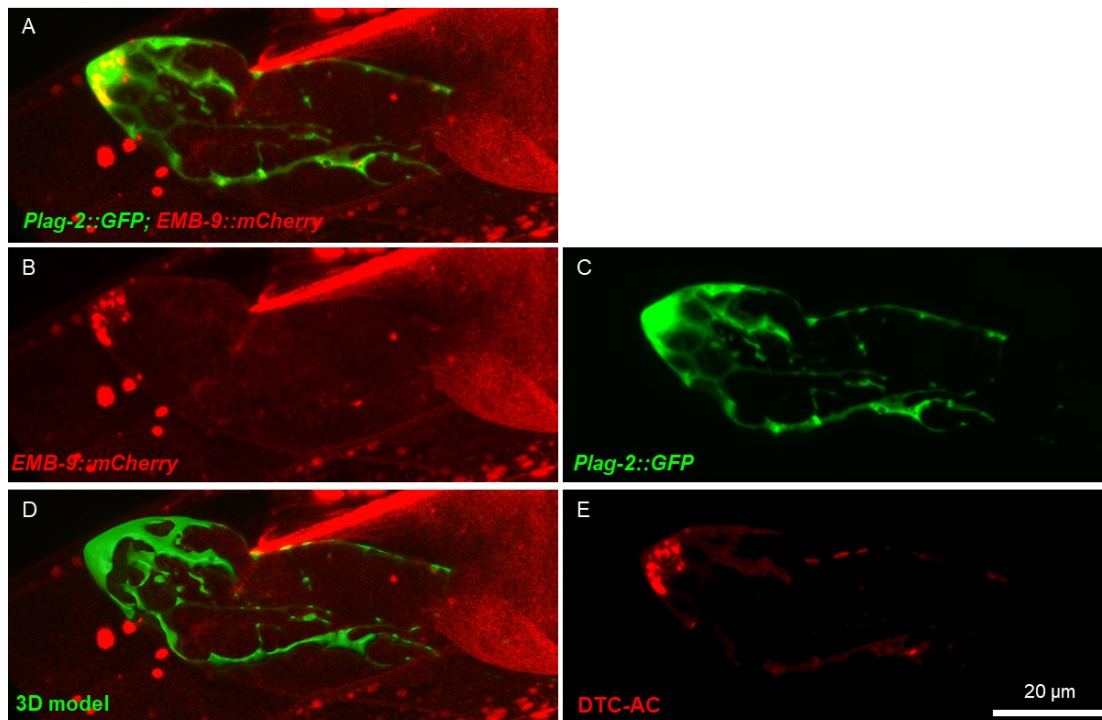
First, we needed to carefully define the impact of the novel *mig-6(qz2)* allele on the animal, given that, to our knowledge, it was the first of its kind to be fertile for *mig-6L*. Before we dwell on the intricacies of its interaction with Notch signalling, multiple observations needed to be made on the single mutant. We quantified the reduction of gonad elongation that we could visually appreciate (Fig. 11). This was done by simple 4',6-diamidino-2-phenylindole (DAPI) staining and measurements of the gonad following microscopic image acquisition. While our preliminary results propose an absence of tumour formation in the *mig-6(qz2)* single mutants, we stained additional animals to confirm. Then, we assessed the animal brood size and the viability of its offspring, a standard, well-documented procedure in *C. elegans*<sup>87</sup>.

##### 2.1.2 Objective 1.1: Defining the nature of the interaction between *mig-6* and *glp-1*.

As we suspected an interaction between *mig-6* and *glp-1*, we made the same observations described in objective 1 on wild type, then *glp-1* single mutants and finally *glp-1; mig-6* double mutant animals, all at the same permissive temperature of 15°C. Doing so allowed us to compare the impact of the single mutation alone or combined and determine that *mig-6(qz2)* was genetically interacting with *glp-1(ar202)*. Indeed, the two mutations synergistically increased both larval and embryonic lethality and caused severe tumour formation in the double mutant.

### 2.1.3 Objective 1.2: Defining the impact of *mig-6(qz2)* on collagen IV levels.

Since MIG-6 short isoform was shown to negatively regulate COL IV levels, we next asked if the ability of *mig-6(qz2)* to negatively regulate COLV was also altered as the mutation specifically affect the long isoform. To test this, we generated a strain bearing two fluorescent markers by a genetic cross (Fig. 20A-C). One expressed the GFP under the control of the *lag-2* promoter, therefore highlighting the position of the DTC, where it is expressed, in green. The other was a single insertion of a mCherry tagged copy of the orthologue of the human COL IV  $\alpha$ 1 chain, EMB-9 in *C. elegans*. Using a confocal microscope, we acquired fluorescent Z-stacks and transferred them to Imaris, an advanced microscopy image processing software. Since the *mig-6(qz2)* allele specifically affects the gene long isoform expressed by the DTC, we focussed on the COL IV closely localised to this structure. To do so, we used Imaris to generate 3D DTC models based on the green channel (Fig. 20D). This allowed us to obtain only the collagen signal overlapping with this model (Fig. 20E), which we refer to as DTC associated collagen (DTC-AC) thus enabling us to compare their abundance between different strains.

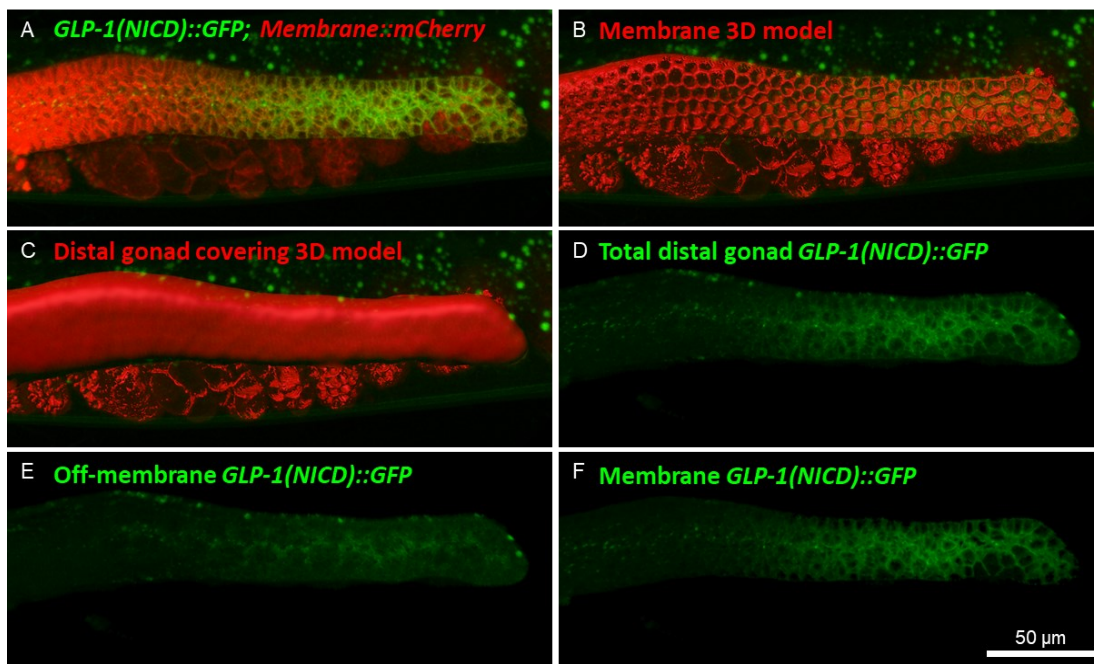


**Figure 20: COL IV quantification workflow**

(A) Representative Imaris's 3D view of a control worm DTC region with both red and green channel (B) red channel only (C) green channel only (D) Imaris 3D model overlapping with the *Plag-2::GFP* signal (E) DTC-AC obtained from the deletion of all the red signal outside the 3D model shown in D.

### **2.1.4 Objective 1.3: Define whether reduced *mig-6l* function improves Notch signalling.**

As the interaction between *mig-6(qz2)* and *glp-1(ar202)* led to tumour formation, we suspected that Notch signalling might be enhanced in *mig-6(qz2)* mutants. To test this, we used two different techniques. For the first, we will refer to as the "Cleaving assay", we generated a strain bearing two fluorescent markers by a genetic cross (Fig. 21A). One expressed a membrane-bound TAGRFPT fluorescent protein in the germline, effectively marking all the GSC and their differentiated cells in red (Fig. 21). The other was a C-Term tagged copy of GLP-1, effectively allowing for the Notch intracellular domain (NICD) to be tracked in green (Fig. 21,22). Just like in objective 1.2, we used a confocal microscope to acquire fluorescent Z-stacks we transferred to Imaris. This time, we generated 3D models covering the cell membrane and the distal gonad as a whole (Fig. 21B-C), allowing us to obtain the signal localising to the GSC membrane versus their cytoplasm (Fig. 21D-F).



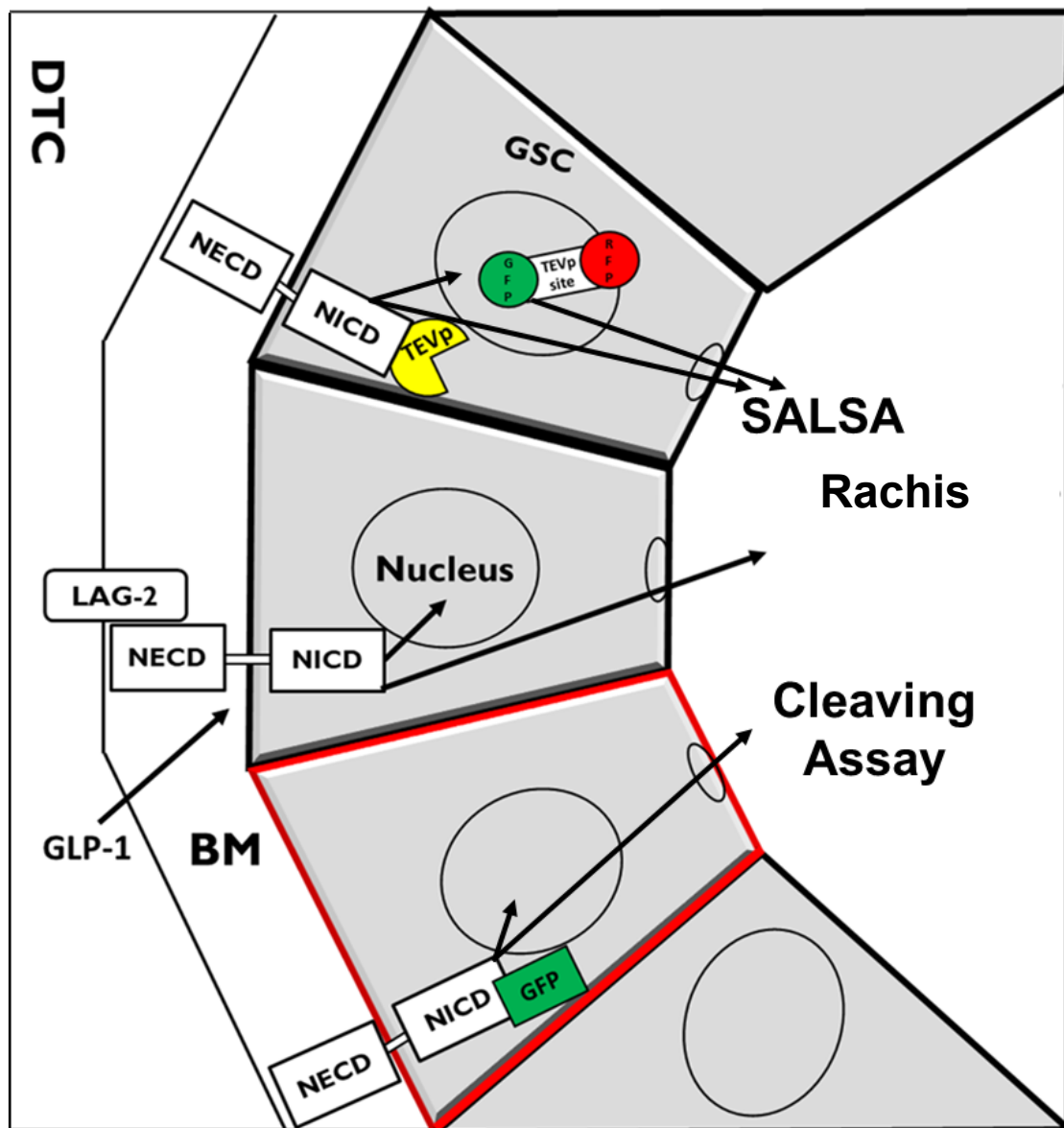
**Figure 21 : Cleaving assay workflow**

(A) Representative Imaris 3D view of a control worm distal gonad region with both red and green channel (B) Imaris 3D model overlapping with the GSC membranes (C) Imaris 3D model encompassing the distal gonad as a whole (D) New channel obtained from the deletion of all the green signal outside the red 3D model shown in C (E) New channel obtained from the deletion from the channel in D of all the green signal inside the red 3D model shown in B (F) New channel obtained from the deletion from the channel in D of all the green signal outside the red 3D model shown in B.

### **2.1.5 Objective 1.4: using the SALSA sensor to define Notch activity more precisely.**

The second Notch activity assessment technique made use of a recent biosensor developed by the Greenwald lab, the Sensor able to detect lateral signalling (SALSA)<sup>88</sup>. Compared to the cleaving assay that allowed for a global evaluation of Notch activity in the distal gonad, SALSA allowed us to assess the Notch activity of single nuclei (Fig. 22,23).



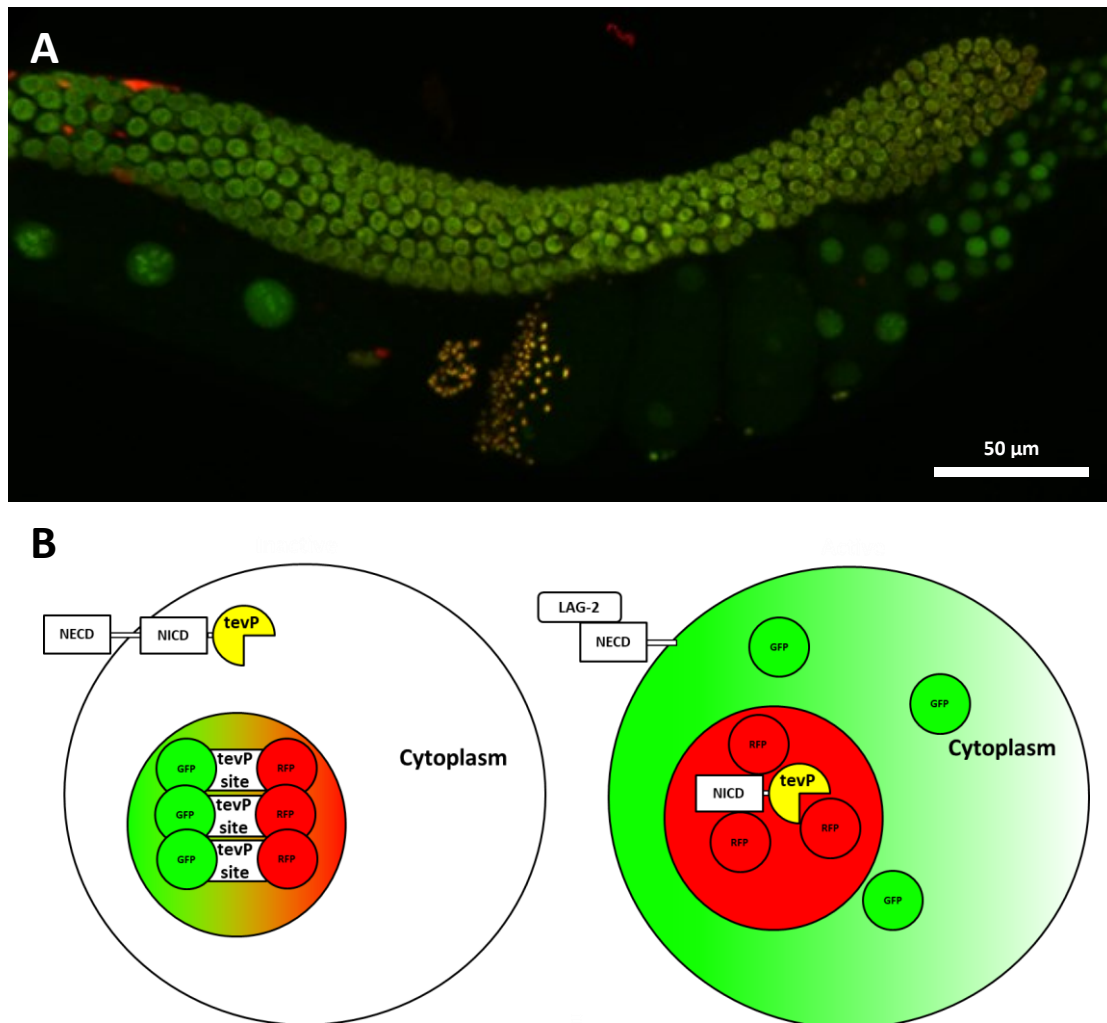


**Figure 22: Graphical representation of the two techniques used to assess Notch activity.**

For objective 1.3, cleaving assay: The NICD is tagged with GFP. Upon activation, the NICD is cleaved and freed into the GSC cytoplasm, from where it can enter the nucleus or their shared cytoplasm, the Rachis. Therefore, we can assess Notch activity based on the GFP localisation at the membrane(inactive) or in the nucleus and cytoplasm(active). As they all share their cytoplasmic content, it allows for the evaluation of Notch activity as a whole since the GFP present in the rachis can come from any cell as opposed to the more recent and precise SALSA sensor that allow for Notch activity assessment in individual nucleus.

For objective 1.4, SALSA assay, as explained in Figure 23, Notch activity allows for the release in the cytoplasm of the GFP from the nucleus tethered RFP. This allows us to obtain precise data for every individual nucleus since we observe an RFP/GFP ratio in the nucleus.

the evaluation of Notch activity as a whole since the GFP present in the rachis can come from any cell.



**Figure 23: SALSA sensor explanation**

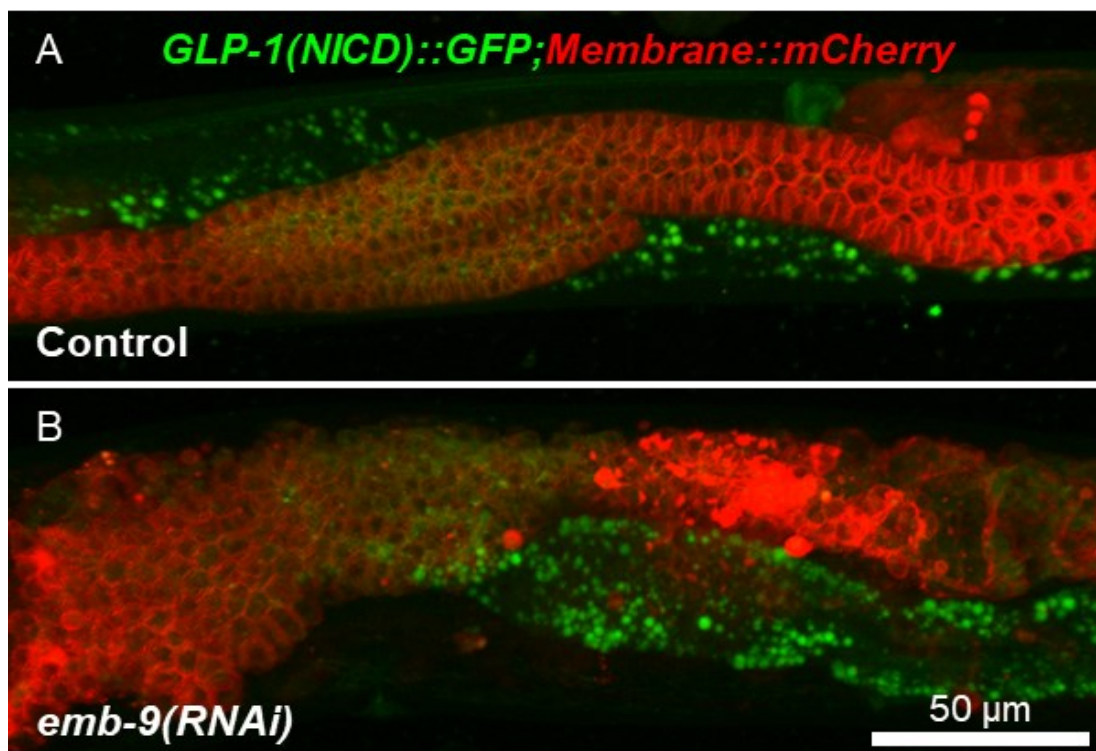
(A) Representative Imaris's 3D view of a control SALSA worm in which every germline cell expresses nuclear RFP and GFP (B) Graphical representation of the SALSA sensor workings. An RFP is tethered to an H2B histone and therefore localizes inside the GSC nucleus. A GFP is tethered to the RFP by a linker containing a tobacco etch virus protease (teVP) site. On the endogenous *glp-1*, they added a teVP. When Notch is inactive, and the NICD is at the membrane, there are equal quantities of RFP and GFP in the nucleus. When LAG-2 binds to the NECD, the NICD is released and can translocate to the nucleus, where it cleaves the teVP site, effectively allowing the GFP to diffuse outside the nucleus. To Assess Notch activity, we calculated the RFP/GFP ratio in each individual nucleus.

### 2.1.6 Objective 2: does collagen deposition correlate with Notch activity in *C. elegans*?

As fibrosis and Notch signalling are both hallmarks of cancer and Notch is seen as causing fibrosis, we asked if we could use the results from Objective 1 to detect a correlation between Notch activity and COL IV abundance.

### 2.1.7 Objective 2.1: Does a decrease of collagen levels cause a reduction in Notch activity?

As the *mig-6(qz2)* mutants seemingly caused an increase in Notch activity by increasing collagen levels, we asked if reducing collagen levels would, in turn, reduce Notch activity. First, to test this, we used RNAi to selectively silence *emb-9*. However, the effect proved to be too strong as without *emb-9* expression, the basement membrane ruptured during development (Fig. 24). Therefore, we used a temperature-sensitive allele of *let-2*, the ortholog of the human COL IV 2 chain that, at restrictive temperature, would prevent the assembly of the COL IV heterotrimer.



**Figure 24: Silencing of *emb-9* expression by RNAi causes gonad rupture.**

(A) Representative Imaris 3D view of a control adult two gonad arms. (B) Representative Imaris 3D view of a worm subjected to *emb-9(RNAi)* by raising them on *emb-9* dsRNA expressing bacteria, which caused the gene silencing and gonad basement membrane rupture.

### 2.1.8 Objective 2.2: How will other collagen-affecting mutations affect Notch activity?

It is possible that *mig-6(qz2)* was altering Notch activity in another way apart from its impact on COL IV levels. Therefore, we asked how other genes that are known to increase collagen levels would affect Notch signalling. To test this, we chose a *lon-2* mutant that was known to upregulate TGF- $\beta$  signalling, leading to increased collagen

synthesis<sup>62,89</sup>. Using the same methodology as objectives 1.2 and 1.3, we assessed the impact of this *lon-2* mutant on both COL IV levels and Notch activity.

### **2.1.9 Objective 3: Determine whether collagen IV regulates notch activity or Notch activity regulates collagen IV.**

While the literature seems to support the idea that fibrosis is a consequence of Notch signalling, it was strange that a basement membrane mutation that would potentially increase collagen levels resulted in what was probably an increase in Notch signalling. Therefore, we performed two experiments to shed light on this irregularity using the same methodology as in objective 1.2.

### **2.1.10 Objective 3.1: How will a decrease in the expression of LAG-2, the Notch ligand, impact collagen IV?**

At first, we had used a mutant allele of *daf-7* to alter collagen levels. However, we found that the allele we used was also reported to be reducing LAG-2 levels<sup>56</sup>. After confirming this reduction, we aimed to evaluate the impact of the resulting lowered Notch activity on COL IV levels. Sadly, no conditional allele of *lag-2* was available or had the phenotype needed for this test.

### **2.1.11 Objective 3.2: How will changes in Notch receptor-dependent activity impact COL IV?**

We next aimed to assess the changes on COL IV resulting from the alteration of Notch activity by using the mutant allele of the Notch receptor, GLP-1. We first used the already described *glp-1(ar202)* that caused constitutive activation of Notch signalling. Secondly, we used another temperature-sensitive allele, *glp-1(e2141)*. This allele is a conditional mutation that led to the receptor's complete loss of function at the restrictive temperature of 25°C, effectively reducing Notch activity to zero and leading to the loss of the germline as every SC will differentiate.

## Submitted manuscript.

### Niche-associated Type IV collagen promotes GLP-1/Notch receptor activation in the *C. elegans* germline

Pier-Olivier Martel<sup>1,3</sup>, Julia Degrémont<sup>2</sup>, Sarah Turmel-Couture<sup>1,3</sup>, Eden Dologuele<sup>1,3</sup>, Lucie Beaulieu<sup>1,3</sup>, Alexandre Clouet<sup>1,3</sup> & Patrick Narbonne<sup>1,3\*</sup>

<sup>1</sup> Département de Biologie Médicale, Université du Québec à Trois-Rivières, Québec, Canada.

<sup>2</sup> Département de Pathologie et Biologie Cellulaire, Institut de Recherche en Immunologie et en Cancérologie (IRIC), Université de Montréal, Montréal, Québec, Canada.

<sup>3</sup> Groupe de Recherche en Signalisation Cellulaire, Université du Québec à Trois-Rivières, Québec, Canada

\* Correspondence should be addressed to: patrick.narbonne@uqtr.ca

#### Abstract

Basement membranes are thin and dense proteinaceous layers of specialized extracellular matrix that surround tissues to maintain their structure and function<sup>90</sup>. With age, chronic inflammation typically stiffens this basement membrane in a phenomenon called fibrosis, the progression of which is reflected by increasing levels of the basement membrane's main component, type IV collagen (COL IV)<sup>69,91</sup>. Tissue fibrosis and elevated Notch signaling are two co-occurring hallmarks of many inflammation-linked diseases, including cancer<sup>4,69,92,93</sup>. Many reasoned that fibrosis may be a consequence of elevated Notch signaling, a belief that has led to Notch targeting antifibrotic therapy attempts<sup>70,72,94</sup>. Yet, the *in vivo* relationship between Notch activity and fibrosis has not been clearly defined. Here, we show that accumulation of EMB-9/COL IV associated to the *C. elegans* germline stem cell niche promotes GLP-1/Notch receptor activation in germline stem cells. Increased Notch activity is therefore a consequence of high basement membrane COL IV contents. Moreover, we find that reducing GLP-1/Notch activity *in vivo* leads to a generalized dramatic increase in EMB-9/COL IV levels, and thereby promotes fibrosis. The generalized fibrosis that comes along with inflammaging may therefore act as a root cause for cancer by promoting Notch signaling, and perhaps more widely, many other ligand-receptor interactions.

## Main

Fibrosis increases with age and promotes cancer by stiffening basement membranes, altering several biophysical cues that impact on the phenotype, differentiation, and growth/proliferation of neighboring cells<sup>95,96</sup>. Whether it is in skin, liver, kidney, lung or breast cancer, the fibrotic state of the tissue is often accompanied by increased Notch signaling<sup>70,97</sup>, an evolutionarily conserved pathway that plays an important role in development and homeostasis<sup>98</sup>. Hence, Notch signaling inhibition has been investigated as a potential therapy for the treatment of fibrosis-related pathologies<sup>70,72,94</sup>. However, such strategies have led to conflicting results and overall fail to meet expectations<sup>93,99,100,101</sup>, potentially due to the use of unspecific Notch receptor targeting drugs, such as gamma secretase inhibitors<sup>78,79</sup>, and/or *in vitro* models. We therefore aimed to better define the *in vivo* relationship between Notch signaling and fibrosis, two major actors in cancer, using the genetically tractable *C. elegans* model.

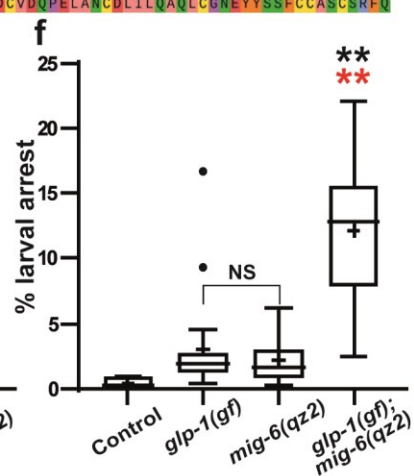
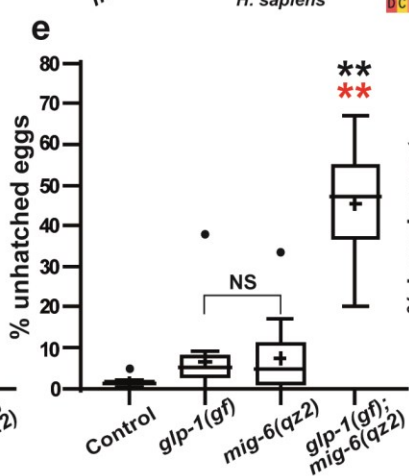
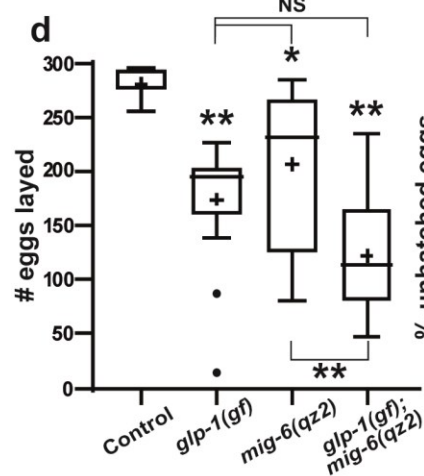
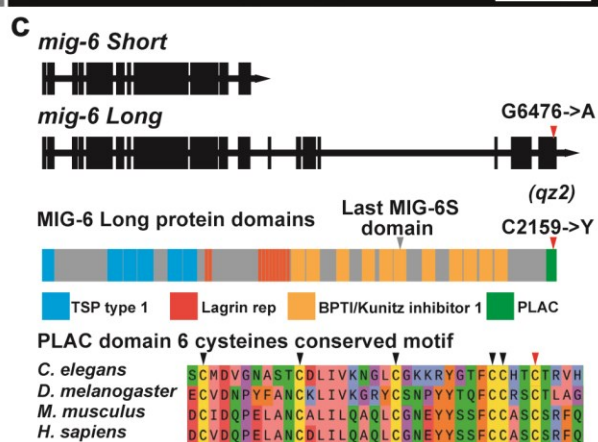
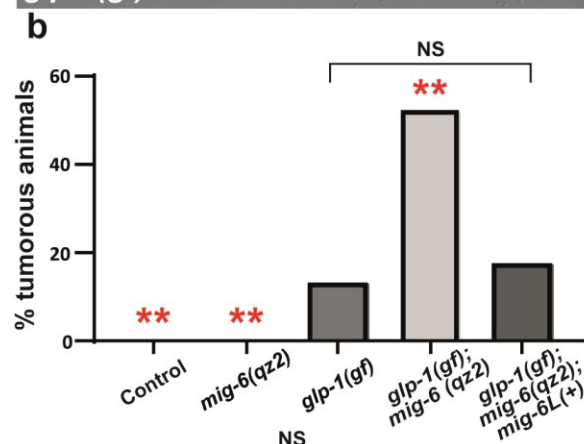
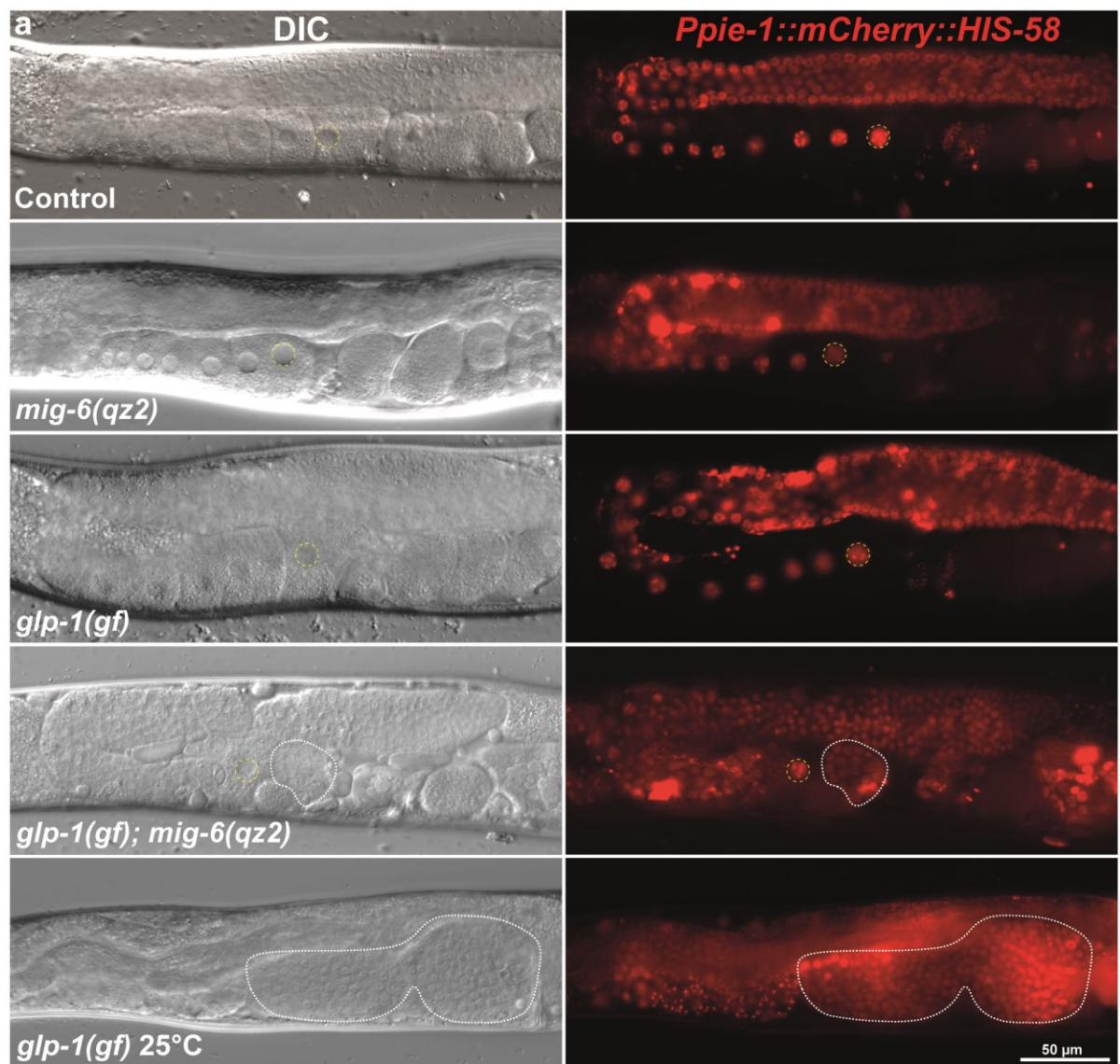
### A basement membrane glycoprotein synergistically interacts with *glp-1*/Notch

In *C. elegans*, the Notch ligand LAG-2 is expressed by the distal tip cells (DTCs) and binds to the Notch receptor GLP-1 at the surface of adjacent germline stem cells (GSC)<sup>3,102</sup>. This releases the Notch intracellular domain (NICD), allowing its translocation to the nucleus where it promotes expression of the *lst-1* and *sygl-1* stemness genes, and acts as the niche signal allowing GSCs to proliferate<sup>25,30,103,104</sup>.

To identify new regulators of GSC proliferation, we used ethyl methane sulfonate (EMS) to mutagenize a mutant strain carrying a conditional *glp-1* gain-of-function (*gf*) allele, which causes the formation of undifferentiated benign germline tumours under restrictive conditions<sup>105-107</sup>. We screened for *glp-1(gf)* enhancers that would cause the formation of germline tumours even under permissive conditions, and isolated a novel allele of the *mig-6L* gene, coding for the long isoform of the *C. elegans* Papilin homolog (Fig.1a,b). MIG-6L has mainly been implicated in the regulation of DTC migration<sup>3</sup>, while this new *mig-6L(qz2)* allele specifically affects its C-terminal protease and lacunin (PLAC) domain via a typical EMS-induced G/C to A/T transition that replaces the last cysteine within the highly conserved six-cysteine region by a tyrosine (Fig.1c)<sup>108</sup>. We confirmed that this was the causal mutation by transformation-rescue (Fig.1b and Extended Data Fig.1a,b). Papilin is a highly conserved basement membrane protein that negatively regulates procollagen peptidases, thus acting to reduce collagen levels<sup>2</sup>. The *mig-6L(qz2)* allele was removed from the *glp-1(gf)* background and outcrossed 4 times prior to all subsequent analyses. Since the *qz2* allele specifically disrupts MIG-6L's PLAC domain, its phenotype informs on the function of this poorly characterized domain.

Single *mig-6L(qz2)* mutants did not develop any tumours (Fig.1a,b) but had a mild phase III DTC migration defect, where the final elongation of the gonad arms was reduced by roughly 25% (Extended Data Fig.1b,c), and a slightly reduced brood size (Fig.1d). In contrast, all three phases of DTC migration are severely impacted in *mig-6L(∅)* mutants, such that these animals are completely sterile<sup>3</sup>, indicating that *mig-6L(qz2)* is hypomorphic. The reduced brood size of *mig-6L(qz2)* animals was similar to that of *glp-1(gf)* single mutants grown under permissive conditions, yet the double *glp-1(gf); mig-6L(qz2)* laid even fewer eggs, the numbers being consistent with each mutation having an additive effect on egg production (Fig.1d). There however was a synergistic effect between *mig-6L(qz2)* and *glp-1(gf)* on embryonic and larval lethality. Namely, the double mutants showed more than three times the embryonic lethality,

and more than twice the larval lethality than what would have been expected from additive effects (Fig.1e,f). We conclude that *mig-6L*, through its PLAC domain, interacts synergistically with *glp-1* during embryonic and larval development, in addition to within the context of GSC niche signaling, and acts to restrict *glp-1*/Notch signaling.





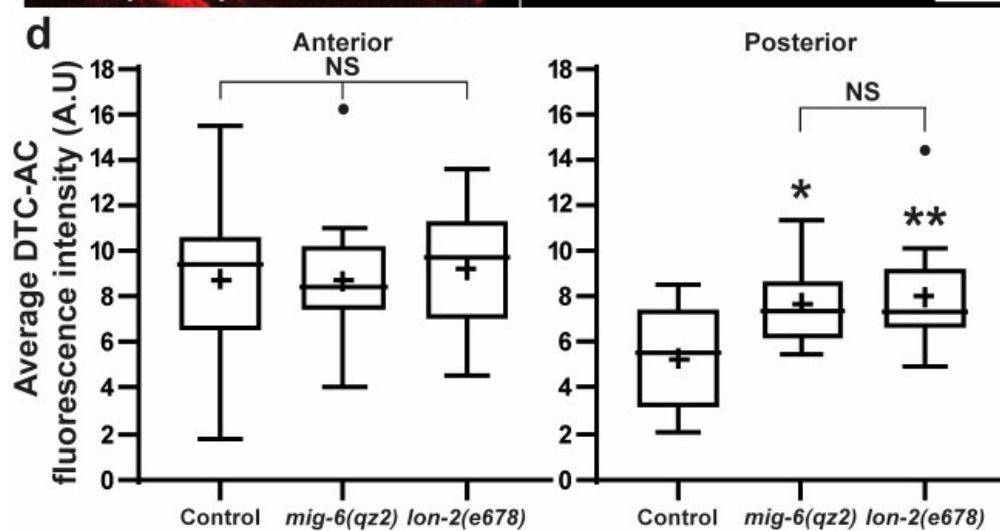
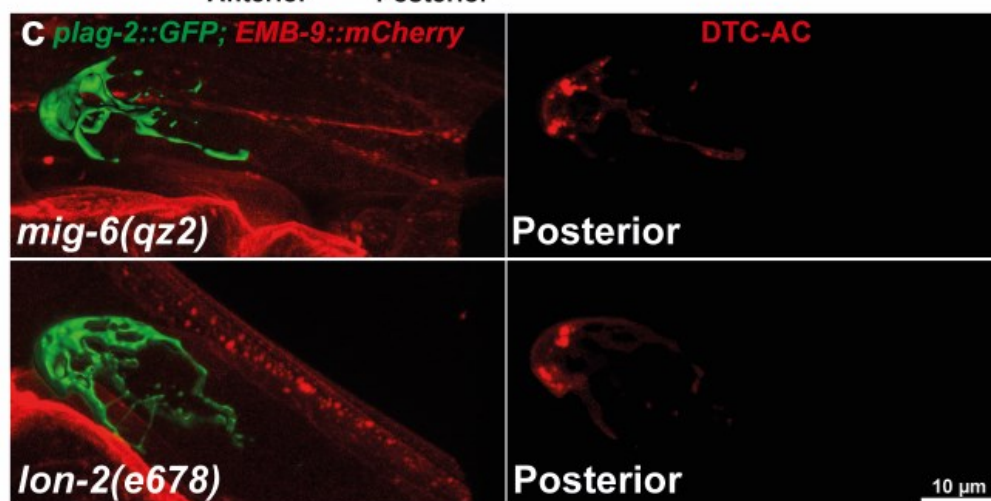
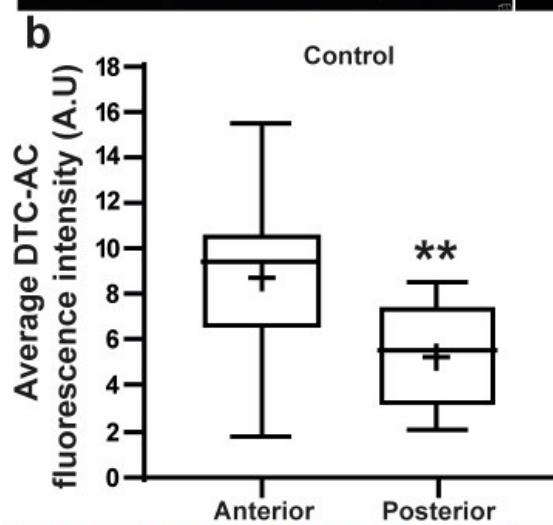
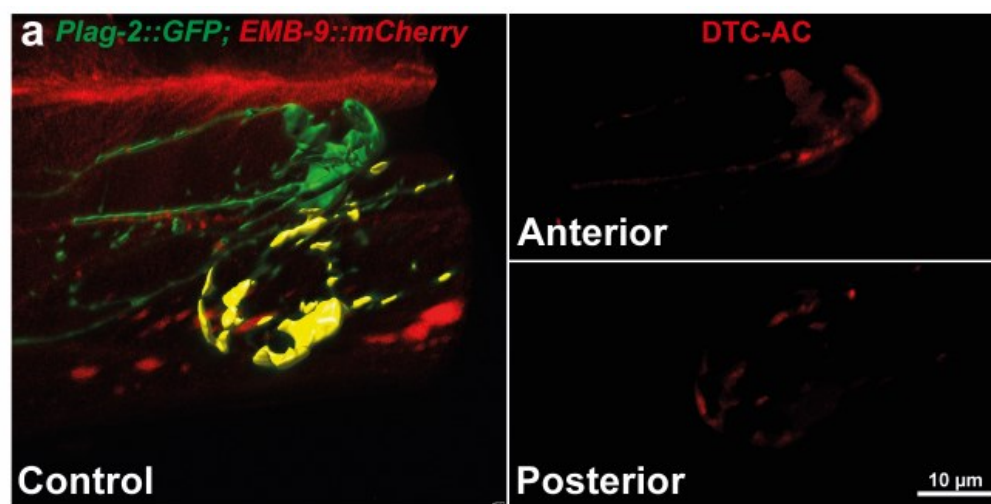
**Figure 1. Synergistic interaction between MIG-6L/Papilin and GLP-1/Notch.** (a) Representative DIC (left) and fluorescence micrographs (right) showing adult (mid L4 +72h) hermaphrodite germlines of the indicated genotypes, raised at 15°C (a permissive temperature for *glp-1(gf)*<sup>105</sup>, except for the bottom panel, which shows a *glp-1(gf)* hermaphrodite that was upshifted to the restrictive temperature of 25°C at the late-L4 stage for 24 hours. Yellow dashed circles highlight the proximal-most (-1) oocyte nuclei (absent in *glp-1(gf)* at 25°C). White dotted lines delineate proximal undifferentiated germline tumours. (b) Quantification of proximal germline tumour formation (mid L4 +72h, 15°C). Three independent replicates were pooled together. For the transgenic rescue, *glp-1(gf); mig-6(qz2); mig-6L(+)* animals carried the *qzEx4[mig-6L(+); Pmyo-3::mCherry]* transgene (see Methods). Sample sizes, from left to right: 52, 54, 75, 98, 53. (c) Top: DNA structure of the *mig-6* short (*mig-6S*) and *mig-6L* isoforms. Exons are depicted as thicker sections, and introns, thinner. Middle: simplified MIG-6L protein domains (Uniprot)<sup>109</sup>, grey sections represent unconserved regions. Red arrowheads show the G6476A; C2159Y, *qz2* substitution in the C-term PLAC domain found only in the MIG-6L isoform. Bottom: alignment showing where this substitution (red arrowhead) lies in the conserved PLAC six cysteine (arrowheads) motif. (d-f) Boxplots showing (d) the number of eggs laid, (e) embryonic and (f) larval lethality of animals of the indicated genotypes (15°C). Data from independent replicates were pooled. Sample sizes, from left to right: (d) 14, 19, 16, 24, (e,f) 8, 19, 16, 24. (a,b,d-f) The *glp-1(gf)* allele is *ar202*<sup>105</sup>. Asterisks (\*) mark significant differences versus the control (black) or versus any other samples (red). One asterisk, (p<0.05); two asterisks, (p<0.01) by (b) Fisher's exact test or (d-f) Kruskal-Wallis with Dunn's multiple comparisons test. NS, Not significant.

#### MIG-6L limits collagen accumulation at the DTC-GSC interface

Reduced function of MIG-6S, a widely-expressed shorter MIG-6 isoform that lacks the PLAC domain<sup>3,44</sup>, was reported to broadly increase type IV collagen (COL IV) levels across the animal<sup>2</sup>. MIG-6L is however specifically secreted by the DTC<sup>3</sup>, a pattern that is unaffected in *qz2* mutants (Extended Data Fig.1d). We therefore asked whether *mig-6L(qz2)* affected COL IV deposition around the DTC. We used an established *EMB-9::mCherry* marker<sup>110</sup> to visualize and quantify the COL IV  $\alpha$ 1 chain, and the *Plag-2::GFP* reporter<sup>111</sup> to mark the DTC. We imaged the anterior and posterior DTCs of control and *mig-6(qz2)* animals to create tri-dimensional (3D) DTC models based on the green fluorescent signal (Fig.2a). We did not detect any differences in *Plag-2::GFP* fluorescence intensities between control and *mig-6(qz2)* mutants DTCs (Extended Data Fig.2a), indicating that *lag-2* expression was unaffected. Cropping out the volume corresponding to the GFP-labelled DTC from the red fluorescent channel allowed the quantification of COL IV levels associated to the DTC (hereafter referred to as DTC-associated COL IV or DTC-AC), at the interface with the GSCs (Fig.2a). Surprisingly, in control animals, we found that DTC-AC levels were significantly higher in the anterior than in the posterior DTC (Fig.2a,b). We therefore considered DTC position in all subsequent analyses. Regarding *mig-6(qz2)* mutants, we found that they had increased DTC-AC, but specifically in the posterior gonad arm (Fig.2c,d). We therefore conclude that the MIG-6L PLAC domain negatively regulates DTC-AC COL IV levels.

Since DTC migration is reduced in *mig-6(qz2)* mutants, we considered the possibility that increased DTC-AC could be linked to reduced gonad elongation. However, DTC migration was equally reduced in both gonad arms in *mig-6(qz2)* mutants, but only the posterior DTC had increased COL IV levels (Fig.2d and Extended Data Fig.1c). We also quantified DTC-AC in *lon-2(e678)* mutants, which specifically have longer anterior distal gonad arms (Extended Data

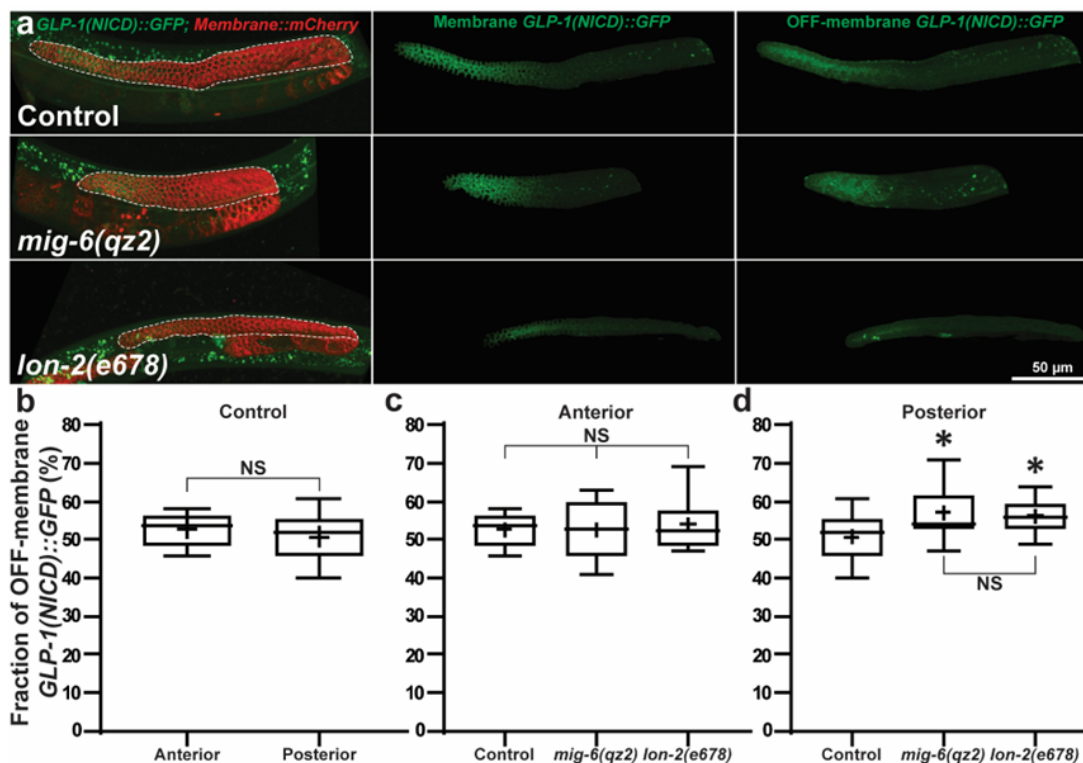
Fig.1c), but again, found that DTC-AC levels varied independently of distal gonad elongation, as these mutants also had a posterior-specific increase in DTC-AC (Fig.2d). We therefore conclude that MIG-6L PLAC domain acts to restrict DTC-AC levels, independently of DTC migration or gonad elongation.



**Figure 2. Increased posterior DTC-AC levels in *mig-6L* and *lon-2* mutants.** (a) Left, representative Imaris-generated 3D view of a control adult (mid L4 + 24h at 25°C) hermaphrodite section where both anterior (green model) and posterior (yellow model) DTCs are visible in the same focal plane. DTCs are labelled in green using a *Plag-2::GFP* transgene<sup>111</sup>, and COL IV is labelled in red by an *EMB-9::mCherry* transgene<sup>110</sup>. Right, *EMB-9::mCherry* signal overlapping with the anterior (top) and posterior (bottom) DTC models. (b) Boxplot scoring the average *EMB-9::mCherry* fluorescence intensity overlapping with the DTC models (mid L4 +24h at 15°C). Sample sizes, from left to right: 25, 12. (c) Left, representative 3D view of a posterior DTC-containing section of hermaphrodite of the indicated genotypes (mid L4 +24h at 15°C), Right, *EMB-9::mCherry* signal overlapping with their respective 3D DTC model. (d) Boxplots scoring the average *EMB-9::mCherry* fluorescence intensity overlapping with the anterior (left) and posterior (right) DTCs of animals of the indicated genotypes. Sample sizes, from left to right: 25, 13, 15, 12, 14, 16. (b,d) Asterisks (\*) mark significant differences. One asterisk,  $p < 0.05$ ; two asterisks,  $p < 0.01$  versus (b) the anterior gonad; unpaired two-tailed t-test, or (d) control; one way ANOVA with Tukey's multiple comparison test.

### **MIG-6L reduces GLP-1(NICD) presence at the GSC plasma membrane**

Since *mig-6(qz2)* enhanced *glp-1(gf)* defects (Fig.1b), and specifically increased posterior DTC-AC levels (Fig.2d), we asked if it led to higher Notch receptor activation, also specifically in the posterior gonad arm. To evaluate GLP-1 activation, we marked all germ membranes with red fluorescence (*Pmex-5::TAGRFPT::PH*)<sup>112</sup> and the GLP-1(NICD) in green (*GLP-1(NICD)::GFP*) [Saravanapriah Nadarajan, David Greenstein and Tim Schedl, personal communication]. Using the red channel, we generated a 3D model of distal germ membranes. We used this mask to separate the fraction of *GLP-1(NICD)::GFP* localizing to the germ membranes from that localizing OFF from the cell membranes, either to the cytoplasm, nuclei or rachis, and thus presumably representing the cleaved or "activated" GLP-1(NICD) fraction (Fig.3a-d and Extended Data Video 1). Of note, we did not detect any differences between distal germline *GLP-1(NICD)::GFP* fluorescence intensities between control and *mig-6(qz2)* animals (Extended Data Fig.2b), indicating that GLP-1 levels were unaffected. We first compared the OFF-membrane fraction of *GLP-1(NICD)::GFP* in the anterior and posterior gonads of controls but found no significant differences ( $p=0.37$ ) (Fig.3b). Yet, in *mig-6(qz2)* mutants, the fraction of OFF-membrane *GLP-1(NICD)::GFP* was significantly and specifically higher in the posterior gonad (fig.3a,c,d). These results raised the possibility that *mig-6L* could modify posterior GLP-1 activation through reducing DTC-AC *EMB-9/COL IV* levels, thereby jeopardizing the LAG-2-GLP-1 interaction.



**Figure 3. DTC-AC levels are linked to GLP-1 activation.** (a) Left, representative Imaris view of generated 3D models of the posterior gonad arm (white dashed lines delineate the distal half) of adult hermaphrodites of the indicated genotypes (mid L4 + 24h at 15°C). A *Pmex-5::TAGRFPT::PH* transgene<sup>113</sup> marks GSCs membranes (red), and a *GLP-1(NICD)::GFP* transgene [Saravanapriah Nadarajan, David Greenstein and Tim Schedl, personal communication] labels the GLP-1(NICD) (green). Middle, *GLP-1(NICD)::GFP* signal overlapping with germ cell membranes. Right, Germ nuclear or cytoplasmic *GLP-1(NICD)::GFP* signal (not overlapping with cell membranes, or “OFF-membrane”). (b) Boxplot scoring the fraction of “OFF-membrane” *GLP-1(NICD)::GFP* fluorescence for the anterior and posterior gonads of control animals. Sample sizes, from left to right: 10, 17. (c-d) Boxplots scoring the fraction of “OFF-membrane” *GLP-1(NICD)::GFP* fluorescence for the anterior (c) or posterior (d) distal gonad arms of animals of the indicated genotypes. Sample sizes, from left to right: (c) 10, 9, 16; (d) 17, 10, 17. Asterisks (\*) mark significant differences versus control ( $p < 0.05$ ) by (b) unpaired two-tailed t-test (c-d) one way ANOVA with Tukey’s multiple comparison test.

#### GLP-1/Notch activation varies together with DTC-AC Col IV levels

To test whether COL IV levels influence GLP-1 activation, we used TGF- $\beta$  pathway mutants to alter DTC-AC COL IV levels. The *lon-2(e678)* mutant is known to upregulate TGF- $\beta$  signaling, leading to increased collagen synthesis<sup>62,89</sup>. Indeed, we measured a significant COL IV increase, specifically associated with the posterior DTC of these mutants (Fig.2d). Accordingly, the fraction of OFF-membrane *GLP-1(NICD)::GFP* was also specifically increased in the posterior gonad of *lon-2* mutants (Fig.3a,c,d).

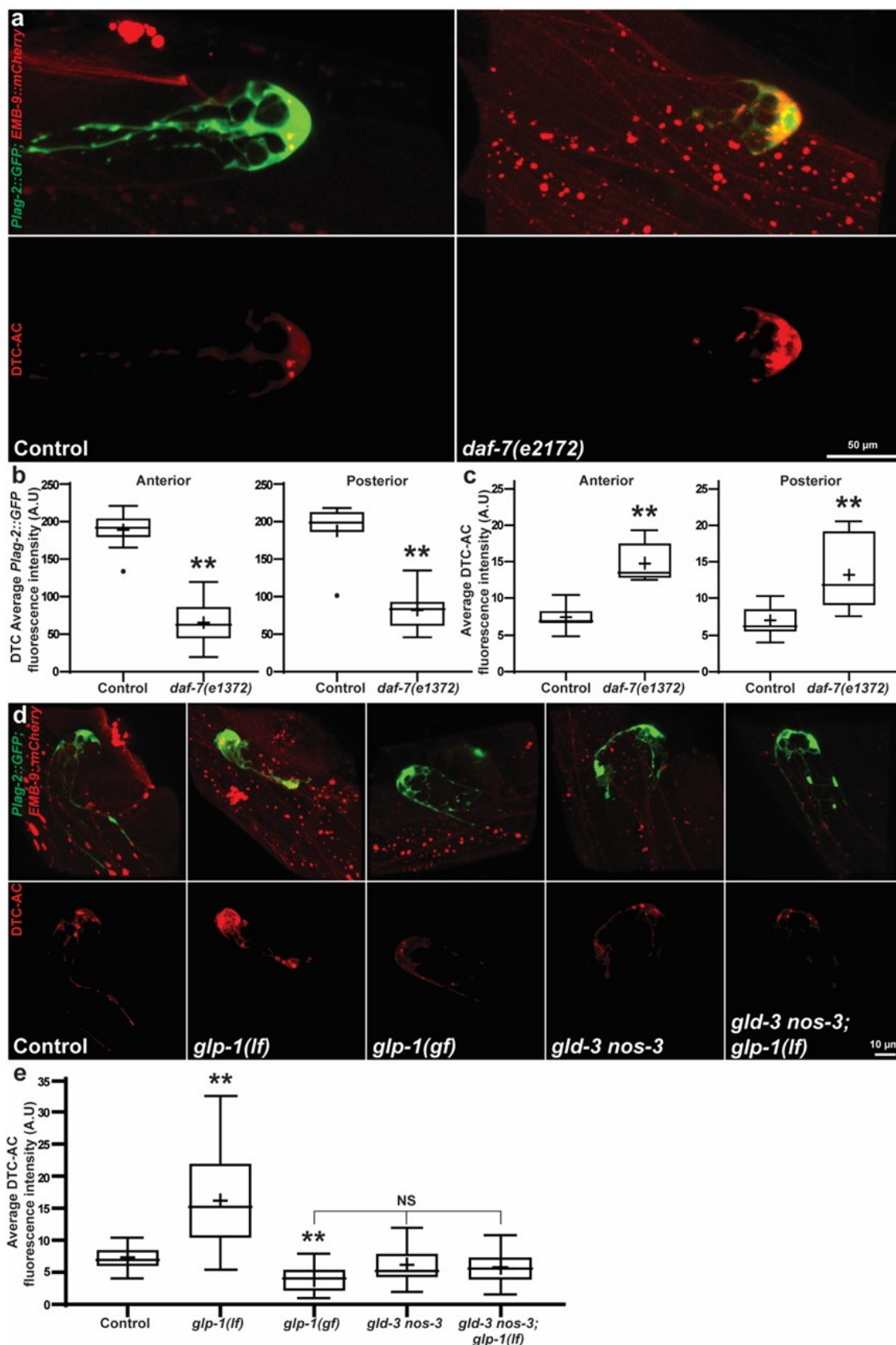
Next, we used *daf-7(e1372)* mutants to downregulate TGF- $\beta$  signaling, and potentially alter COL IV levels<sup>56,62</sup>. This *daf-7* mutation was however reported to reduce *lag-2* expression by the DTC<sup>56</sup>, results that we reproduced using the *Plag-2::GFP* reporter (Fig.4a,b). This reduction in Notch ligand expression would have precluded the direct association of any observed reduction in GLP-1 activation to a variation in DTC-AC levels, hence we did not measure the

ratio of OFF-membrane GLP-1(NICD)::GFP in *daf-7* mutants. We nevertheless measured their DTC-AC levels, and found that it was drastically higher in both the anterior and posterior gonad arms relative to control animals (Fig.4a,c). This unexpected result raised the new possibility that reduced *lag-2* expression, either directly or through the resulting decrease in Notch activity, led to an increase in DTC-AC.

#### **GLP-1/Notch activity inversely affects COL IV levels**

To investigate whether Notch activity influences DTC-AC levels, we first quantified DTC-AC levels in both *glp-1(lf)* and *glp-1(gf)* mutants<sup>105,114</sup>. We found that a decrease in Notch activity caused a dramatic increase in both anterior and posterior DTC-AC levels (Fig.4d,e and Extended Data Fig.3a). In addition, we reported that increasing Notch activity significantly reduced DTC-AC levels (Fig.4d,e and Extended Data Fig.3b). Interestingly, the negative effects Notch signaling had on COL IV levels were not restricted to the area associated with the DTC, but more broadly affected the specimen. Indeed, COL IV levels were significantly increased in the body wall muscles and distal gonad basement membranes of *glp-1(lf)* mutants, but decreased in the body wall muscles of *glp-1(gf)* mutants (Fig.4d and Extended Data Fig.3c,d). These results show that *glp-1*/Notch signaling broadly restricts COL IV accumulation in *C. elegans*, likely through cell non-autonomous systemic effects.

Changes in GLP-1 activity could affect COL IV levels directly. However, since *glp-1(lf)* mutants quickly lose their GSC pools to differentiation<sup>115</sup>, while *glp-1(gf)* mutants grow GSC tumours<sup>105</sup>, changes in GLP-1 activity could instead regulate COL IV levels indirectly, through an effect on germline identity/status. To discern between a direct or indirect effect, we measured DTC-AC levels in triple *gld-3(lf) nos-3(lf); glp-1(lf)* mutants that lacked *glp-1* activity, but conserved a GSC pool and grew germline tumours due to the simultaneous lack of *gld-3* and *nos-3* function, two redundant *glp-1* downstream inhibitory targets<sup>34,114</sup>. The absence of a functional GLP-1 receptor *per se* did not perturb DTC-AC levels as it remained undistinguishable across control, *gld-3; nos-3* doubles and *gld-3 nos-3; glp-1* triples (Fig.4d,e). Similarly, body wall muscle and distal germline basement membrane COL IV levels were undistinguishable between *gld-3 nos-3* doubles and *gld-3 nos-3; glp-1(lf)* triples (Extended data Fig.3c,d). These results suggest that the animal's COL IV levels, both globally and locally around the DTCs, may be systemically adjusted in response to germline states, and do not directly depend on Notch receptor activity.



**Figure 4. Reduced Notch activity increases DTC-AC levels through downstream effects.** (a) Top, representative Imaris-generated 3D view of a DTC-containing section of adult hermaphrodites of the indicated genotypes (mid L4 + 24h at 25°C). Bottom, DTC-overlapping *EMB-9::mCherry* signal. (b) Boxplots scoring the average *Plag-2::GFP* fluorescence intensity in anterior (left) and posterior (right) DTCs of control and *daf-7(e1372)* animals. (c) Boxplots

scoring the average DTC-overlapping *EMB-9::mCherry* fluorescence intensity in anterior (left) and posterior (right) DTCs of control and *daf-7(e1372)* animals. **(b-c)** Sample sizes, from left to right: **(b)** 12, 10, 7, 12; **(c)** 11, 6, 17, 10. **(d)** Top, representative Imaris-generated 3D view of a DTC-containing section of adult hermaphrodites of the indicated genotypes (15°C until L2 + 40 hours at 25°C). Bottom, DTC-overlapping *EMB-9::mCherry* signal. **(a, d)** A *Plag-2::GFP* transgene marks DTCs<sup>116</sup> (green), and an *EMB-9::mCherry* transgene labels COL IV<sup>110</sup> (red). **(e)** Boxplot scoring the average DTC-associated *EMB-9::mCherry* fluorescence intensity in animals of the indicated genotypes. No differences were observed between anterior and posterior DTC-AC levels for both *glp-1(lf)* and *glp-1(gf)* mutants (Extended data Fig.3a,b). Sample sizes, from left to right: 25, 34, 24, 21, 22. Alleles: *glp-1(e2141)lf*, *glp-1(ar202)gf*, *gld-3(q730)*, *nos-3(q650)*. **(b-c,e)** Asterisks (\*) mark significant differences versus control. One asterisk,  $p < 0.05$ ; two asterisks,  $p < 0.01$ ; by **(b)** anterior: unpaired two-tailed t-test, posterior: Mann-Whitney test, **(c)** anterior: unpaired two-tailed t-test, posterior: Welch's t-test **(e)** Brown-Forsythe and Welch's ANOVA with Dunnett's T3 multiple comparisons test.

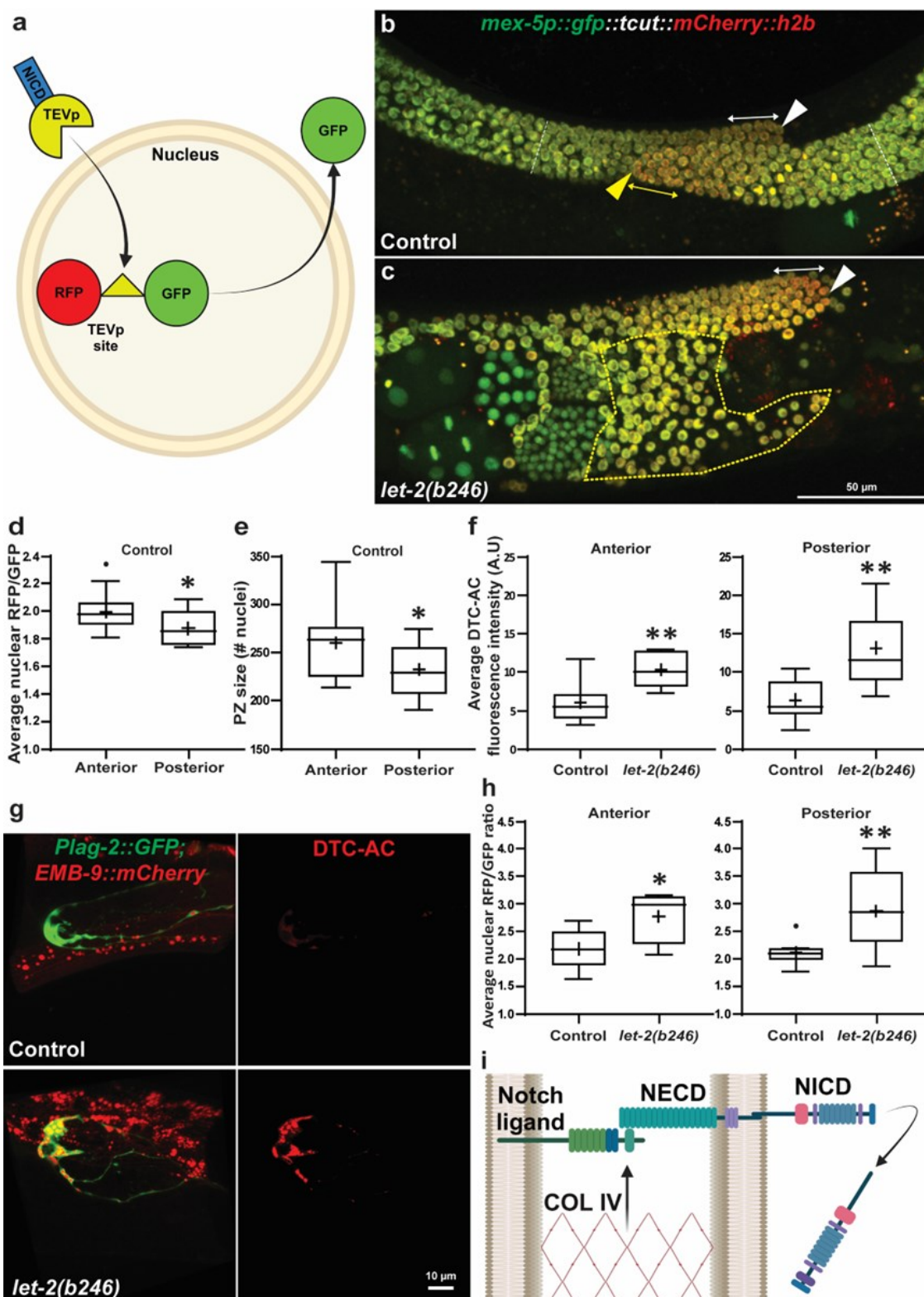
### GLP-1/Notch activation is tied to DTC-associated COL IV levels

After having better defined the influence of Notch activity on DTC-AC levels, we returned to defining the impact of DTC-AC levels on Notch receptor activation, this time using a genetically-encoded sensitive *in vivo* sensor able to detect lateral signaling activity (SALSA)<sup>88</sup>. This sensor combines GFP with a nuclear localized RFP, the two fluorophores being separated by a Tobacco etch virus protease (TEVp) site. The sensor strain also carries a *glp-1(ar648)* switch, in which a TEV protease was added to the NICD. Upon Notch activation, the NICD::TEVp is released from the membrane, enters the nucleus, and frees GFP from its nuclear RFP tether (Fig.5a), allowing Notch activation to be quantified as a nuclear RFP/GFP ratio<sup>88</sup>. As such, a greater RFP/GFP ratio indicates greater Notch receptor activation, and greater NICD-mediated transcription in germ nuclei. Using high-resolution confocal microscopy and 3D modeling, we generated microspheres overlapping with germ nuclei to obtain their RFP/GFP ratios (Fig.5b and Extended Data Video 2). Since GLP-1 activity gradually declines as a function of the distance from the DTC<sup>88,117</sup>, we focused on nuclei located 0 to 5 cell diameters from the DTC, where activity is strongest (Fig.5b). As expected, GSCs from switchless control animals had a RFP/GFP ratio near 1, being half-red, half-green (Extended Data Fig.4a), lower than those within animals bearing the switch (Fig.5b-d)<sup>88</sup>. Interestingly, Notch receptor activation was significantly higher in the anterior GSCs of control animals than in their posterior GSCs (Fig.5b,d), thereby erasing the only instance where we had not observed Notch activation to follow significant changes in DTC-AC levels (Figs.2b,3b). This is presumably due to the increased sensitivity of the SALSA *versus* GLP-1(NICD)::GFP assay. Moreover, we had not detected any differences in DTC-AC levels between the anterior and posterior gonad arms of *mig-6(qz2)* mutants (Fig.2d;  $p = 0,3$ ), and accordingly, the SALSA assay showed no differences in GLP-1/Notch activity (Extended Data Fig.4b). These results therefore further strengthen the potential direct relationship between DTC-AC levels and GLP-1/Notch receptor activation.

Notch activation controls the size of the germ stem and progenitor pool<sup>118</sup>. To further validate this intriguing difference in Notch activity between the anterior and posterior gonad arms in control animals, we measured their respective proliferative zone (PZ) size. Consistent with the observed variations in Notch activity, we found that control animals have a slightly but significantly smaller posterior PZ size (Fig.5e). In *mig-6(qz2)* mutants however, in which anterior and posterior DTC-AC were similar, both gonad arms had undistinguishable PZ sizes



(Extended Data Fig.4c). Collectively, and across two Notch activation assays (*GLP-1(NICD)::GFP* and SALSAs), our data strongly support a positive relationship between DTC-AC levels and GLP-1/Notch receptor activation.



**Figure 5. DTC-AC promotes Notch activation.**

(a) Graphical representation of the SALSA assay created with BioRender.com. When the NICD is released and enters the nucleus, the attached TEVp cleaves the TEVp site linking GFP to a membrane tethered RFP, allowing GFP to diffuse out of the nucleus, thereby increasing the nuclear RFP/GFP ratio<sup>88</sup>. (b) Representative Imaris-generated 3D view showing the anterior (left) and posterior (right) gonad arms of a control adult hermaphrodite (15°C until mid L4 +

24h at 25°C) expressing the SALSA sensor. White (anterior) and yellow (posterior) arrowheads indicate the distal-most nucleus of each gonad arms. White dashed lines mark the first row containing two crescent shaped differentiating nuclei, at the proximal extremities of the progenitor zones (PZs). (c) Representative Imaris-generated 3D view of the SALSA sensor in *let-2(b246)* mutants raised in parallel. Yellow dashed lines indicate germ cells located outside the gonad following its rupture, a common defect for *let-2(b246)* mutants raised under these conditions (12/25 arms were ruptured). (d) Boxplot scoring Notch activity in control anterior and posterior gonad arms, based on the RFP/GFP ratio averaged from nuclei located in the distal 1 to 5 cell diameters, indicated by double headed arrows. Sample sizes, from left to right: 12, 11. (e) Boxplot scoring the number of nuclei in control anterior and posterior PZs. Sample sizes, from left to right: 13, 15. (f) Boxplots scoring the average DTC-overlapping *EMB-9::mCherry* fluorescence intensity in anterior (left) and posterior (right) DTCs of control and *let-2(b246)* animals. Sample sizes, from left to right: 10, 8, 9, 7. (g) Representative Imaris-generated 3D views of DTC-containing sections of adult hermaphrodites of the indicated genotypes (mid L4 + 24h at 25°C). A *Plag-2::GFP* transgene<sup>111</sup> marks DTCs (green), and an *EMB-9::mCherry* transgene<sup>110</sup> labels COL IV (red). Left, Merged GFP and RFP channels. Right, DTC-overlapping *EMB-9::mCherry* signal. (h) Boxplots scoring Notch activity in anterior (left) and posterior (right) gonad arms of control and *let-2(b246)* animals, based on the average nuclear RFP/GFP ratio from GSCs located within 1-5 cell diameters from the DTC. Sample sizes, from left to right: 6, 6, 8, 11. Asterisks (\*) mark significant differences versus (d,e) anterior or (f,h) control. One asterisk,  $p < 0.05$ ; two asterisks,  $p < 0.01$ ; by (d-f) unpaired two-tailed t-test, (h) anterior: unpaired two-tailed t-test posterior: Welch's t-test. (i) Model created with BioRender.com in which basement membrane COL IV promotes Notch activity.

#### DTC-associated COL IV promotes GLP-1/Notch receptor activation

We next aimed to establish whether DTC-AC levels promote GLP-1/Notch receptor activation. To manipulate COL IV levels, we used a conditional allele of the *C. elegans* COL IV  $\alpha 2$  chain, *let-2(b246)*<sup>119-121</sup>. This mutation prevents proper assembly and secretion of the COL IV heterotrimeric complex, such that most of it remains stuck in the muscles, the main COL IV producing tissue of the animal<sup>119,122</sup>. As expected, *let-2(b246)* mutants had an obvious overall increase in body wall muscle *EMB-9::mCherry* levels, balanced by a systemic decrease in basement membrane EMB-9 levels (Extended Data fig.5). Surprisingly however, there was a striking increase in the anterior and posterior DTC-AC levels in *let-2(b246)* mutants (Fig.5f,g). Consistent with this, however, GLP-1 activity was increased in both distal *let-2(b246)* gonad arms relative to within control animals (Fig.5b-c,h). These results demonstrate that increasing DTC-AC levels promotes GLP-1/Notch receptor activation (Fig.5i).

#### Discussion

Due to the broad and severe adverse effects associated with *in vivo* COL IV level manipulations<sup>120-122</sup>, the relationship between tissue fibrosis and Notch signaling has remained largely unclear. *In vitro* analyses that varied matrix stiffness, on the other hand, have led to conflicting results<sup>123,124</sup>. In this study, we clearly show that the interaction between a Delta-like membrane-bound ligand and the Notch receptor at the surface of stem cells within an adjacent tissue is favored by increasing levels of COL IV in the intervening basement membrane. Namely, the efficiency of GLP-1/Notch receptor activation in GSCs decreases when DTC-AC levels are low and increases when DTC-AC levels are higher. These results were somewhat surprising since basement membrane fibrosis is generally presented as a

consequence of elevated Notch signaling, and hence focused on targeting this pathway to treat both cancer and fibrotic diseases<sup>70,93</sup>. Direct downregulation of GLP-1/Notch receptor activity increased COL IV basement membrane deposition, while upregulation had the opposite effect. Fibrosis is therefore not a consequence of high Notch activity. Fibrosis may instead result from the indirect consequences of reduced Notch signaling – in the *C. elegans* case, the loss of its GSCs to differentiation.

It is therefore unclear whether the pharmacological inhibition of Notch signaling to treat cancer or fibrotic diseases will pan out as a successful strategy. Strengthening this view, Notch deficiency was shown to lead to hypertrophy and fibrosis in the mouse heart<sup>125</sup>. Developing strategies to modify basement membrane collagen levels, for example by altering precise components of TGF-beta signaling, or collagenase activity<sup>126-128</sup>, could provide more efficient and specific therapeutic approaches.

## Methods

### *C. elegans* maintenance

*C. elegans* were grown on standard nematode growth medium (NGM) seeded with OP50 *E. coli* bacteria<sup>20</sup>. Animals were grown at 15°C, and when indicated, upshifted to 25°C at the indicated stage and for the indicated period in the figure legend. When animals were upshifted at the L2 stage, they were further resynchronized at L4, based on vulva development<sup>129</sup>. Extended Data Table 1 lists all strains used.

### Cloning of the *mig-6(qz2)* allele

A standard EMS forward genetic screen<sup>20</sup> was performed using a *fog-1(q785)/hT2 [bli-4(e937) let-?(q782) qIs48]; glp-1(ar202)gf* strain. Briefly, after P0 mutagenesis, *fog-1(q785); glp-1(ar202)gf* F2 L4s were upshifted to 25°C and screened for germline tumour formation<sup>130</sup>. The *mig-6(qz2)* allele was subsequently identified by whole-genome sequencing and RNAi screening to phenocopy candidate genes. Finally, molecular identity was confirmed by Sanger sequencing and transformation rescue experiments (Fig.1b and Extended Data Fig.1a,b).

### Transgenics

For *mig-6(qz2)* transformation rescue, the *qzEx4[mig-6L(+); Pmyo-3::mCherry]* extra-chromosomal array was generated by standard microinjections<sup>60</sup> of a mixture of pZH117[*mig-6L(+)* genomic/cDNA minigene]<sup>3</sup> (40ng/μl), pKSII (100 ng/μl), and pCFJ104[*Pmyo-3::mCherry*]<sup>61</sup> (40 ng/μL).

For CRISPR/Cas9-mediated endogenous *mig-6L* tagging, we used the self-excising cassette method as described<sup>131</sup>. However, to improve knock-in efficiency, animals were grown on *cku-80(RNAi)* prior to microinjections<sup>132</sup>. Extended Data Table 2 lists all plasmids and primers used.

### Imaging

Animals of the indicated stage were paralyzed by soaking in an 8 μL drop of a 0.1% Tetramizole (Sigma, L9756) M9 solution on a glass coverslip that was then flipped onto a 3% agarose/M9 pad placed on a microscope slide. Since the gut and germline are intertwined such that when

one gonad arm is on top of the gut, the other arm is usually underneath, resulting in fainter fluorescence signals. This most often prevents same-animal antero-posterior fluorescence intensity comparisons. Therefore, except on the rare occasions where both arms were in the same focal plane, only either the anterior or posterior gonad arm or DTC was imaged for each animal.

Whole-animal differential interference contrast (DIC) and or epifluorescence images (Fig.1a and Extended Data Fig.1a,d) were acquired every  $\mu\text{m}$  using a Plan-Apochromat 20x dry objective (NA 0.8) mounted on an inverted Zeiss Axio Observer.Z1 with an AxioCam 506 mono camera and Zeiss 38 HE GFP or 45 HQ Texas Red shift free fluorescence filter sets. Images were stitched using the Zen 2.6 software, and using ImageJ, brightness was uniformly adjusted and animal were straightened for ease of visualization. All DIC images show single focal planes, and where applicable, fluorescent images also show the corresponding single focal plane.

For all confocal acquisitions (Figs. 2a,b, 3a, 4,a,d, 5,a,b,f, and Extended Data Fig.4d), coverslips were sealed with VALAP (1:1:1 vaseline, lanolin, paraffin), and 0.35  $\mu\text{m}$  z-step stacks were acquired with a Leica SP8 point scanning confocal microscope with a HC PL APO CS2 40x/1.30 numerical aperture oil objective.

For *EMB-9::mCherry* quantification (Figs.2c, 4a,d, 5,f), mCherry was excited/collected at 590/632nm with 0,6% laser intensity. The *Plag-2::GFP* was excited/collected at 487/520nm with a laser intensity that varied between 1-5% to detect most of the signal, but avoid saturation, in order to model the DTC as accurately as possible.

For *Plag-2::GFP* quantification (Figs.4b and Extended Data Fig.2a), GFP and mCherry were excited/collected at 487/520nm with 0,4% laser intensity, and 600/620nm with a 0.6% laser intensity, respectively.

For the GLP-1(NICD) cleaving assay (Fig.3), *GLP-1(NICD)::GFP* was excited/collected at 495/538nm with 6% laser intensity. *Pmex-5::PH::TAGRFPT* was excited/collected at 590/632nm with a laser intensity that varied between 2-5% to detect most of the signal, but avoid saturation, in order to model distal germ membranes as accurately as possible.

For the SALSA assay (Figs.5a-c,e and Extended Data Fig.4.a,b), GFP and RFP were excited/collected at 495/539nm and 590/632nm, respectively, each with 1% laser intensity.

For global *EMB-9::mCherry* visualization (Extended Data Fig.4c) *PAT-2::mNG* and *EMB-9::mCherry* were excited/collected at 487/520nm with 4% laser intensity, and 590/632nm with 2% laser intensity, respectively.

#### **Tumour formation assay**

Larvae were grown at 15°C, synchronized by picking mid-L4 stage individuals<sup>129</sup>, to a new plate for an additional 72 hours, still at 15°C, except for the *glp-1(gf)* shown at the bottom of Fig.1a, which were upshifted to 25°C for 24 hours. The presence of proximal germline tumours was scored using DIC and *Ppie-1::mCherry::HIS-58* epifluorescence with a Plan-Apochromat 20x dry objective (NA 0.8) mounted on an inverted Zeiss Axio Observer.Z1.

#### **Distal gonad length measurement**

Larvae were grown at 15°C and late L4s were picked to a new plate for 24 more hours at 15°C before they were imaged. FIJI was used to measure distal gonad length by drawing a

segmented line along the center of the distal half of the gonad arm, from the bend to the distal tip.

#### **Brood size, embryonic and larval lethality**

For fecundity, according to standard procedures<sup>87</sup>, late L4 larvae were singled at 15°C. Animals were transferred to a new plate every 24 hours, after which the number of eggs laid and hatched larvae were scored. The assay was stopped when an individual laid no eggs for 24 hours. For embryonic lethality, the number of unhatched eggs after 24 hours was recorded (2x checked after 48 hours). For larval lethality, the number of dead or arrested larvae was scored 4 days later.

#### ***Plag-2::GFP* and *EMB-9::mCherry* fluorescence intensity quantification**

Confocal z-stacks were transferred to Imaris 9.2.1, and based on the green channel (*Plag-2::GFP*), 3D surfaces were generated using identical settings. The 3D models were individually thresholded to optimally match the DTC surfaces. All surfaces corresponding to the DTC and its cytonemes were grouped as one structure. For DTC-AC quantification, the GFP surface object was selected and using the edit tool, a new mCherry channel corresponding to the DTC-AC was obtained, and its mean intensity was pulled from the statistics tab. For *pLAG-2::GFP* quantification, the mean intensity for the GFP channel was instead pulled.

For average body wall muscle and distal gonad basement membrane *EMB-9::mCherry* quantification, based on the red channel, 3D surfaces were generated as described above to optimally fit the body wall muscles or gonad membrane. For body wall muscles, a  $\approx 40 \times 20 \times 5 \mu\text{m}$  thick section was selected using the edit tool. For the gonad basement membrane, a  $\approx 20 \times 10 \times 1 \mu\text{m}$  thick distal gonad basement membrane section,  $\approx 20 \mu\text{m}$  away from the DTC cell body was selected using the edit tool (see Extended data Video 3). For both sections, the mean intensity for the red channel was pulled from the statistics tab.

#### **Notch signaling quantification using *GLP-1(NICD)::GFP***

For *GLP-1(NICD)::GFP* fluorescence quantifications, images were processed as above, except that 3D surfaces were generated based on the red channel (*Pmex-5::PH::TAGRFPT*) to obtain a distal gonad containing surface. This surface was manually refined using the edit tool delete unwanted surfaces (*e.g.* proximal gonad, unspecific signal, etc; see Extended data Video 1). A new green channel was obtained based on the final trimmed red surface object, containing only the *GLP-1(NICD)::GFP* signal from within the distal gonad. The GFP intensity sum was then pulled from the statistics tab. Another 3D surface was generated based on the red channel with the same methodology, but using different settings, this time to obtain a surface matching GSC membranes. This new red surface was selected, and the intensity sum for the corresponding GFP channel, localizing to the distal germ membranes, was pulled. These two sums were used to calculate the ratio of OFF-membrane *GLP-1(NICD)::GFP*.

#### **Notch signaling quantification using SALSA**

For SALSA quantifications<sup>88</sup>, we imported images into Imaris 9.2.1 as above, and using the spots tool, generated  $3.6 \mu\text{m}$  diameter spheres based on the red (*mCherry::H2B*) channel corresponding to individual germ nuclei, using the same batch settings for all images. The edit tool was used to refine the selection to only the spheres corresponding to germ nuclei located

within 5 cell diameters of the DTC (Extended data Video 2). The intensity sums for both the red and green channels from these spheres were pulled to generate individual RFP/GFP ratios for each nuclei. Ratios from single gonad arms were averaged and normalized to the switchless control averaged anterior and posterior ratio ( $\approx 0,51$ ). Note that the switchless control RFP/GFP ratio was fixed to 1, to correspond to the expected equimolar nuclear quantities of GFP and RFP<sup>88</sup>.

### PZ size evaluation

Initial Imaris files used for the SALSA assay were reused and, based on the red (*mCherry::H2B*) channel generated using the same batch settings for every image, 2.6  $\mu\text{m}$  diameter spheres, corresponding to germ nuclei, were generated using the spots tool. We found that using a diameter slightly smaller than the actual nuclei diameter improved identification efficiency. The edit tool was used to manually delete spheres that did not correspond to PZ nuclei. We defined the PZ as distal to the first row of cells where at least two distinctive crescent shaped germ nuclei were present<sup>133</sup> and obtained the total number of PZ spheres.

### Statistics

All statistical analysis were performed using GraphPad Prism 10.2.0. Each dataset normality was verified using the Shapiro-Wilk test. Variance was verified by F test for comparing 2 samples and Brown-Forsythe test for comparing more than 2 samples. The test used are indicated in the figure legend and were chosen consistent with the following criteria.

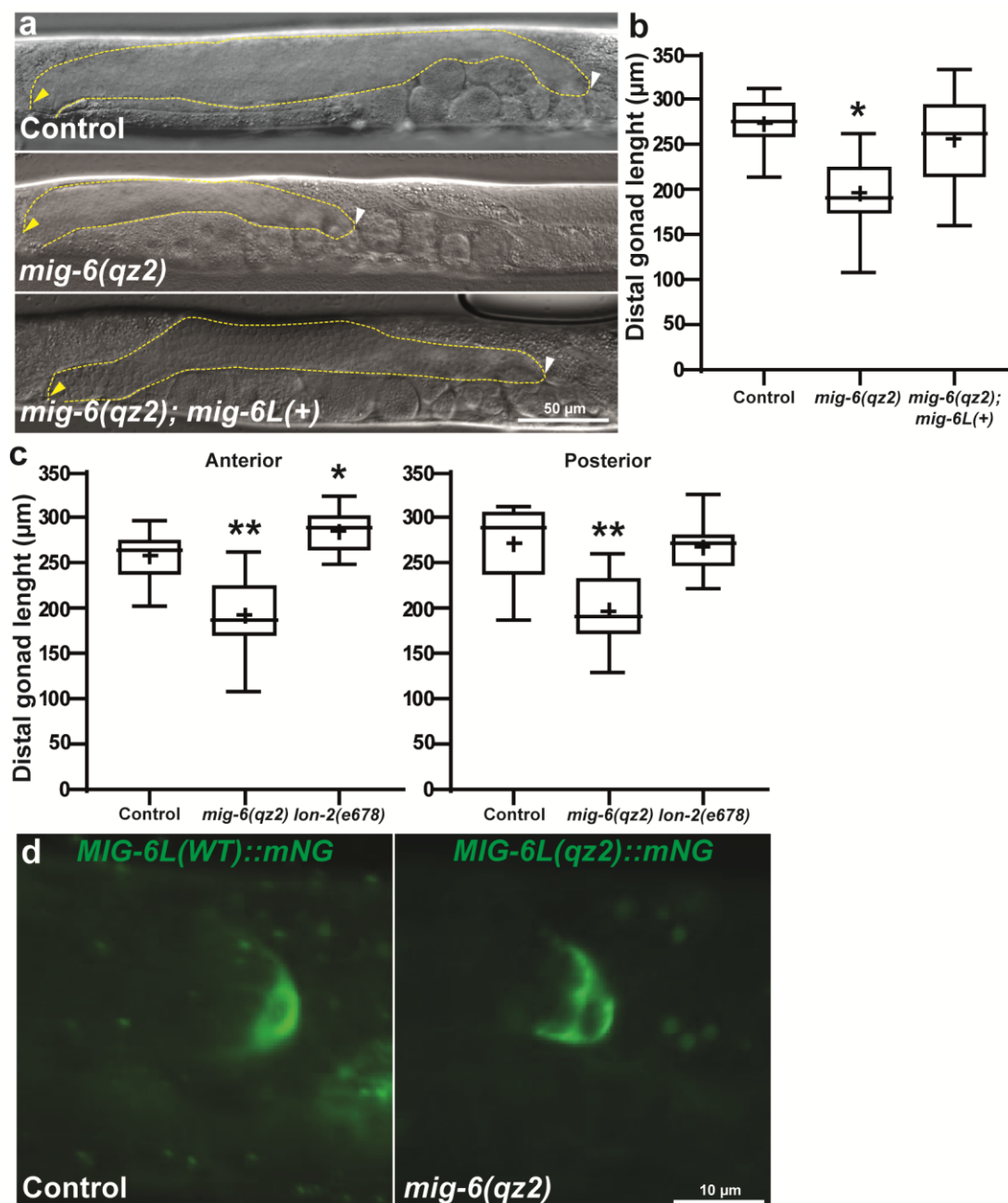
For 2 sample comparison with normal distribution and equal variance we used unpaired two-tailed t-test. When the distribution was not gaussian, we used the Mann-Whitney test. When the distribution was normal, but the variance was unequal, we used the Welch's t-test.

For comparison of more than 2 sample with normal distribution and equal variance we used one way ANOVA with Tukey's multiple comparison test. When the distribution was not gaussian, we used the Kruskal-Wallis with Dunn's multiple comparisons test. When the distribution was normal, but the variance was unequal, we used the Brown-Forsythe and Welch's ANOVA with Dunnett's T3 multiple comparisons test.

### Acknowledgements

We thank Jean-Philippe Leduc Gaudet, Claire Bénard, Lise Rivollet and Malika Nadour for comments on the manuscript. We thank Hugo Germain for the Imaris 9.2.1 licence, Iva Greenwald for the SALSA biosensor strains, David Sherwood for the *EMB-9::mCherry* strain, David Greenstein and Dave Hansen for the *GLP-1(NICD)::GFP* strain. We also thank Judith Kimble, Sarah Crittenden and Claire Bénard for precious suggestions, reagents and strains, and Mélodie B. Plourde for technical support and advice. Finally, we thank WormBase for its essential role in *C. elegans* research. Some strains were provided by the CGC, which is funded by NIH Office of Research Infrastructure Programs (P40 OD010440). The Narbonne laboratory is funded by grants from the Fondation Marcel et Rolande Gosselin, NSERC (RGPIN-2019-06863, RGPAS-2019-00017, and DGEER-2019-00326), and CIHR (PJT-169138) to P.N. P.N. is a FRQ-S Junior 2 Bursary Scholar (310643).

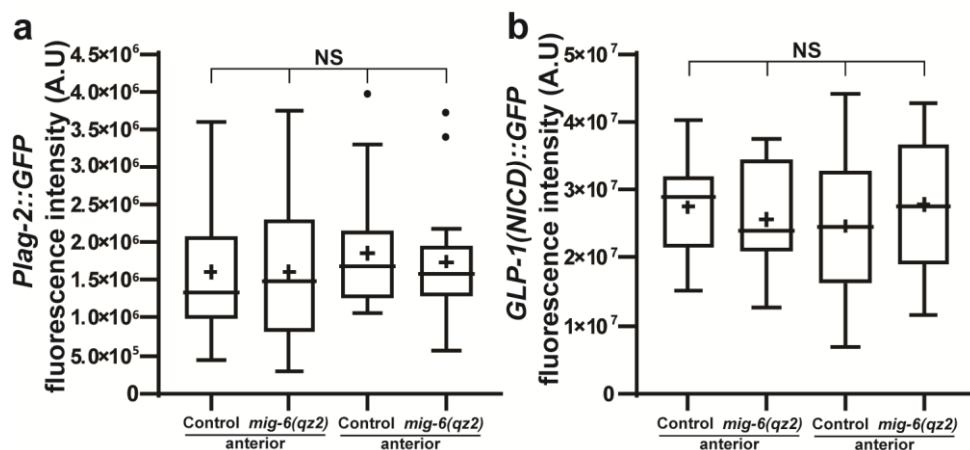
## Extended Data



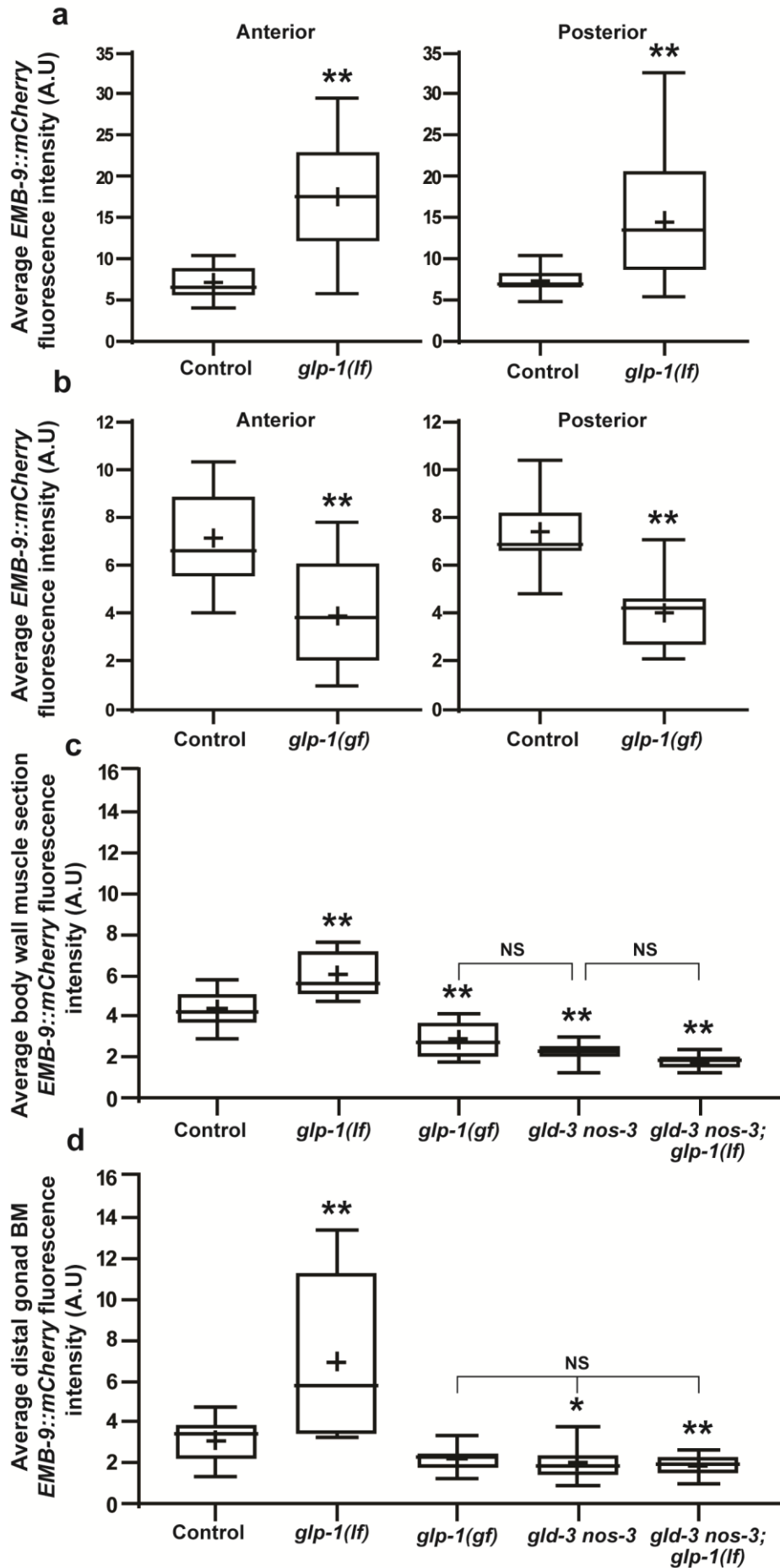
**Extended Data Figure 1. Effect of *mig-6(qz2)* and *lon-2(e678)* on distal gonad elongation.** (a) Representative DIC micrographs of anterior gonad arms from adult hermaphrodites of the indicated genotypes (late L4 + 24h at 15°C). Yellow dashed lines delineate the distal gonad. Yellow arrowheads mark gonadal bends, and white arrowheads mark distal extremities. A *Pmyo-3::mCherry* marker was used to mark the extrachromosomal *mig-6L(+)* transgene but the fluorescence signal is not shown in this image. (b) Boxplot scoring the distal gonad lengths (from the distal tip to the bend; see Methods) of adult hermaphrodites of the indicated genotypes (late L4 + 24h at 15°C). Anterior and posterior gonad arm measurements were pooled together as they were similar. Sample sizes, from left to right: 34, 46, 17 gonad arms. (c) Boxplots scoring anterior (left) and posterior (right) distal gonad lengths of adult hermaphrodites of the indicated genotypes (late L4 + 24h at 15°C). Sample sizes, from left to right: 17, 22, 19. (b,c) Asterisks (\*) mark significant differences versus the control. One asterisk,  $p < 0.05$ ; two asterisks,  $p < 0.01$ ; by (b) one way ANOVA with Tukey's multiple comparison test, (c) anterior: one way ANOVA with Tukey's multiple comparison test, posterior: one way ANOVA with Tukey's multiple comparison test.



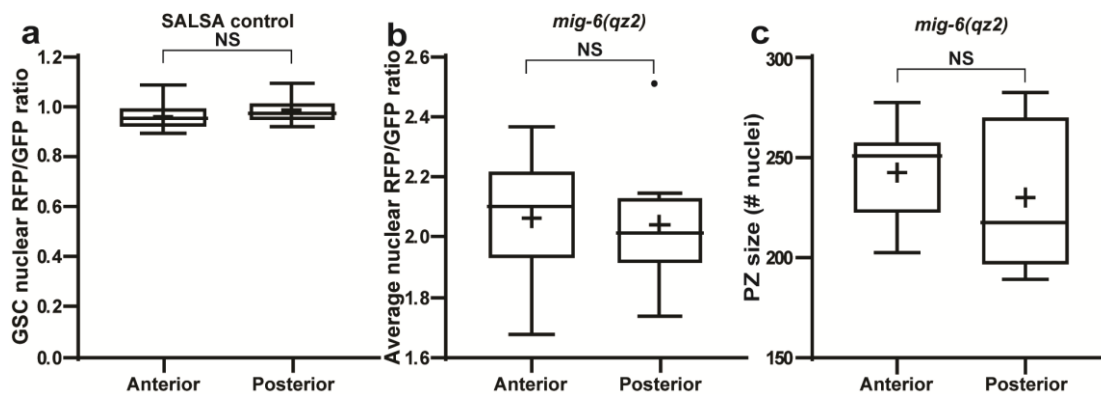
posterior: Kruskal-Wallis with Dunn's multiple comparisons test. **(d)** Representative single focal plane image of a DTC containing region of a mid L4 hermaphrodite with endogenous *MIG-6L::mNG*, in control (left) or *qz2* mutants (right).



**Extended Data Figure 2. Reduced *mig-6L* function does not impact *Plag-2::GFP* or *GLP-1(NICD)::GFP* expression.** **(a)** Boxplot scoring the total *Plag-2::GFP* fluorescence intensity in anterior and posterior DTCs of adult hermaphrodites of the indicated genotypes (mid L4 + 24h at 15°C). Sample sizes, from left to right: 15, 12, 15, 15. **(b)** Boxplot scoring the total *GLP-1(NICD)::GFP* fluorescence intensity in anterior and posterior distal gonads of adult hermaphrodites of the indicated genotypes (mid L4 + 24h at 15°C). Sample sizes, from left to right: 16, 14, 15, 14. **(a,b)** NS, Not significant ( $p > 0.05$ ) by **(a)** Kruskal-Wallis with Dunn's multiple comparisons **(b)** one way ANOVA with Tukey's multiple comparison test.

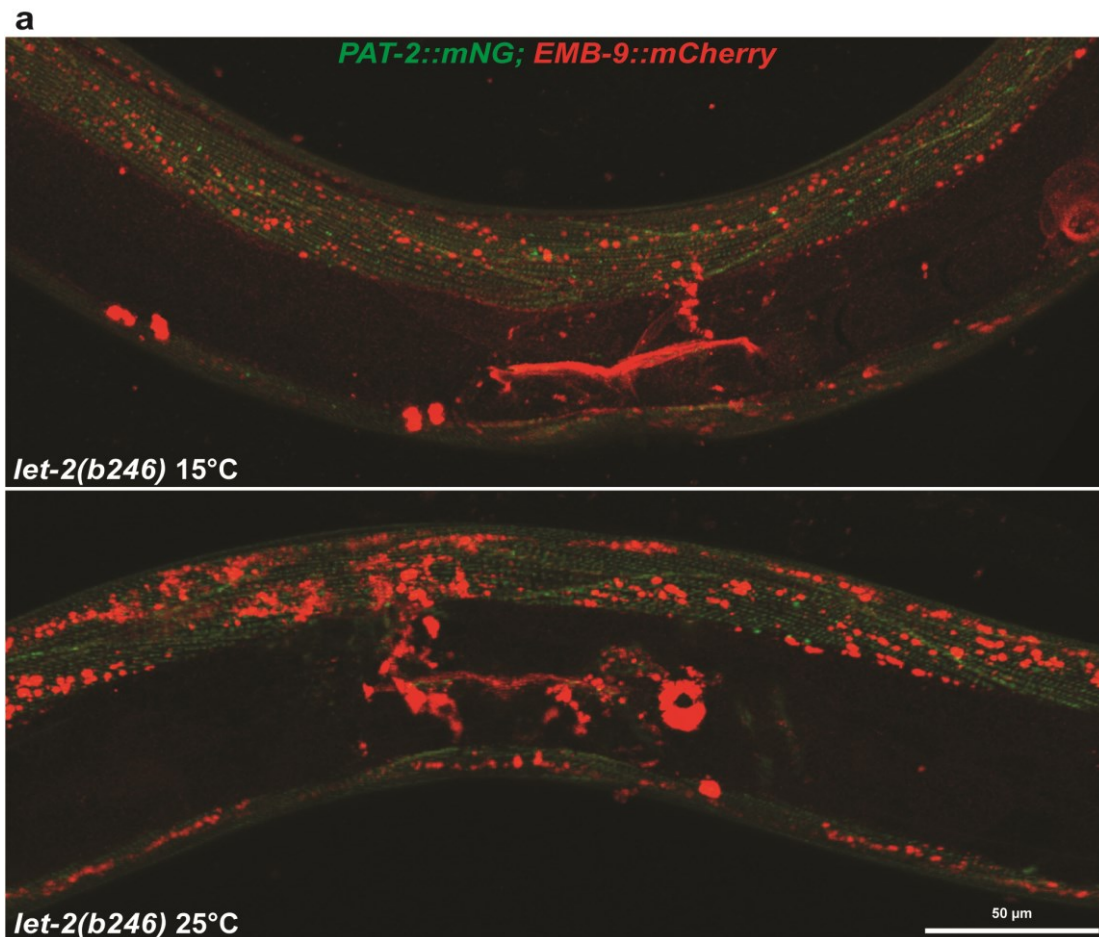


**Extended Data Figure 3. Effects of Notch signaling mutations on DTC-associated and global *EMB-9::mCherry* levels.** (a) Boxplots scoring the average *EMB-9::mCherry* fluorescence intensity overlapping with anterior (left) or posterior (right) DTCs of control and *glp-1(lf)* adult hermaphrodites (15°C until L2 + 40 hours at 25°C). Sample sizes, from left to right: 14, 18, 11, 16. (b) Boxplots scoring the average *EMB-9::mCherry* fluorescence intensity overlapping with anterior (left) or posterior (right) DTCs of control and *glp-1(gf)* adult hermaphrodites raised in parallel. Sample sizes, from left to right: 14, 15, 11, 10. (a,b) Note that when animals were upshifted to 25°C from the L2 stage, the antero-posterior asymmetry in DTC-AC levels seen at 15°C in control hermaphrodites (Fig. 2b) is no longer detected. (c) Boxplot scoring the average *EMB-9::mCherry* fluorescence intensity in a  $\approx 40 \times 20 \times 5 \mu\text{m}$  thick body wall muscle section (see Extended data Video 3) of adult hermaphrodites of the indicated genotypes (15°C until L2 + 40 hours at 25°C). Sample sizes, from left to right: 14, 11, 12, 10, 12. (d) Boxplot scoring the average *EMB-9::mCherry* fluorescence intensity in a  $\approx 20 \times 10 \times 1 \mu\text{m}$  thick distal gonad basement membrane section (see Extended data Video 3) located 20  $\mu\text{m}$  from the DTC body of adult hermaphrodites of the indicated genotypes (15°C until L2 + 40 hours at 25°C) Sample sizes, from left to right: 15, 11, 13, 16, 15. Alleles: *glp-1(e2141)lf*, *glp-1(ar202)gf*, *gld-3(q730)*, *nos-3(q650)*. (a-d) Asterisks (\*) mark significant differences versus the control. One asterisk,  $p < 0.05$ ; two asterisks,  $p < 0.01$ ; by (a) Welch's t-test, (b) unpaired two-tailed t-test, (c,d) Brown-Forsythe and Welch's ANOVA with Dunnett's T3 multiple comparisons test.



**Extended Data Figure 4. Switchless SALSA baseline fluorescence ratios and Notch activity in *mig-6(qz2)* mutants.**

(a) Boxplot scoring baseline RFP/GFP fluorescence in anterior and posterior GSCs (located 1 to 5 cell diameters from the DTC) of SALSA switchless controls. Sample sizes, from left to right: 12, 11. (b) Boxplot scoring Notch activity in anterior and posterior gonad arms of *mig-6(qz2)* mutants, based on the average GSC SALSA RFP/GFP ratio. Sample sizes, from left to right: 12, 10. (c) Boxplot scoring the number of nuclei in *mig-6(qz2)* anterior and posterior PZs. Sample sizes, from left to right: 10, 10. (a-c) NS, Not significant ( $p > 0.05$ ) by (a-c) unpaired two-tailed t-test.



**Extended data Figure 5. Global *EMB-9::mCherry* distribution in *let-2(b246)* mutants.**

(a) Representative Imaris-generated 3D views showing a vulva centered section of *let-2(b246)* adult hermaphrodites grown for 24 hours after the mid-L4 stage at the permissive (15°C, top), or restrictive (25°C, bottom) temperature. A *PAT-2::mNG* transgene marks M-lines in the body wall muscles<sup>134</sup> (green), and an *EMB-9::mCherry* transgene labels COL IV<sup>110</sup> (red). Animals show obvious muscle COL IV accumulation and reduced basement membrane COL IV levels under restrictive conditions (25°C).

Extended data table 1

Strain	Genotype	Reference
N2	WT	Brenner <sup>20</sup>
BS4048	<i>glp-1(q175); tnl39[GLP-1::GFP::3xFLAG]</i>	Saravanapriah Nadarajan, David Greenstein, and Tim Schedl, personal communication
CB4037	<i>glp-1(e2141)lf III</i>	<i>Kodoyianni, et al.</i> <sup>114</sup>
GC833	<i>glp-1(ar202)gf III</i>	<i>Pepper, et al.</i> <sup>105</sup>
GS9317	<i>arSi85[Pmex-5::GFP::TCUT::mCherry::H2B::tbb-2 3'UTR] I</i>	<i>Shaffer and Greenwald</i> <sup>88</sup>
GS9447	<i>arSi85[Pmex-5::GFP::TCUT::mCherry::H2B::tbb-2 3'UTR] I; glp-1(ar648) III</i>	<i>Shaffer and Greenwald</i> <sup>88</sup>
LP193	<i>cpSi20[Pmex-5::TAGRFPT::PH::tbb-2 3'UTR; unc-119(+)]II; unc-119(ed3)III</i>	<i>Heppert, et al.</i> <sup>112</sup>
NK364	<i>qyls46[EMB-9::mCherry] X</i>	<i>Ihara, et al.</i> <sup>110</sup>
UM367	<i>glp-1(ar202)gf III; mig-6(qz2)V</i>	This paper
UM385	<i>qzEx5[mig-6L((+)pZH117)]; Pmyo-3::mCherry]</i>	This paper
UTR162	<i>mig-6(qz2)V</i>	This paper
UTR229	<i>qls57[Plag-2::GFP; unc-119(+)]II; qyls46[EMB-9::mCherry] X</i>	This paper
UTR236	<i>cpSi20[Pmex-5::TAGRFPT::PH::tbb-2 3'UTR; unc-119(+)]II; unc-119(ed3)III; glp-1(q175) tnl39[GLP-1::GFP::3xFLAG]III</i>	This paper
UTR237	<i>cpSi20[Pmex-5::TAGRFPT::PH::tbb-2 3'UTR; unc-119(+)]II; unc-119(ed3)III; glp-1(q175) tnl39[GLP-1::GFP::3xFLAG]III; mig-6(qz2)V</i>	This paper
UTR246	<i>qls57[Plag-2::GFP; unc-119(+)]II; mig-6(qz2) V; qyls46[EMB-9::mCherry] X</i>	This paper
UTR269	<i>fog-1(q785) I/hT2 [bli-4(e937) let-?(q782) qls48] (I;III); glp-1(ar202)gf III</i>	<i>Narbonne, et al.</i> <sup>130</sup>
UTR289	<i>cpSi20[Pmex-5::TAGRFPT::PH::tbb-2 3'UTR; unc-119(+)]II; glp-1(q175) tnl39[GLP-1::GFP::3xFLAG]III; lon-2(e678)X</i>	This paper
UTR312	<i>qls57[Plag-2::GFP; unc-119(+)]II; glp-1(e2141)III; qyls46[EMB-9::mCherry] X</i>	This paper
UTR317	<i>qls57[Plag-2::GFP; unc-119(+)]II; lon-2(e678) qyls46[EMB-9::mCherry] X</i>	This paper
UTR319	<i>qls57[Plag-2::GFP; unc-119(+)]II; glp-1(ar202)gf III; qyls46[EMB-9::mCherry] X</i>	This paper
UTR343	<i>qls57[Plag-2::GFP; unc-119(+)]II; daf-7(e1372)III; qyls46[EMB-9::mCherry] X</i>	This paper
UTR344	<i>cpSi20[Pmex-5::TAGRFPT::PH::tbb-2 3'UTR + unc-119(+)]II; daf-7(e1372); GLP-1(q175)III; tnl39[GLP-1::GFP::3xFLAG]IV</i>	This paper
UTR385	<i>qls56[Plag-2::GFP; unc-119(+)]V; qyls46[EMB-9::mCherry] X</i>	This paper

UTR386	<i>arSi85[Pmex-5::GFP::TCUT::mCherry::h2b::tbb-2 3'UTR]I; mig-6(qz2)V</i>	This paper
UTR387	<i>arSi85[Pmex-5p::GFP::TCUT::mCherry::h2b::tbb-2 3'UTR] I; glp-1(ar648)III; mig-6(qz2)V,</i>	This paper
UTR402	<i>gld-3(q730) nos-3(q650)/mIn1 [mIs14 dpy-10(e128)]II; qIs56[Plag-2::GFP; unc-119(+)]V; qyIs46[EMB-9::mCherry] X</i>	This paper
UTR403	<i>gld-3(q730) nos-3(q650)/mIn1 [mIs14 dpy-10(e128)]II; glp-1(e2141)III; qIs56[Plag-2::GFP; unc-119(+)]V; qyIs46[EMB-9::mCherry] X</i>	This paper
UTR433	<i>glp-1(ar202)gf III; mig-6(qz2)V; qzEx5[mig-6L(+); Pmyo-3::mCherry]</i>	This paper
UTR434	<i>arSi85[Pmex-5p::GFP::TCUT::mCherry::h2b::tbb-2 3'UTR] I; glp-1(ar648)III; let-2(b246)X</i>	This paper
UTR447	<i>arSi85[Pmex-5p::GFP::TCUT::mCherry::h2b::tbb-2 3'UTR] I; let-2(b246)X</i>	This paper
UTR450	<i>qIs57[Plag-2::GFP; unc-119(+)]II; qyIs46[EMB-9::mCherry] let-2(b246)X</i>	This paper
UTR453	<i>arSi85[Pmex-5p::GFP::TCUT::mCherry::h2b::tbb-2 3'UTR] I; mig-6(oz113)V/nT1[qIs51]IV;V</i>	This paper

Extended data table 2

name	Description	Primer (5'->3')	Reference
pCFJ104	<i>Pmyo-3::mCherry</i>		Frokjaer-Jensen, et al. 135
pKSII	Used as filler DNA		
pPOM18	pDD162 (ref) + sgRNA1 for making <i>mig-6L::mNG::5XFLAG</i>	AAATTTAAAATTATGAACCCG TTTAGAGCTAGAAATAGCAA GT  CAAGACATCTCGCAATAGG	This paper
pPOM19	<i>mig-6L::mNG::5Xflag</i> sgRNA2(Made from KLD recircularised PCR on pDD162)	Forward:ATAATTTTAAATTTT AAGTTGTTTTAGAGCTAGAAA TAGCAAGT Reverse:CAAGACATCTCGCAA TAGG	This paper
pPOM20	<i>mig-6L::mNG::5Xflag</i> repair template for N2 worms. AvrII and SpeI digested pDD268 [Dickinson, et al. <sup>131</sup> ] and homology arms amplified from N2 genomic DNA were assembled by Gibson assembly.	Forward:ACGTTGTAAAACGA CGGCCAGTCGCCGGCATTACG CCTCCACTTTT Reverse:CATCGATGCTCCTGA GGCTCCCGATGCTCCGAAGT AAAATTATGAACCCGTGTGCA AGT  Forward:CGTGATTACAAGGA TGACGATGACAAGAGATAAG TTTGATTTTTGATTTCAAAT TTTC Reverse:GGAAACAGCTATGA CCATGTTATCGATTTCCAGGT AAGGCAGGGAAATGA	This paper
pPOM21	<i>mig-6L(qz2)::mNG::5Xflag</i> repair template for <i>mig-6(qz2)</i> worms. AvrII and SpeI digested pDD268 [Dickinson, et al. <sup>131</sup> ] and homology arms amplified from UTR162 genomic DNA were assembled by Gibson assembly.	Forward:ACGTTGTAAAACGA CGGCCAGTCGCCGGCATTACG CCTCCACTTTT Reverse:CATCGATGCTCCTGA GGCTCCCGATGCTCCGAAGT AAAATTATGAACCCGTGTGTA AGT  Forward:CGTGATTACAAGGA TGACGATGACAAGAGATAAG TTTGATTTTTGATTTCAAAT TTTC Reverse:GGAAACAGCTATGA CCATGTTATCGATTTCCAGGT AAGGCAGGGAAATGA	This paper
pZH117	<i>mig-6L</i> genomic/cDNA minigene		Kawano, et al. <sup>3</sup>

[https://drive.google.com/file/d/1z6kMZOpGltPzDPPj7\\_AXzi-7lrsBv\\_d/view?usp=sharing](https://drive.google.com/file/d/1z6kMZOpGltPzDPPj7_AXzi-7lrsBv_d/view?usp=sharing)

### **Extended data Video 1. Cleaving assay workflow**

The video starts with a close-up of a distal (distal is to the right) *GLP-1(NICD)::GFP; Pmex-5::TAGRFPT::PH* gonad section of a control adult (mid L4 + 24h at 15°C) in which the green and red channels are overlaid. Then, a first 3D model is generated over the GSC membranes to generate a red alveoli-like structure. Next, another red surface is generated to enwrap the distal gonad as a whole and is used to delete the GFP locating outside of this object. Finally, images showing the total distal gonad *GLP-1(NICD)::GFP* signal, the *GLP-1(NICD)::GFP* signal localizing to the plasma membrane, and the *GLP-1(NICD)::GFP* localizing OFF from the membranes are successively shown.

<https://drive.google.com/file/d/1YONyVTLBD3pbUWT2I9BMKxnHzhLImqKz/view?usp=sharing>

### **Extended data Video 2. SALSA quantification workflow**

The video begins with a 3D view of the distal gonad arms of the control adult hermaphrodite (15°C until mid L4 + 24h at 25°C) shown in Fig.5b. Spot clouds are first added for both gonad arms, and most aberrantly placed spots that do not correspond to germ nuclei are manually deleted. Further editions are made to preserve only the five first distal rows of germ nuclei for both gonad arms, and to delete any spot that are not accurately centered on a nucleus.

<https://drive.google.com/file/d/1Ov6RXbkN0votR540aTf7VBfTadEHE9h3/view?usp=sharing>

### **Extended data Video 3. Body wall muscle and gonad basement membrane COL IV quantification workflow**

The video starts with a merge of the *Plag-2::GFP* and *EMB-9::mCherry* signals in a control adult hermaphrodite (mid L4 + 24h at 15°C). First, a 3D model is thresholded based on the red channel to simultaneously fit body wall muscle and gonad basement membrane sections. Next, a  $\approx 40 \times 20 \times 5 \mu\text{m}$  thick body wall muscle section (shown in red) is extracted from the body wall muscle to evaluate its average *EMB-9::mCherry* fluorescence intensity. A smaller  $\approx 20 \times 10 \times 1 \mu\text{m}$  thick distal gonad basement membrane section, located 20  $\mu\text{m}$  from the DTC body, is then extracted, this time to obtain the average distal gonad basement membrane *EMB-9::mCherry* fluorescence intensity.



## Chapter III

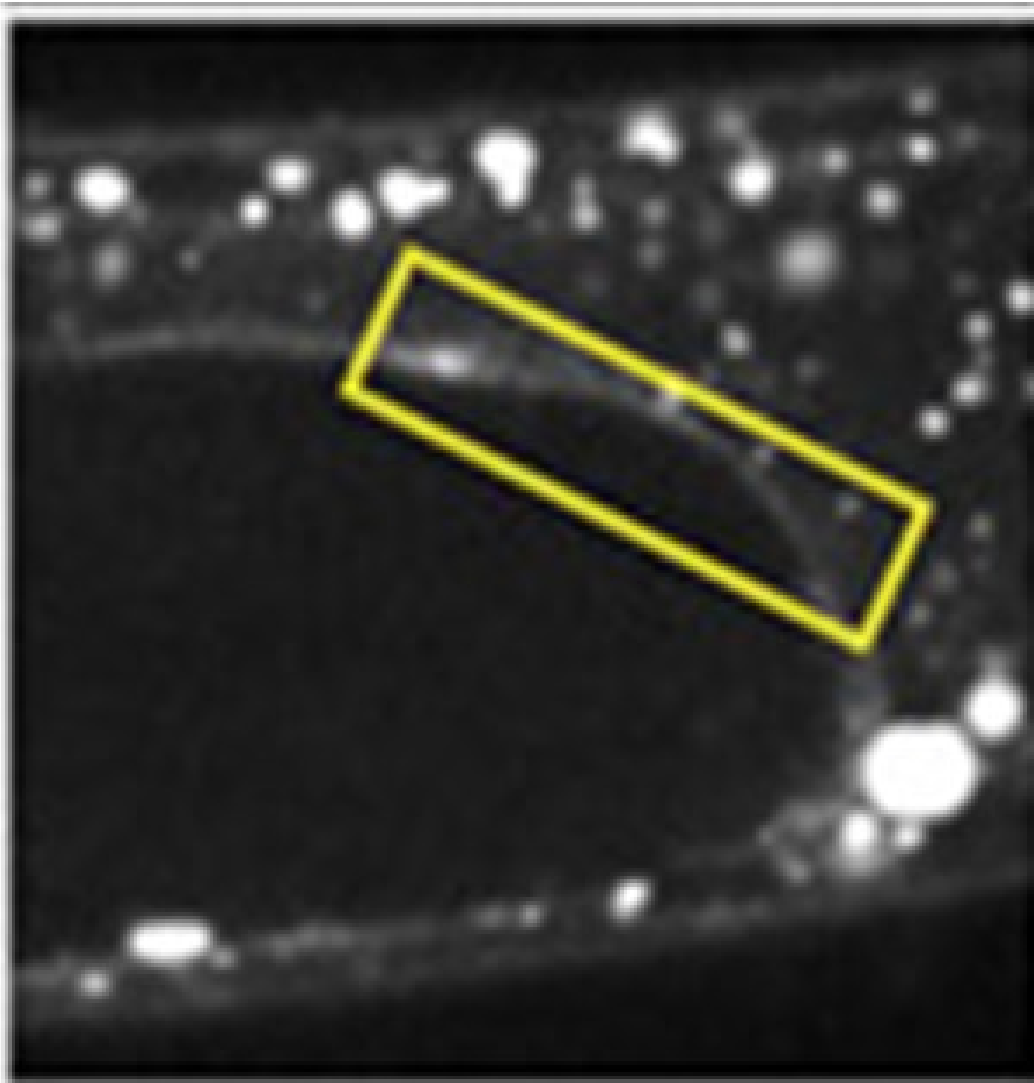
### Discussion

In the following discussion, we will return to the content presented in the article while outlining both minor and major results and trying to appreciate how they integrate into the field of actual knowledge.

#### 3.1 MIG-6 PLAC domain

As previously mentioned, the precise function of the PLAC domain remains elusive to date. While our findings do not yet provide a definitive answer, they offer some insights.

Following their work, Kawano et al., suggested that *mig-6* may play a role in regulating the localisation or activity of ADAMTS in the gonadal basement membrane during development and DTC migration<sup>3</sup>. More recently, Keeley et al., based on their findings using the *mig-6L(0)* allele, proposed that it might not be directly involved in collagen remodelling, as they did not observe any fibrotic phenotype in those mutants. However, our research indicates that DTC-AC levels are increased in the *mig-6(qz2)* mutants<sup>2</sup>. This apparent contradiction can potentially be attributed to methodological differences. Keeley et al.<sup>2</sup> quantified collagen in the gonadal basement membrane using a single, mid-dorsal line measuring 0.5 wide and 4.5  $\mu\text{m}$  long on a single confocal z-slice, which represent a very small fraction of the whole structure (Fig. 25). In contrast, we employed 3D models encompassing the entire DTC associated basement membrane region (see Chapter 2 Fig. 2). It is worth pointing out that MIG-6L is expressed by the DTC<sup>3</sup>. Our finding, therefore, challenges the current understanding of *mig-6L* and its PLAC domain function and suggests that it may play a role in distal collagen remodelling in the *C. elegans* gonad.



**Figure 25: Keeley et al. COL IV quantification**

Picture of a single confocal z-stack slice near the gonad bend where the collagen was quantified in the basement membrane (white line inside the yellow box). Adapted from Keeley, et al. <sup>2</sup>.

### **3.2 How does *mig-6(qz2)* interact with *glp-1(qr202)*?**

At first, we had difficulty explaining how *mig-6(qz2)* was enhancing the tumorous phenotype of *glp-1(ar202)* mutants. We can now propose that it does so through its impact on COL IV deposition in the basement membrane at the interface between the DTC and the GSCs. Even in permissive conditions, *glp-1(ar202)* animals still produce a slightly altered protein<sup>105</sup> that causes tumour formation approximately 10 % of the time (see Chapter 2, Fig. 1b). This, combined with an increase in COL IV levels further promoting Notch activity, could, therefore, explain the synergistic interaction between the two mutants.

### 3.3 Anterior/posterior gonad asymmetry

Our analysis unveiled a notable anteroposterior asymmetry in DTC-AC levels, resulting in lower Notch activation and a slightly smaller progenitor zone (PZ) size in wild-type posterior gonad arms of worms raised at 15°C (see Chapter 2 Fig. 5e). This result was surprising as there are very few instances of papers reporting differential effects on the anterior and posterior gonad arms<sup>3,136</sup>. *C. elegans*' two gonad arms have always been regarded as being exactly symmetrical, ever since the very early studies<sup>137</sup>, motivating the pooling of anterior and posterior gonad data by most investigators.

Consistent with this, the difference seems to apply only to animals raised at 15°C, as our experiments conducted under other conditions (see Extended Data Fig. 3a) did not display this antero-posterior difference. In most cases in the literature, experiments are performed at 20°C. Even though this anteroposterior asymmetry appears to be specific to a growing temperature of 15°C, this observation highlights the need for future caution when studying seemingly symmetrical structures.

### 3.4 Type IV collagen promotes Notch ligand/receptor activity.

At first, the results we obtained from assessing DTC-AC levels and cleaving assay allowed us to highlight a correlation between COL IV levels and Notch activity. At this point, each time we observed an increase in DTC-AC (see Chapter 2 Fig. 2), it was accompanied by an increase in Notch signalling, reflected by the higher NICD OFF-membrane (activated) levels (see Chapter 2 Fig. 3c,d). Yet, in wild-type animals, where DTC-AC is significantly lower in the posterior versus the anterior arm, we could not at first detect any significant differences in OFF-membrane NICD levels (see Chapter 2 Fig. 2b,3b). However, using the recently developed in vivo Notch activity SALSA reporter<sup>88</sup>, we were able to detect lower Notch activity in the animal's posterior gonad (see Chapter 2 Fig. 5d). Yet, at this point, our results were still strictly correlative, and apart from the lower levels of posterior DTC-AC in the wild type, we had no examples of mutants that caused a decrease in collagen levels. We tried to reduce COL IV levels by RNAi, but it had too severe and global impact on COL IV silencing and resulted in basement membrane rupture, which prevented analysis (see

Fig. 24). In *C. elegans*, RNAi is easily achieved by feeding the worm bacteria expressing specific double Stranded DNA<sup>138</sup>. We tried to dilute the COL IV RNAi bacteria to perhaps obtain a milder effect and observe a decrease in DTC-AC all while avoiding gonad rupture. In these more favourable conditions, which did not lead to gonad rupture, we however did not detect any significant reduction in DTC-AC. Since we failed to reduce COL IV by RNAi in a way that still allowed us to quantify Notch activity, meaning an absence of gonad rupture, we had to use another approach. Still aiming to prove that a decrease in DTC-AC levels would lead to a reduction of Notch activity, we next used a temperature-sensitive mutant of *let-2*, coding for the COL IV  $\alpha 2$  chain. After some tests, we found conditions that did not lead to systematic gonad rupture. Still, we were surprised to find an increase of both DTC-AC levels and Notch activity as opposed to the expected decrease we were after (see Chapter 2, Fig. 5g). We are confident that the gonad basement membrane COL IV content was indeed decreased as we observed gonad rupture about half of the time and an increase in muscle sequestered COLV IV levels (see Chapter 2 Extended Data Fig. 5). Before this experiment with *let-2*, we could only claim that there was a correlation between COL IV levels and Notch activity. However, now that we had altered only one of the COL IV chains and still observed a change in Notch activity, we can conclude that COL IV levels promotes Notch activity.

This goes against the recent literature, where fibrosis is instead seen as a consequence of high Notch activity<sup>70,72,93,94,139,140</sup>. An *in vitro* experiment found that COL IV binds to both the Notch ligand and receptor<sup>141</sup>. To fit with the literature, it was proposed that COL IV binding would inhibit Notch activity. Our results now suggest the opposite, namely that COL IV binding to the notch ligand and/or receptor promotes Notch signalling.

To our knowledge, there is no *in vivo* evidence in the literature that Notch signalling would directly promote the expression of collagen IV. However, there has been a multitude of trials up to this very day that aim to reduce fibrosis by targeting Notch signalling, therefore assuming that it is a consequence of high Notch signalling. The main issue with these approaches is that they mostly rely on gamma-secretase inhibitors to target Notch signalling<sup>78</sup>. In Notch signalling, the gamma-secretase is needed for the release of the NICD upon the receptor and ligand binding. Thus,

inhibiting the gamma-secretase prevents NICD release and effectively prevents Notch signalling. The issue as already stated is that gamma-secretase is not specific to Notch signalling<sup>78,79</sup>. Therefore, we think that in those articles, when they improved fibrosis by inhibiting Notch activity, it may instead be due to the unspecific impact of the gamma-secretase inhibitor that, amongst multiple other processes, hinders parts of TGF- $\beta$  signalling, and at the same time COL IV synthesis.

### **3.5 Notch activity does not promote collagen production.**

Still in opposition to the literature, our results clearly showed that loss of Notch activity does not cause a decrease in COL IV production. We rather observed a notable increase in COL IV levels throughout the organism (see Chapter 2 Fig. 4d,e and Extended Data Fig. 3). At first, when comparing only the *glp-1* gain or loss of function mutants to the controls, we could have hypothesised that Notch activity was inhibiting collagen production as its loss instead led to such increase of COL IV levels and its overactivation to a decrease. Next, we performed further experiments with the *gld-3 nos-3; glp-1(lf)* triple mutants, that lack GLP-1 activity but still form GSC tumours because they also lack *gld-3* and *nos-3* activity, which are redundantly required for differentiation<sup>25,142</sup>. This triple mutant, while its distal germline was devoid of Notch receptor activity but also had its downstream inhibitory targets removed, showed, for the most part, no changes in COL IV levels, indicating that GLP-1 receptor activation per se, does not inhibit COL IV synthesis either (see Chapter 2 Fig. 4e). Further research will be needed to fully understand how COL IV levels are adjusted, but we can propose that it has something to do with the state of the germline, whether it be linked to the size of the GSC pool or the presence of differentiated germ cells. On the one hand, in *glp-1(lf)* mutants, the loss of Notch activity causes the loss of the GSC pool as they all enter differentiation. On the other hand, in the *glp-1(gf)* mutants, there is no production of differentiated cells, but there is GSC tumour formation. In addition to proposing that COL IV promotes Notch activity and not the other way around, we also suggest that Notch activity does not directly influence COL IV levels. Notch signalling is a highly conserved pathway, making it safe to propose that our results may be transposable to mammals, as many other cellular processes identified with this model are<sup>143,144</sup>. This finding is of great importance if it

proves to be accurate; even specific inhibition of Notch in human disease, for example, could, in fact, worsen fibrosis instead of alleviating it.

### **3.6 Mutation in the *daf-7* gene could cause changes in COL IV levels through its impact on Notch activity.**

We had initially chosen to study the *daf-7* mutant while trying to alter COL IV levels as it was involved in TGF- $\beta$  signalling. However, the literature stated, and we confirmed that it caused reduced *lag-2* expression (see Chapter 2 Fig. 4b)<sup>56</sup>. It also caused a dramatic increase in DTC-AC levels (see Chapter 2 Fig. 4c). Considering previously discussed results, we propose that this increase in DTC-AC levels that we observed is in fact due to the decrease of the Notch ligand levels, LAG-2 which result in a phenotype like, yet not as severe as the *glp-1(lf)* mutants where complete loss of GLP-1 activity also led to notable increase in DTC-AC levels. An alternative hypothesis could be that *daf-7* is controlling COL IV levels independently from *glp-1*.

### **3.7 Conclusion**

In conclusion, a strength of our study lies in the specificity of our approach to genetically alter single components of the Notch signalling or extracellular matrix. While severe Notch or collagen mutations in more complex organisms are often embryonic lethal<sup>120-122,145</sup>, the generation of conditional and tissue-specific alleles will be necessary to assess whether the relationship between type IV collagen and Notch activity that we've uncovered here in *C. elegans* is conserved<sup>143,146-148</sup>. Further work will also be necessary to elucidate exactly how collagen levels affect Notch receptor activation. Interestingly, collagens have been reported to directly interact with Notch signaling components<sup>141</sup>, potentially providing a starting point.

Our work also gives some new insights into the role of the *mig-6* PLAC domain. Indeed, loss of the MIG-6L PLAC domain causes defects in normal gonad migration and posterior COL IV deposition, suggesting that this domain is necessary for the interaction of MIG-6L with the ADAMTS required for properly regulating COL IV disassembly.

We challenge the paradigm that labels fibrosis as the consequence of Notch signalling. We even showed that the COL IV levels are not directly influenced by Notch receptor

activity but rather by the downstream consequences of GLP-1 signalling, the loss of the GSC pool. These results could change how researchers look at the interaction between Notch signalling and fibrosis that are both increased in cancer and many fibrosis related diseases.

Gamma-secretase inhibitors are presently seen as molecules of choice for inhibition of Notch signalling. These molecules have highly nonspecific effects as they inhibit the cleavage of over 90 other substrates<sup>76</sup>. Furthermore, Notch-targeting therapies have overall failed to meet expectations<sup>101</sup>. In 2023, though, the first and only phase 3 trial occurred for Nirogascestat, a gamma-secretase inhibitor for treating desmoid tumours, also known as aggressive fibromatosis. It showed promising results while, of course, having some adverse effects<sup>149</sup>. We, however, suggest the positive impact may not only be due to the inhibitor's effect on Notch activity. It could also be, in fact, related to the highly fibrotic nature of this disease and the more direct downregulation of collagen synthesis by the gamma-secretase inhibitors? Future trials will be needed using more specific molecules that affect specific collagen-related pathways.

### 3.8 Research Perspectives

#### 3.8.1 How exactly does COL IV promote Notch activity?

From our actual data, we can, at this point, only propose a general model (see Chapter 2 Fig. 5i) based on the solid evidence that there is more release of NICD in the presence of more COL IV, for the same amount of LAG-2. In this work, we focussed on COL IV as it is the main structural component of the basement membrane. However, as we introduced it (Fig. 12), the basement membrane is a complex and dynamic assembly of many proteins. It is, therefore, not impossible that COL IV could promote Notch receptor activity indirectly. However, since *in vitro* experiments showed that mammalian COL IV can bind both to the Notch ligand and receptor<sup>141</sup>, a direct effect is our favoured hypothesis. It would, therefore, be interesting to test whether this interaction occurs *in vivo* in the *C. elegans* germline. One way to achieve this would be the use of split fluorescent proteins<sup>150</sup>. We would split-tag endogenous Notch receptors and ligands to measure their binding to one another in the distal part of the germline. We could express a split-FP version of another ligand in the DTC to make

sure that the signal results from specific Delta-Notch binding. After validating our approach, we would next tag one of the two COL IV components and find out whether it interacts with our previously generated split-FP GLP-1 or LAG-2. If one of *C. elegans* two  $\alpha$ -chain COL IV indeed acted the same way and binds to either or both the ligand and receptor, we could propose that COL IV may spatially stabilise the interaction between the two proteins, thereby facilitating NICD release. This could be tested by modified yeast two-hybrid assays, which would allow us to determine if binding occurs between these proteins<sup>33</sup>.

Next, we could also ask if the increase in OFF-membrane NICD that we observed is due to more frequent, and/or longer interactions between the ligand and receptor. This could be investigated using Förster resonance energy transfer (FRET) which has already been adapted for use in *C. elegans*<sup>24</sup>. This technique allows for the real-time measurement of distance between tagged fluorescent proteins with nanometer precision<sup>24</sup>.

### **3.8.2 Investigating the role of TGF- $\beta$ signalling in COL IV production.**

As fibrosis is a recurrent problem in multiple diseases, and as we found that changes in COL IV production are not a direct consequence of Notch activity, it would be highly interesting to define how exactly COL IV levels are adjusted in response to diverse biological cues. We believe that the TGF- $\beta$  pathway has a very important role to play in the regulation of COL IV levels and would require further investigation. In this study, we only used *daf-7* and *lon-2* mutants that are, respectively, a TGF- $\beta$  pathway ligand and extracellular regulator. Although ample research in *C. elegans* identified many other components of the TGF- $\beta$  pathway (Fig. 16), identifying which ones are specifically promoting COL IV synthesis, however, remains complex. An excellent example of this is our experiment with *daf-7* mutants where we found changes in COL IV levels that could in fact be the indirect consequence of the reduced Notch activity, as these mutants also had lower *lag-2* expression.

To try and narrow down the number of genes we could investigate in this complex pathway, we can first go through the known role of its diverse components in *C. elegans* (Fig. 16).

As *daf-4* is the only type I receptor in *C. elegans*, it would be unwise to use the mutant allele of this gene as it would automatically lead to the inhibition of both the dauer



and the Sma/Mab TGF $\beta$ -related pathway (Fig. 16,17). Next, we can hypothesise that *daf-1*, *daf-8* and *daf-14* would lead to, at the very least, a phenotype similar to the one observed in *daf-7* mutants and cause a decrease in LAG-2 levels. For example, removing *daf-1*, which is required for the binding of the DAF-7 ligand, should replicate the phenotype of *daf-7* mutants. Alternatively, removing *daf-8* and *daf-14*, which are downstream of *daf-7*, should lead to the same problem as with *daf-1*.

That still leaves us with 20 genes that would need to be investigated for their impact on COL IV levels while ensuring they don't affect the abundance of the Notch ligand. However, a possibility is that the Sma/Mab TGF $\beta$ -related pathway (Fig. 17) component will be more directly involved in fibrosis as they work in association with BMP-like ligands<sup>61-64,151</sup>. But before testing all the genes from this part of the pathway, a first test could make use of *tag-68* mutants, which is an ortholog to the human SMAD6 which inhibits R-SMAD phosphorylation by competing with them<sup>152</sup>. Interestingly the *tag-68* mutants were not shown to cause defect in dauer formation, which makes them interesting candidates as they may not affect *lag-2* expression like *daf-7*, which act in dauer TGF- $\beta$ -related pathway, and therefore could be more specific to the regulation of collagen synthesis<sup>153</sup>. We could hypothesise that *tag-68* mutants that can no longer downregulate the Sma/Mab TGF $\beta$ -related pathway will have increased COL IV levels comparable to what we observed in *gfp-1(lf)* worms. If it is the case, it would mean that this pathway deserves further investigation, the end goal being able to draw a clear model linking the SC pool state all the way down to COL IV synthesis.

### **3.8.3 Investigating the impact of gamma-secretase inhibitors on COL IV levels.**

We critiqued the use of gamma-secretase inhibitors as a way to alleviate fibrosis through the inhibition of Notch signalling. However, to strengthen our position we should observe the impact of such inhibitors on both DTC-AC and global COL IV levels. A protocol is already available for *C. elegans* and would provide interesting results by exposing our diverse mutant strains to gamma-secretase inhibitors<sup>154</sup>.

## References

- 1 Tomasetti, C. & Vogelstein, B. Cancer etiology. Variation in cancer risk among tissues can be explained by the number of stem cell divisions. *Science* **347**, 78-81, doi:10.1126/science.1260825 (2015).
- 2 Keeley, D. P. *et al.* Comprehensive Endogenous Tagging of Basement Membrane Components Reveals Dynamic Movement within the Matrix Scaffolding. *Developmental cell* **54**, 60-74 e67, doi:10.1016/j.devcel.2020.05.022 (2020).
- 3 Kawano, T. *et al.* C. elegans mig-6 encodes papilin isoforms that affect distinct aspects of DTC migration, and interacts genetically with mig-17 and collagen IV. *Development* **136**, 1433-1442, doi:10.1242/dev.028472 (2009).
- 4 Piersma, B., Hayward, M. K. & Weaver, V. M. Fibrosis and cancer: A strained relationship. *Biochimica et biophysica acta. Reviews on cancer* **1873**, 188356, doi:10.1016/j.bbcan.2020.188356 (2020).
- 5 Herpin, A., Lelong, C. & Favrel, P. Transforming growth factor-beta-related proteins: an ancestral and widespread superfamily of cytokines in metazoans. *Dev Comp Immunol* **28**, 461-485, doi:10.1016/j.dci.2003.09.007 (2004).
- 6 Trimmer, K. A.
- 7 De Strooper, B. Aph-1, Pen-2, and Nicastrin with Presenilin generate an active gamma-Secretase complex. *Neuron* **38**, 9-12, doi:10.1016/s0896-6273(03)00205-8 (2003).
- 8 Girard, L. R. *et al.* WormBook: the online review of Caenorhabditis elegans biology. *Nucleic Acids Res* **35**, D472-475, doi:10.1093/nar/gkl894 (2007).
- 9 Visvader, J. E. Cells of origin in cancer. *Nature* **469**, 314-322, doi:10.1038/nature09781 (2011).
- 10 Andersson, E. R. & Lendahl, U. Therapeutic modulation of Notch signalling--are we there yet? *Nat Rev Drug Discov* **13**, 357-378, doi:10.1038/nrd4252 (2014).
- 11 Brenner, D. R. *et al.* Projected estimates of cancer in Canada in 2022. *CMAJ* **194**, E601-E607, doi:10.1503/cmaj.212097 (2022).
- 12 Brown, J. S. *et al.* Updating the Definition of Cancer. *Mol Cancer Res* **21**, 1142-1147, doi:10.1158/1541-7786.MCR-23-0411 (2023).
- 13 The Oxford English Dictionary. *Br Med J* **1**, 311-312 (1928).
- 14 Reya, T., Morrison, S. J., Clarke, M. F. & Weissman, I. L. Stem cells, cancer, and cancer stem cells. *Nature* **414**, 105-111, doi:10.1038/35102167 (2001).
- 15 Preston, B. D., Albertson, T. M. & Herr, A. J. DNA replication fidelity and cancer. *Semin Cancer Biol* **20**, 281-293, doi:10.1016/j.semcancer.2010.10.009 (2010).
- 16 Zakrzewski, W., Dobrzynski, M., Szymonowicz, M. & Rybak, Z. Stem cells: past, present, and future. *Stem Cell Res Ther* **10**, 68, doi:10.1186/s13287-019-1165-5 (2019).
- 17 Drake, J. W., Charlesworth, B., Charlesworth, D. & Crow, J. F. Rates of spontaneous mutation. *Genetics* **148**, 1667-1686, doi:10.1093/genetics/148.4.1667 (1998).
- 18 Evans, M. J. & Kaufman, M. H. Establishment in culture of pluripotential cells from mouse embryos. *Nature* **292**, 154-156,

- doi:10.1038/292154a0 (1981).
- 19 Perez-Ramirez, C. A. & Christofk, H. R. Challenges in Studying Stem Cell Metabolism. *Cell Stem Cell* **28**, 409-423, doi:10.1016/j.stem.2021.02.016 (2021).
- 20 Brenner, S. The genetics of *Caenorhabditis elegans*. *Genetics* **77**, 71-94 (1974).
- 21 Consortium, C. e. S. Genome sequence of the nematode *C. elegans*: a platform for investigating biology. *Science* **282**, 2012-2018, doi:10.1126/science.282.5396.2012 (1998).
- 22 Sulston, J. E. & Horvitz, H. R. Post-embryonic cell lineages of the nematode, *Caenorhabditis elegans*. *Dev Biol* **56**, 110-156, doi:10.1016/0012-1606(77)90158-0 (1977).
- 23 Kimble, J. E. & White, J. G. On the control of germ cell development in *Caenorhabditis elegans*. *Dev Biol* **81**, 208-219, doi:10.1016/0012-1606(81)90284-0 (1981).
- 24 Joshi, P. M., Riddle, M. R., Djabrayan, N. J. & Rothman, J. H. *Caenorhabditis elegans* as a model for stem cell biology. *Dev Dyn* **239**, 1539-1554, doi:10.1002/dvdy.22296 (2010).
- 25 Kimble, J. & Crittenden, S. L. Germline proliferation and its control. *WormBook : the online review of C. elegans biology*, 1-14, doi:10.1895/wormbook.1.13.1 (2005).
- 26 Penton, A. L., Leonard, L. D. & Spinner, N. B. Notch signaling in human development and disease. *Semin Cell Dev Biol* **23**, 450-457, doi:10.1016/j.semcdb.2012.01.010 (2012).
- 27 Artavanis-Tsakonas, S., Rand, M. D. & Lake, R. J. Notch signaling: cell fate control and signal integration in development. *Science* **284**, 770-776, doi:10.1126/science.284.5415.770 (1999).
- 28 Aster, J. C., Pear, W. S. & Blacklow, S. C. The Varied Roles of Notch in Cancer. *Annu Rev Pathol* **12**, 245-275, doi:10.1146/annurev-pathol-052016-100127 (2017).
- 29 Kershner, A. M., Shin, H., Hansen, T. J. & Kimble, J. Discovery of two GLP-1/Notch target genes that account for the role of GLP-1/Notch signaling in stem cell maintenance. *Proc Natl Acad Sci U S A* **111**, 3739-3744, doi:10.1073/pnas.1401861111 (2014).
- 30 Chen, J. *et al.* GLP-1 Notch-LAG-1 CSL control of the germline stem cell fate is mediated by transcriptional targets *lst-1* and *sygl-1*. *PLoS Genet* **16**, e1008650, doi:10.1371/journal.pgen.1008650 (2020).
- 31 Tam, P. P. *et al.* The Puf family of RNA-binding proteins in plants: phylogeny, structural modeling, activity and subcellular localization. *BMC Plant Biol* **10**, 44, doi:10.1186/1471-2229-10-44 (2010).
- 32 Spassov, D. S. & Jurecic, R. The PUF family of RNA-binding proteins: does evolutionarily conserved structure equal conserved function? *IUBMB Life* **55**, 359-366, doi:10.1080/15216540310001603093 (2003).
- 33 Ferdous, A. S. *et al.* Functional significance of PUF partnerships in *C. elegans* germline stem cells. *bioRxiv*, doi:10.1101/2023.02.15.528708 (2023).
- 34 Gordon, K. Recent Advances in the Genetic, Anatomical, and Environmental Regulation of the *C. elegans* Germ Line Progenitor Zone. *Journal of developmental biology* **8**, doi:10.3390/jdb8030014 (2020).
- 35 Wilson, A. *et al.* c-Myc controls the balance between hematopoietic

- stem cell self-renewal and differentiation. *Genes Dev* **18**, 2747-2763, doi:10.1101/gad.313104 (2004).
- 36 Liu, L. & Rando, T. A. Manifestations and mechanisms of stem cell aging. *J Cell Biol* **193**, 257-266, doi:10.1083/jcb.201010131 (2011).
- 37 Ceron, J. Caenorhabditis elegans for research on cancer hallmarks. *Dis Model Mech* **16**, doi:10.1242/dmm.050079 (2023).
- 38 Mohammad, K., Dakik, P., Medkour, Y., Mitrofanova, D. & Titorenko, V. I. Quiescence Entry, Maintenance, and Exit in Adult Stem Cells. *Int J Mol Sci* **20**, doi:10.3390/ijms20092158 (2019).
- 39 Michaelson, D., Korta, D. Z., Capua, Y. & Hubbard, E. J. Insulin signaling promotes germline proliferation in *C. elegans*. *Development* **137**, 671-680, doi:10.1242/dev.042523 (2010).
- 40 Narbonne, P., Maddox, P. S. & Labbe, J. C. DAF-18/PTEN signals through AAK-1/AMPK to inhibit MPK-1/MAPK in feedback control of germline stem cell proliferation. *PLoS Genet* **13**, e1006738, doi:10.1371/journal.pgen.1006738 (2017).
- 41 Robinson-Thiewes, S. *et al.* Non-autonomous regulation of germline stem cell proliferation by somatic MPK-1/MAPK activity in *C. elegans*. *Cell Rep* **35**, 109162, doi:10.1016/j.celrep.2021.109162 (2021).
- 42 Nardi, J. B., Gao, C. & Kanost, M. R. The extracellular matrix protein lacunin is expressed by a subset of hemocytes involved in basal lamina morphogenesis. *Journal of insect physiology* **47**, 997-1006, doi:10.1016/s0022-1910(01)00074-9 (2001).
- 43 Nicholson, A. C., Malik, S. B., Logsdon, J. M., Jr. & Van Meir, E. G. Functional evolution of ADAMTS genes: evidence from analyses of phylogeny and gene organization. *BMC Evol Biol* **5**, 11, doi:10.1186/1471-2148-5-11 (2005).
- 44 Nardi, J. B., Martos, R., Walden, K. K., Lampe, D. J. & Robertson, H. M. Expression of lacunin, a large multidomain extracellular matrix protein, accompanies morphogenesis of epithelial monolayers in *Manduca sexta*. *Insect biochemistry and molecular biology* **29**, 883-897 (1999).
- 45 Colige, A. *et al.* Cloning and characterization of ADAMTS-14, a novel ADAMTS displaying high homology with ADAMTS-2 and ADAMTS-3. *The Journal of biological chemistry* **277**, 5756-5766, doi:10.1074/jbc.M105601200 (2002).
- 46 Kelwick, R., Desanlis, I., Wheeler, G. N. & Edwards, D. R. The ADAMTS (A Disintegrin and Metalloproteinase with Thrombospondin motifs) family. *Genome biology* **16**, 113, doi:10.1186/s13059-015-0676-3 (2015).
- 47 Jayadev, R. & Sherwood, D. R. Basement membranes. *Curr Biol* **27**, R207-R211, doi:10.1016/j.cub.2017.02.006 (2017).
- 48 Smyth, N. *et al.* Absence of basement membranes after targeting the LAMC1 gene results in embryonic lethality due to failure of endoderm differentiation. *J Cell Biol* **144**, 151-160, doi:10.1083/jcb.144.1.151 (1999).
- 49 Timpl, R., Wiedemann, H., van Delden, V., Furthmayr, H. & Kuhn, K. A network model for the organization of type IV collagen molecules in basement membranes. *Eur J Biochem* **120**, 203-211, doi:10.1111/j.1432-1033.1981.tb05690.x (1981).
- 50 Halfter, W. *et al.* New concepts in basement membrane biology. *FEBS*

- J* **282**, 4466-4479, doi:10.1111/febs.13495 (2015).
- 51 Yurchenco, P. D., Tsilibary, E. C., Charonis, A. S. & Furthmayr, H. Models for the self-assembly of basement membrane. *J Histochem Cytochem* **34**, 93-102, doi:10.1177/34.1.3510247 (1986).
- 52 Patterson, G. I. & Padgett, R. W. TGF beta-related pathways. Roles in *Caenorhabditis elegans* development. *Trends Genet* **16**, 27-33, doi:10.1016/s0168-9525(99)01916-2 (2000).
- 53 Pawlak, J. B. & Blobe, G. C. TGF-beta superfamily co-receptors in cancer. *Dev Dyn* **251**, 137-163, doi:10.1002/dvdy.338 (2022).
- 54 Goodman, M. B. & Savage-Dunn, C. Reciprocal interactions between transforming growth factor beta signaling and collagens: Insights from *Caenorhabditis elegans*. *Dev Dyn* **251**, 47-60, doi:10.1002/dvdy.423 (2022).
- 55 Ren, P. *et al.* Control of *C. elegans* larval development by neuronal expression of a TGF-beta homolog. *Science* **274**, 1389-1391, doi:10.1126/science.274.5291.1389 (1996).
- 56 Pekar, O. *et al.* Linking the environment, DAF-7/TGFbeta signaling and LAG-2/DSL ligand expression in the germline stem cell niche. *Development* **144**, 2896-2906, doi:10.1242/dev.147660 (2017).
- 57 Savage, C. *et al.* *Caenorhabditis elegans* genes *sma-2*, *sma-3*, and *sma-4* define a conserved family of transforming growth factor beta pathway components. *Proc Natl Acad Sci U S A* **93**, 790-794, doi:10.1073/pnas.93.2.790 (1996).
- 58 Padgett, R. W., Das, P. & Krishna, S. TGF-beta signaling, Smads, and tumor suppressors. *Bioessays* **20**, 382-390, doi:10.1002/(SICI)1521-1878(199805)20:5<382::AID-BIES5>3.0.CO;2-Q (1998).
- 59 Suzuki, Y. *et al.* A BMP homolog acts as a dose-dependent regulator of body size and male tail patterning in *Caenorhabditis elegans*. *Development* **126**, 241-250, doi:10.1242/dev.126.2.241 (1999).
- 60 Savage-Dunn, C. *et al.* Genetic screen for small body size mutants in *C. elegans* reveals many TGFbeta pathway components. *Genesis* **35**, 239-247, doi:10.1002/gene.10184 (2003).
- 61 Katagiri, T. & Watabe, T. Bone Morphogenetic Proteins. *Cold Spring Harb Perspect Biol* **8**, doi:10.1101/cshperspect.a021899 (2016).
- 62 Goto, H. *et al.* Gene therapy for meniscal injury: enhanced synthesis of proteoglycan and collagen by meniscal cells transduced with a TGFbeta(1)gene. *Osteoarthritis Cartilage* **8**, 266-271, doi:10.1053/joca.1999.0300 (2000).
- 63 Wozney, J. M. *et al.* Novel regulators of bone formation: molecular clones and activities. *Science* **242**, 1528-1534, doi:10.1126/science.3201241 (1988).
- 64 Zeisberg, M. *et al.* Bone morphogenic protein-7 inhibits progression of chronic renal fibrosis associated with two genetic mouse models. *Am J Physiol Renal Physiol* **285**, F1060-1067, doi:10.1152/ajprenal.00191.2002 (2003).
- 65 Morita, K., Chow, K. L. & Ueno, N. Regulation of body length and male tail ray pattern formation of *Caenorhabditis elegans* by a member of TGF-beta family. *Development* **126**, 1337-1347, doi:10.1242/dev.126.6.1337 (1999).
- 66 Yin, J., Madaan, U., Park, A., Aftab, N. & Savage-Dunn, C. Multiple cis elements and GATA factors regulate a cuticle collagen gene in

- Caenorhabditis elegans. *Genesis* **53**, 278-284, doi:10.1002/dvg.22847 (2015).
- 67 Gumienny, T. L. *et al.* Glypican LON-2 is a conserved negative regulator of BMP-like signaling in *Caenorhabditis elegans*. *Curr Biol* **17**, 159-164, doi:10.1016/j.cub.2006.11.065 (2007).
- 68 Khalilgharibi, N. & Mao, Y. To form and function: on the role of basement membrane mechanics in tissue development, homeostasis and disease. *Open Biol* **11**, 200360, doi:10.1098/rsob.200360 (2021).
- 69 Wynn, T. A. Cellular and molecular mechanisms of fibrosis. *J Pathol* **214**, 199-210, doi:10.1002/path.2277 (2008).
- 70 Hu, B. & Phan, S. H. Notch in fibrosis and as a target of anti-fibrotic therapy. *Pharmacol Res* **108**, 57-64, doi:10.1016/j.phrs.2016.04.010 (2016).
- 71 Zhu, F. *et al.* Preventive effect of Notch signaling inhibition by a gamma-secretase inhibitor on peritoneal dialysis fluid-induced peritoneal fibrosis in rats. *Am J Pathol* **176**, 650-659, doi:10.2353/ajpath.2010.090447 (2010).
- 72 Chen, Y. *et al.* Inhibition of Notch signaling by a gamma-secretase inhibitor attenuates hepatic fibrosis in rats. *PLoS One* **7**, e46512, doi:10.1371/journal.pone.0046512 (2012).
- 73 Condorelli, A. G. *et al.* Gamma-secretase inhibitors down-regulate the pro-fibrotic Notch signaling pathway in recessive dystrophic epidermolysis bullosa. *J Invest Dermatol*, doi:10.1016/j.jid.2023.10.045 (2024).
- 74 Bielez, B. *et al.* Epithelial Notch signaling regulates interstitial fibrosis development in the kidneys of mice and humans. *J Clin Invest* **120**, 4040-4054, doi:10.1172/JCI43025 (2010).
- 75 Yonemura, Y. *et al.* Comparison of presenilin 1 and presenilin 2 gamma-secretase activities using a yeast reconstitution system. *J Biol Chem* **286**, 44569-44575, doi:10.1074/jbc.M111.270108 (2011).
- 76 Shih le, M. & Wang, T. L. Notch signaling, gamma-secretase inhibitors, and cancer therapy. *Cancer Res* **67**, 1879-1882, doi:10.1158/0008-5472.CAN-06-3958 (2007).
- 77 De Strooper, B. *et al.* A presenilin-1-dependent gamma-secretase-like protease mediates release of Notch intracellular domain. *Nature* **398**, 518-522, doi:10.1038/19083 (1999).
- 78 McCaw, T. R. *et al.* Gamma Secretase Inhibitors in Cancer: A Current Perspective on Clinical Performance. *Oncologist* **26**, e608-e621, doi:10.1002/onco.13627 (2021).
- 79 Dong, Z. *et al.* Gamma-Secretase Inhibitor (DAPT), a potential therapeutic target drug, caused neurotoxicity in planarian regeneration by inhibiting Notch signaling pathway. *Sci Total Environ* **781**, 146735, doi:10.1016/j.scitotenv.2021.146735 (2021).
- 80 Haapasalo, A. & Kovacs, D. M. The many substrates of presenilin/gamma-secretase. *J Alzheimers Dis* **25**, 3-28, doi:10.3233/JAD-2011-101065 (2011).
- 81 Kim, K. K., Sheppard, D. & Chapman, H. A. TGF-beta1 Signaling and Tissue Fibrosis. *Cold Spring Harb Perspect Biol* **10**, doi:10.1101/cshperspect.a022293 (2018).
- 82 Chen, L., Klass, C. & Woods, A. Syndecan-2 regulates transforming growth factor-beta signaling. *J Biol Chem* **279**, 15715-15718,

- doi:10.1074/jbc.C300430200 (2004).
- 83 Blair, C. R., Stone, J. B. & Wells, R. G. The type III TGF-beta receptor betaglycan transmembrane-cytoplasmic domain fragment is stable after ectodomain cleavage and is a substrate of the intramembrane protease gamma-secretase. *Biochim Biophys Acta* **1813**, 332-339, doi:10.1016/j.bbamcr.2010.12.005 (2011).
- 84 Blobe, G. C. *et al.* Functional roles for the cytoplasmic domain of the type III transforming growth factor beta receptor in regulating transforming growth factor beta signaling. *J Biol Chem* **276**, 24627-24637, doi:10.1074/jbc.M100188200 (2001).
- 85 Tian, X. *et al.* E-cadherin/beta-catenin complex and the epithelial barrier. *J Biomed Biotechnol* **2011**, 567305, doi:10.1155/2011/567305 (2011).
- 86 Zheng, G. *et al.* Disruption of E-cadherin by matrix metalloproteinase directly mediates epithelial-mesenchymal transition downstream of transforming growth factor-beta1 in renal tubular epithelial cells. *Am J Pathol* **175**, 580-591, doi:10.2353/ajpath.2009.080983 (2009).
- 87 Hodgkin, J. & Barnes, T. M. More is not better: brood size and population growth in a self-fertilizing nematode. *Proc Biol Sci* **246**, 19-24, doi:10.1098/rspb.1991.0119 (1991).
- 88 Shaffer, J. M. & Greenwald, I. SALSA, a genetically encoded biosensor for spatiotemporal quantification of Notch signal transduction in vivo. *Developmental cell* **57**, 930-944 e936, doi:10.1016/j.devcel.2022.03.008 (2022).
- 89 Massague, J. TGFbeta in Cancer. *Cell* **134**, 215-230, doi:10.1016/j.cell.2008.07.001 (2008).
- 90 Sekiguchi, R. & Yamada, K. M. Basement Membranes in Development and Disease. *Curr Top Dev Biol* **130**, 143-191, doi:10.1016/bs.ctdb.2018.02.005 (2018).
- 91 Sanada, F. *et al.* Source of Chronic Inflammation in Aging. *Front Cardiovasc Med* **5**, 12, doi:10.3389/fcvm.2018.00012 (2018).
- 92 Christopoulos, P. F. *et al.* Targeting the Notch Signaling Pathway in Chronic Inflammatory Diseases. *Front Immunol* **12**, 668207, doi:10.3389/fimmu.2021.668207 (2021).
- 93 Kavian, N., Servettaz, A., Weill, B. & Batteux, F. New insights into the mechanism of notch signalling in fibrosis. *Open Rheumatol J* **6**, 96-102, doi:10.2174/1874312901206010096 (2012).
- 94 Dees, C. *et al.* Inhibition of Notch signaling prevents experimental fibrosis and induces regression of established fibrosis. *Arthritis Rheum* **63**, 1396-1404, doi:10.1002/art.30254 (2011).
- 95 Park, J. S. *et al.* The effect of matrix stiffness on the differentiation of mesenchymal stem cells in response to TGF-beta. *Biomaterials* **32**, 3921-3930, doi:10.1016/j.biomaterials.2011.02.019 (2011).
- 96 Miller, A. E., Hu, P. & Barker, T. H. Feeling Things Out: Bidirectional Signaling of the Cell-ECM Interface, Implications in the Mechanobiology of Cell Spreading, Migration, Proliferation, and Differentiation. *Advanced healthcare materials*, e1901445, doi:10.1002/adhm.201901445 (2020).
- 97 Li, Q., Li, M., Zheng, K., Tang, S. & Ma, S. Expression pattern analysis and drug differential sensitivity of cancer-associated fibroblasts in triple-negative breast cancer. *Transl Oncol* **14**, 100891,

- doi:10.1016/j.tranon.2020.100891 (2021).
- 98 Hori, K., Sen, A. & Artavanis-Tsakonas, S. Notch signaling at a glance. *J Cell Sci* **126**, 2135-2140, doi:10.1242/jcs.127308 (2013).
- 99 Li, Y. *et al.* Hepatocyte CD36 protects mice from NASH diet-induced liver injury and fibrosis via blocking N1ICD production. *Biochim Biophys Acta Mol Basis Dis* **1869**, 166800, doi:10.1016/j.bbadis.2023.166800 (2023).
- 100 Li, B. *et al.* NOTCH signaling inhibition after DAPT treatment exacerbates alveolar echinococcosis hepatic fibrosis by blocking M1 and enhancing M2 polarization. *FASEB J* **37**, e22901, doi:10.1096/fj.202202033R (2023).
- 101 Zhou, B. *et al.* Notch signaling pathway: architecture, disease, and therapeutics. *Signal Transduct Target Ther* **7**, 95, doi:10.1038/s41392-022-00934-y (2022).
- 102 Sorensen, E. B., Seidel, H. S., Crittenden, S. L., Ballard, J. H. & Kimble, J. A toolkit of tagged glp-1 alleles reveals strong glp-1 expression in the germline, embryo, and spermatheca. *microPublication biology* **2020**, doi:10.17912/micropub.biology.000271 (2020).
- 103 Fiuza, U. M. & Arias, A. M. Cell and molecular biology of Notch. *The Journal of endocrinology* **194**, 459-474, doi:10.1677/JOE-07-0242 (2007).
- 104 Merritt, C. & Seydoux, G. Transgenic solutions for the germline. *WormBook : the online review of C. elegans biology*, 1-21, doi:10.1895/wormbook.1.148.1 (2010).
- 105 Pepper, A. S., Killian, D. J. & Hubbard, E. J. Genetic analysis of *Caenorhabditis elegans* glp-1 mutants suggests receptor interaction or competition. *Genetics* **163**, 115-132, doi:10.1093/genetics/163.1.115 (2003).
- 106 Berry, L. W., Westlund, B. & Schedl, T. Germ-line tumor formation caused by activation of glp-1, a *Caenorhabditis elegans* member of the Notch family of receptors. *Development* **124**, 925-936 (1997).
- 107 Valet, M. & Narbonne, P. Formation of benign tumors by stem cell deregulation. *PLoS Genet* **18**, e1010434, doi:10.1371/journal.pgen.1010434 (2022).
- 108 Cal, S. *et al.* Cloning, expression analysis, and structural characterization of seven novel human ADAMTSs, a family of metalloproteinases with disintegrin and thrombospondin-1 domains. *Gene* **283**, 49-62, doi:10.1016/s0378-1119(01)00861-7 (2002).
- 109 Ramirez-Suarez, N. J. *et al.* Axon-Dependent Patterning and Maintenance of Somatosensory Dendritic Arbors. *Developmental cell* **48**, 229-244 e224, doi:10.1016/j.devcel.2018.12.015 (2019).
- 110 Ihara, S. *et al.* Basement membrane sliding and targeted adhesion remodels tissue boundaries during uterine-vulval attachment in *Caenorhabditis elegans*. *Nature cell biology* **13**, 641-651, doi:10.1038/ncb2233 (2011).
- 111 Blelloch, R. *et al.* The gon-1 gene is required for gonadal morphogenesis in *Caenorhabditis elegans*. *Dev Biol* **216**, 382-393, doi:10.1006/dbio.1999.9491 (1999).
- 112 Heppert, J. K. *et al.* Comparative assessment of fluorescent proteins for in vivo imaging in an animal model system. *Mol Biol Cell* **27**, 3385-



- 3394, doi:10.1091/mbc.E16-01-0063 (2016).
- 113 Das, A., Dickinson, D. J., Wood, C. C., Goldstein, B. & Slep, K. C. Crescerin uses a TOG domain array to regulate microtubules in the primary cilium. *Mol Biol Cell* **26**, 4248-4264, doi:10.1091/mbc.E15-08-0603 (2015).
- 114 Kodoyianni, V., Maine, E. M. & Kimble, J. Molecular basis of loss-of-function mutations in the *glp-1* gene of *Caenorhabditis elegans*. *Mol Biol Cell* **3**, 1199-1213, doi:10.1091/mbc.3.11.1199 (1992).
- 115 Austin, J. & Kimble, J. *glp-1* is required in the germ line for regulation of the decision between mitosis and meiosis in *C. elegans*. *Cell* **51**, 589-599, doi:10.1016/0092-8674(87)90128-0 (1987).
- 116 Henderson, S. T., Gao, D., Lambie, E. J. & Kimble, J. *lag-2* may encode a signaling ligand for the GLP-1 and LIN-12 receptors of *C. elegans*. *Development* **120**, 2913-2924, doi:10.1242/dev.120.10.2913 (1994).
- 117 Lee, C., Sorensen, E. B., Lynch, T. R. & Kimble, J. C. *C. elegans* GLP-1/Notch activates transcription in a probability gradient across the germline stem cell pool. *eLife* **5**, doi:10.7554/eLife.18370 (2016).
- 118 Haupt, K. A. *et al.* The molecular basis of LST-1 self-renewal activity and its control of stem cell pool size. *Development* **146**, doi:10.1242/dev.181644 (2019).
- 119 Graham, P. L. *et al.* Type IV collagen is detectable in most, but not all, basement membranes of *Caenorhabditis elegans* and assembles on tissues that do not express it. *J Cell Biol* **137**, 1171-1183, doi:10.1083/jcb.137.5.1171 (1997).
- 120 Gupta, M. C., Graham, P. L. & Kramer, J. M. Characterization of alpha1(IV) collagen mutations in *Caenorhabditis elegans* and the effects of alpha1 and alpha2(IV) mutations on type IV collagen distribution. *J Cell Biol* **137**, 1185-1196, doi:10.1083/jcb.137.5.1185 (1997).
- 121 Sibley, M. H., Graham, P. L., von Mende, N. & Kramer, J. M. Mutations in the alpha 2(IV) basement membrane collagen gene of *Caenorhabditis elegans* produce phenotypes of differing severities. *EMBO J* **13**, 3278-3285, doi:10.1002/j.1460-2075.1994.tb06629.x (1994).
- 122 Holster, T. *et al.* Loss of assembly of the main basement membrane collagen, type IV, but not fibril-forming collagens and embryonic death in collagen prolyl 4-hydroxylase I null mice. *J Biol Chem* **282**, 2512-2519, doi:10.1074/jbc.M606608200 (2007).
- 123 Matsuo, E. *et al.* Substrate stiffness modulates endothelial cell function via the YAP-Dll4-Notch1 pathway. *Exp Cell Res* **408**, 112835, doi:10.1016/j.yexcr.2021.112835 (2021).
- 124 Kretschmer, M., Mamistvalov, R., Sprinzak, D., Vollmar, A. M. & Zahler, S. Matrix stiffness regulates Notch signaling activity in endothelial cells. *J Cell Sci* **136**, doi:10.1242/jcs.260442 (2023).
- 125 Del Gaudio, F. *et al.* Left ventricular hypertrophy and metabolic resetting in the Notch3-deficient adult mouse heart. *Sci Rep* **13**, 15022, doi:10.1038/s41598-023-42010-7 (2023).
- 126 Henderson, N. C., Rieder, F. & Wynn, T. A. Fibrosis: from mechanisms to medicines. *Nature* **587**, 555-566, doi:10.1038/s41586-020-2938-9 (2020).

- 127 Staab-Weijnitz, C. A. Fighting the Fiber: Targeting Collagen in Lung Fibrosis. *Am J Respir Cell Mol Biol* **66**, 363-381, doi:10.1165/rcmb.2021-0342TR (2022).
- 128 Donoughe, S. *et al.* BMP signaling is required for the generation of primordial germ cells in an insect. *Proc Natl Acad Sci U S A* **111**, 4133-4138, doi:10.1073/pnas.1400525111 (2014).
- 129 Seydoux, G., Savage, C. & Greenwald, I. Isolation and characterization of mutations causing abnormal eversion of the vulva in *Caenorhabditis elegans*. *Dev Biol* **157**, 423-436, doi:10.1006/dbio.1993.1146 (1993).
- 130 Narbonne, P., Maddox, P. S. & Labbe, J. C. DAF-18/PTEN locally antagonizes insulin signalling to couple germline stem cell proliferation to oocyte needs in *C. elegans*. *Development* **142**, 4230-4241, doi:10.1242/dev.130252 (2015).
- 131 Dickinson, D. J., Pani, A. M., Heppert, J. K., Higgins, C. D. & Goldstein, B. Streamlined Genome Engineering with a Self-Excising Drug Selection Cassette. *Genetics* **200**, 1035-1049, doi:10.1534/genetics.115.178335 (2015).
- 132 Ward, J. D. Rapid and precise engineering of the *Caenorhabditis elegans* genome with lethal mutation co-conversion and inactivation of NHEJ repair. *Genetics* **199**, 363-377, doi:10.1534/genetics.114.172361 (2015).
- 133 Crittenden, S. L., Leonhard, K. A., Byrd, D. T. & Kimble, J. Cellular analyses of the mitotic region in the *Caenorhabditis elegans* adult germ line. *Mol Biol Cell* **17**, 3051-3061, doi:10.1091/mbc.e06-03-0170 (2006).
- 134 Jayadev, R. *et al.* alpha-Integrins dictate distinct modes of type IV collagen recruitment to basement membranes. *J Cell Biol* **218**, 3098-3116, doi:10.1083/jcb.201903124 (2019).
- 135 Frokjaer-Jensen, C. *et al.* Single-copy insertion of transgenes in *Caenorhabditis elegans*. *Nature genetics* **40**, 1375-1383, doi:10.1038/ng.248 (2008).
- 136 Large, E. E. & Mathies, L. D. *Caenorhabditis elegans* SWI/SNF subunits control sequential developmental stages in the somatic gonad. *G3 (Bethesda)* **4**, 471-483, doi:10.1534/g3.113.009852 (2014).
- 137 Kimble, J. & Hirsh, D. The postembryonic cell lineages of the hermaphrodite and male gonads in *Caenorhabditis elegans*. *Dev Biol* **70**, 396-417, doi:10.1016/0012-1606(79)90035-6 (1979).
- 138 Conte, D., Jr., MacNeil, L. T., Walhout, A. J. M. & Mello, C. C. RNA Interference in *Caenorhabditis elegans*. *Curr Protoc Mol Biol* **109**, 26 23 21-26 23 30, doi:10.1002/0471142727.mb2603s109 (2015).
- 139 Zmorzynski, S., Styk, W., Filip, A. A. & Krasowska, D. The Significance of NOTCH Pathway in the Development of Fibrosis in Systemic Sclerosis. *Ann Dermatol* **31**, 365-371, doi:10.5021/ad.2019.31.4.365 (2019).
- 140 Condorelli, A. G. *et al.* Notch-ing up knowledge on molecular mechanisms of skin fibrosis: focus on the multifaceted Notch signalling pathway. *J Biomed Sci* **28**, 36, doi:10.1186/s12929-021-00732-8 (2021).
- 141 Zhang, X., Meng, H. & Wang, M. M. Collagen represses canonical Notch signaling and binds to Notch ectodomain. *Int J Biochem Cell Biol* **45**, 1274-1280, doi:10.1016/j.biocel.2013.03.020 (2013).

- 142 Eckmann, C. R., Crittenden, S. L., Suh, N. & Kimble, J. GLD-3 and control of the mitosis/meiosis decision in the germline of *Caenorhabditis elegans*. *Genetics* **168**, 147-160, doi:10.1534/genetics.104.029264 (2004).
- 143 Liu, J. & Chin-Sang, I. D. C. *elegans* as a model to study PTEN's regulation and function. *Methods* **77-78**, 180-190, doi:10.1016/j.ymeth.2014.12.009 (2015).
- 144 Silverman, G. A. *et al.* Modeling molecular and cellular aspects of human disease using the nematode *Caenorhabditis elegans*. *Pediatr Res* **65**, 10-18, doi:10.1203/PDR.0b013e31819009b0 (2009).
- 145 Xue, Y. *et al.* Embryonic lethality and vascular defects in mice lacking the Notch ligand Jagged1. *Hum Mol Genet* **8**, 723-730, doi:10.1093/hmg/8.5.723 (1999).
- 146 O'Kane, C. J. Modelling human diseases in *Drosophila* and *Caenorhabditis*. *Semin Cell Dev Biol* **14**, 3-10, doi:10.1016/s1084-9521(02)00162-3 (2003).
- 147 Aboobaker, A. A. & Blaxter, M. L. Medical significance of *Caenorhabditis elegans*. *Ann Med* **32**, 23-30, doi:10.3109/07853890008995906 (2000).
- 148 Ahringer, J. Turn to the worm! *Curr Opin Genet Dev* **7**, 410-415, doi:10.1016/s0959-437x(97)80157-8 (1997).
- 149 Gounder, M. *et al.* Nirogacestat, a gamma-Secretase Inhibitor for Desmoid Tumors. *N Engl J Med* **388**, 898-912, doi:10.1056/NEJMoa2210140 (2023).
- 150 Feng, S. *et al.* Bright split red fluorescent proteins for the visualization of endogenous proteins and synapses. *Commun Biol* **2**, 344, doi:10.1038/s42003-019-0589-x (2019).
- 151 Frangogiannis, N. Transforming growth factor-beta in tissue fibrosis. *J Exp Med* **217**, e20190103, doi:10.1084/jem.20190103 (2020).
- 152 Miyazawa, K. & Miyazono, K. Regulation of TGF-beta Family Signaling by Inhibitory Smads. *Cold Spring Harb Perspect Biol* **9**, doi:10.1101/cshperspect.a022095 (2017).
- 153 Consortium, C. e. D. M. large-scale screening for targeted knockouts in the *Caenorhabditis elegans* genome. *G3 (Bethesda)* **2**, 1415-1425, doi:10.1534/g3.112.003830 (2012).
- 154 Sarasija, S. & Norman, K. R. A gamma-Secretase Independent Role for Presenilin in Calcium Homeostasis Impacts Mitochondrial Function and Morphology in *Caenorhabditis elegans*. *Genetics* **201**, 1453-1466, doi:10.1534/genetics.115.182808 (2015).

